Fall November 2014

ENGINEERED NANOPARTICLES FOR DETECTION AND TREATMENT OF BACTERIA AND BIOFILMS

Xiaoning Li

ENGINEERED NANOPARTICLES FOR DETECTION AND TREATMENT OF BACTERIA AND BIOFILMS

A Dissertation Presented

By

XIAONING LI

Submitted to the Graduate School of the
University of Massachusetts Amherst in partial fulfillment
of the requirements for the degree of

DOCTOR OF PHILOSOPHY

September 2014

Chemistry

ENGINEERED NANOPARTICLES FOR DETECTION AND TREATMENT OF BACTERIA AND BIOFILMS

A Dissertation Presented

By

XIAONING LI

Approved as to style and content by:

Vincent M. Rotello, Chair

Dhandapani Venkataraman, Member

Michael J. Knapp, Member

Harry Bermudez, Member

Craig T. Martin, Department Head

Department of Chemistry

DEDICATION

To my parents and my love

献给我最敬爱的父母和我的爱人！

ACKNOWLEDGMENTS

My PhD life has been an adventurous, challenging, yet rewarding journey, of which I have arrived to the last stop by writing this thesis. Chapters, words, and figures written here can only state my research achievement, but they are not able to reveal the tremendous help, support, and inspiration I have received from the people mentioned here. Without them, this journey would have been extremely difficult and dull.

First, I would like to express my sincere and greatest gratitude to my advisor, Prof. Vincent M. Rotello, for his influential guidance and constant encouragement. He opened the gate to science for me, passed scientific vision to me, and taught me research skills. Most importantly, he showed me that all roads lead to science, for which Prof. Rotello has offered me the incredible freedom and flexibility to explore the vast world of science and to find my own path. I deeply appreciate him being my mentor and teacher and it is my great honor and fortune to work with him.

I would like to acknowledge my dissertation committee members, Prof. Dhandapani Venkataraman (DV), Prof. Michael Knapp, and Prof. Harry Bermudez, for their constructive insights and academic support throughout this work.

I am deeply appreciative to Prof. Margaret Riley, Dr. Y. S. Prakash, Prof. Xinrong Zhang, Dr. Fang Wen, Dr. Hao Kong, and Ms. Sandra Robinson for their advice, support, and especially expertise in their field to make our successful and productive research collaboration possible.

I am truly thankful to all the past and present members in the Rotello group for their warm support and help all these years. They have been amazing colleagues, leaders, team members, teachers, mentees, and friends. In particular, I would like to thank Dr. Oscar Miranda and Dr. Chandra Subramani for introducing me to research and for sharing their research experience with me. I would also like to acknowledge the contributions that Dr. Miranda, Dr.

Rana, Krish, Brian, Rubul, Daniel, Ali, Akash, Bo, Yi-Cheun, and Brad made to the work in this thesis.

My warm and sincere thank also goes to all my friends who ensured my colorful and energetic life during my study in UMass Amherst: Jing, Yao, Zhongjing, Yuxi, Zhengjiang, Rui, NLe, Sung Tae, Youngdo, Chang Soo, Deb, Daniel, Ziwen, Tsukasa, Moumita, Vikas, Diego, Carol, Ari, and Mike. The joy we shared together, the tears we shed together, the time we spent together, and your helping hands on raining days will always be my treasured memory.

Last but not least, I wish to give my sincerest and hearty thanks to my family for their endless love and unconditioned support. My grandparents and parents are the best teachers I could ever ask for. Their selfless love makes my wings so powerful that I can soar freely in this foreign sky. I am genuinely grateful to have Krish, my fiancée, to be my best friend and partner, who showed me my potential both in research and in life that I did not even know. His love, encouragement, and inspiration drove me to pursue my PhD degree and accomplish this thesis.

ABSTRACT

ENGINEERED NANOPARTICLES FOR DETECTION AND TREATMENT OF BACTERIA DN BIOFILMS

SEPTEMBER 2014

XIAONING LI

B.S., UNIVERSITY OF SCIENCE AND TECHNOLOGY OF CHINA

Ph.D., UNIVERSITY OF MASSACHUSETTS AMHERST

Directed by: Professor Vincent M. Rotello

Rapid and sensitive detection and identification of bacteria woud control and prevent bacterial infection and disease, enhancing the likelihood of early diagnosis and treatment. Especially developing effective biosensor for identification of bacteria species involved in formation of biofilms, which cause chronic and persistent diseases, would promote diagnostic and therapeutic efficiency. Conventional detection methods are limited by sensitivity and required time. First part of my research has been focused on developing a rapid, simple, and sensitive biosensor aiming at portable device application for detection of bacteria in water samples. This sensor is able to detect bacteria at low concentration and generate colorimetric readouts that can be interpreted without aid of instrumentation. A prototype inkjet printed test strip is fabricated to demonstrate the low-cost and sensitive bacteria detecting approach. For detection and identification of the higher and more complex state of bacterial life, biofilms, I developed a multi-channel biosensor to profile biofilms based on their global signature patterns. With the emergence of antibiotic especially multi-drug resistance in bacteria, prevention and detection is no longer efficient, and novel strategies are in great demand for treatment of these multi-drug resistant bacteria as well as bacterial biofilms which possess intrinsic antibiotic resistance. Thus the second part of my research is focused on exploring and tuning nanoparticles antimicrobial properties for treatment of bacteria and biofilms.

TABLE OF CONTENTS

Page

LIST OF TABLES

LIST OF FIGURES

Figure Page

CHAPTER 1

INTRODUCTION

1.1 Global microbial threats

Microbial infections cause 300 million cases of severe illness every year, and 16 million people including 2 million children are estimated to be killed by infectious diseases every year.[1] Recent outbreaks, such as *Escherichia coli* in Germany and the New Delhi Metallo-beta-lactamase-expressing "superbug" in Asia, remind us that microbes are still one of the greatest threats to public health and wellness on a global scale. As a result, rapid detection of microorganisms, especially bacteria, is a key requirement in environmental monitoring, water and food safety, and clinical diagnosis and treatment.

Conventional method for detection and identification of bacteria is plating and culture.[2] After sampling, it generally requires at least 24 hours for analysis and demands selective and differential mediums during culture.[3] Additionally, due to the low sensitivity and limited countable colonies required, samples often need to be collected in large volumes. However, bacteria number can change very rapidly and greatly during the culture and analysis time, which may result in incorrect or belated assessment. Since short term peaks of bacteria concentration can lead to considerably increased outbreaks of disease, rapid and sensitive methods for detection of bacteria are in great demand to address the urgency need for monitoring food/water quality as well as clinical diagnosis.

Quantitative polymerase chain reaction (q-PCR) allows amplification and simultaneous quantification of target bacterial DNA, providing a more sensitive technique capable of detecting and identifying bacteria in less than 24 hours.[4] This molecular technique has been eventually adapted by the U.S. Environmental Protection Agency and clinical diagnosis. Similarly, other methods have been proposed and investigated by researchers using high technology, such as luminescence,[5] immunological methods,[6] and mass spectrometry.[7] Each of these systems has

advantages and offers new aspects into promoting rapid microbial detection. However, the requirement of expensive instrument and trained personnel may substantially limit their application, especially for on-site detection and widespread application in emerging countries where bacteria-contaminated water and food take a majority part of global deaths caused by bacterial diseases. Therefore, technological platforms that possess rapid, sensitive, simple, and potentially low-cost detection features are still the focus of pioneer research.

1.2 Biosensor

A biosensor is generally defined as a device that utilizes biological components to detect a target substance, often a biological analyte. The essential device-based detection technique of biosensors makes them a more suitable approach for on-site application. A biosensor usually consists of a receptor for recognition of analytes and a transducer for transduction of signals to interpretation (Figure 1.1).

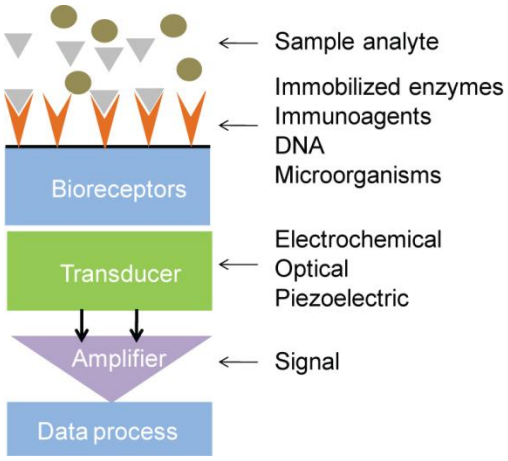

Figure 1.1. Schematic illustration of a general biosensor design including bioreceptor, transducer, amplifier, and data process.

In a biosensor, a receptor is mostly a biological species (e.g., an enzyme, an antibody, or a nucleic acid) or a biological living system (e.g., cells or microorganisms), and such bioreceptors can be incorporated in the sampling portion of a biosensor via either covalent or non-covalent attachment. Analytes are often recognized by interaction with receptors through

biochemical/biophysical mechanisms. And the interaction event between analytes and receptors is converted by transducer into a measurable effect, such as an electrochemical, mass-sensitive, or optical signal.

The two key steps involved in the detection process using a biosensor are analyte recognition and signal transduction. The sensitivity of a biosensor is therefore dependent upon these two key designs. One commonly employed strategy to increase biosensor sensitivity is signal amplification during/after signal transduction process. For example, optical or electronic sandwich bioaffinity assays capture and recognize analytes on one layer of receptors, followed by labeling of analytes with another layer of secondary receptors/amplifiers which then generate amplified signals (Figure 1.2).[8] The challenge in these approaches is the disadvantages of capturing a small number of labels per binding event. Therefore, innovative materials and platforms are needed in order to achieve ultrahigh sensitivity during analyte recognition process.

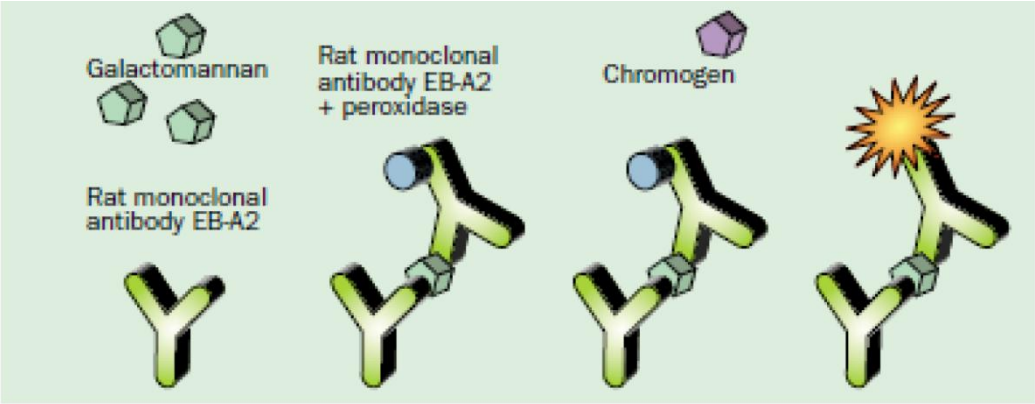

Figure 1.2. A sandwich bioaffinity assay for detection of galactomannan. Analyte galactomanna is captured by the antibody EB-A2 receptor then is labeled by another layer of EB-A2 receptors plus peroxidase. Signals were then generated and amplified by peroxidase catalyzed chromogenic reaction. Adapted from reference 8.

1.3 Nanoparticles for biosensing

The distinctive physical and chemical properties of nanoscale particles offer unique prospects for designing highly sensitive receptors in biorecognition process, potentially

increasing biosensor sensitivity (Figure 1.3). First, the tiny size and large surface-to-volume ratio of NPs guarantees increased receptor-analyte interaction, amplifying number of binding events (Figure 1.4).[9] Additionally, surface functionalization of NPs can provide stable, sensitive, and specific or selective recognition elements of interest in biosensor design.[10]

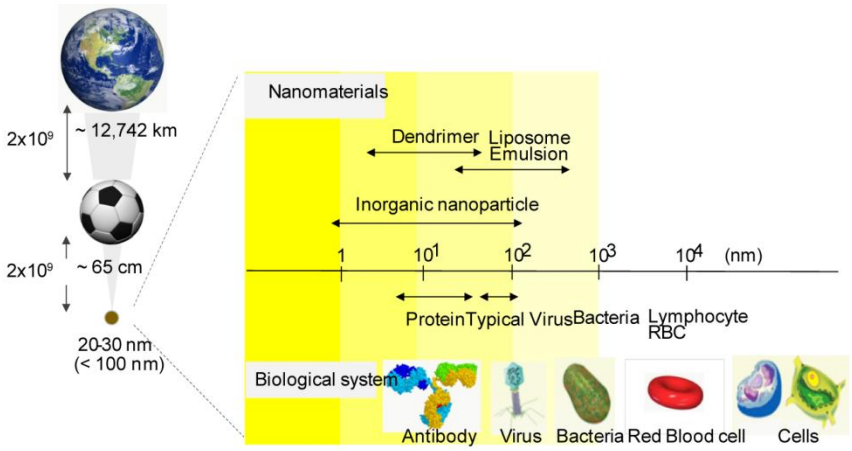

Figure 1.3. Schematic illustration of nanoparticle size compared to biomolecules and bio-species.

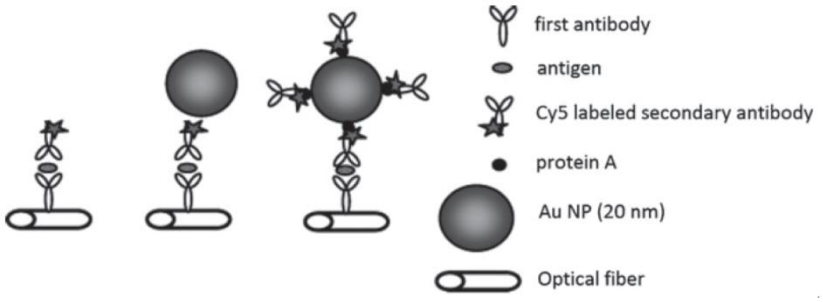

Figure 1.4. A NP-based sandwich bioaffinity assay for detection of protein. By conjugation with NP, number of Cy5 labeled secondary antibody increased compared to the original sandwich assay design, hence improving biosensor sensitivity. Adapted from reference 9.

Furthermore, NPs possess distinctive attributes such as optical, photophyscial, electronic, and catalytic properties, which make them ideal labels for the biorecognition process. These properties can be further tuned by size, shape, dimensions, and compositions. In addition, the nanoscale size of NPs dictates that their properties can be strongly affected by the binding with

analyte molecules,[11] providing pronounced affect for signal generation and transduction (Figure 1.5).[12,13]

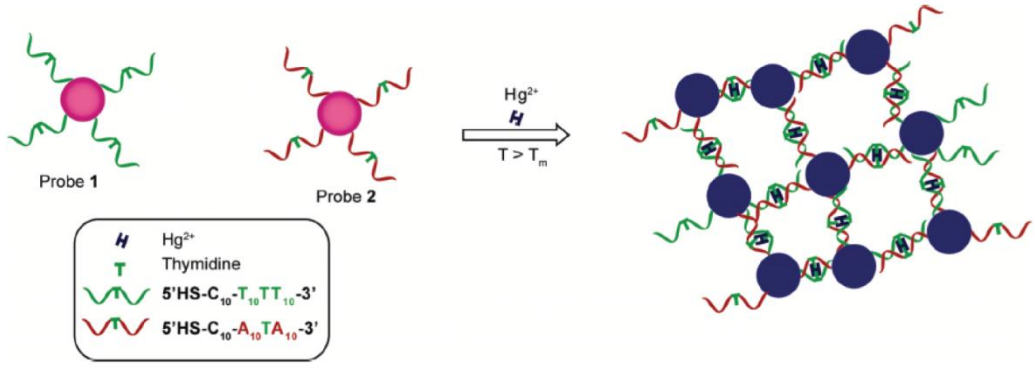

Figure 1.5. Colorimetric detection of Hg2+ using DNA functionalized gold nanoparticles. Thymidine-Hg2+-thymidine coordination chemistry is exploited and results in gold nanoparticle aggregation. The aggregation of gold nanoparticles of appropriate sizes (diameter bigger than 3.5 nm) induces interparticle surface plasmon coupling, resulting a visible color change from red to blue. This phenomenon provides a practical platform for absorption-based colorimetric sensing. Adapted from reference 12.

Given the enormous amplification afforded by NPs as well as the NP size-dependent properties, such as enhanced surface activity, surface plasmon resonance, quantum confinement, and superparamagnetism, nanoparticles make remarkable platforms for designing novel and highly sensitive biosensors (Table 1.1).[14] More importantly, by engineering core composition, size, and shape, NP properties can be tuned to give a variety of signal types for amplification and outputs. Similarly, engineered NPs can afford multifunction, presenting various yet controllable interaction profiles on NP surface to meet requirements of different analyte target. Hence, the use of properly engineered NPs could realize the high demand of rapid, sensitive, and simple methods for detection of bacteria.

Table 1.1. Characteristics, ligands and representative applications for various metal and semiconductor materials. Adapted from reference 14.

Core materials	Characteristics	Ligand(s)	Applications

Au	Optical absorption, fluorescence and fluorescence quenching, stability	Thiol, disulfide, phosphine, amine	Biomolecular recognition, delivery, sensing
Ag	Surface-enhanced fluorescence	Thiol	Sensing
Pt	Catalytic property	Thiol, phosphine, amine, isocyanide	Bio-catalyst, sensing
CdSe	Luminescence, photo-stability	Thiol, phosphine, pyridine	Imaging, sensing
Fe_2O_3	Magnetic property	Diol, dopamine derivative, amine	MIR imaging and biomolecule purification
SiO_2	Biocompatibility	Alkoxysilane	Biocompatible by surface coating

1.4 Bacterial infections and treatment

Pathogenic bacteria are referred to those that cause or are capable of causing disease. Some pathogens are unequivocally pathogenic, whereas others are generally harmless and they cause disease only under certain conditions, for example, when being introduced into a normally sterile body site, or infection of an immunocompromised host.[15] Pathogenic bacteria can enter the host body through a variety of means, including inhalation, ingestion, or sexual contact. Upon evasion of host primary defense, bacteria usually adhere to host cells and proliferate, causing infections by damaging host cells via toxins or an inflammatory response. Furthermore, if bacteria successfully evade host secondary defenses, infections, in turn, can have severe consequences, leading to serious bacterial diseases and even life-threatening complications, such as sepsis, organ failure, toxic shock syndrome, and death.[16] In some cases, bacterial infections can result in chronic disease state, where the involved bacterial colonization often develops into a biofilm, a complex three-dimensional bacterial community.[17] The biofilm-associated diseases are clinically more challenging than acute bacterial infections in both diagnosis and treatment (Figure 1.6).[18]

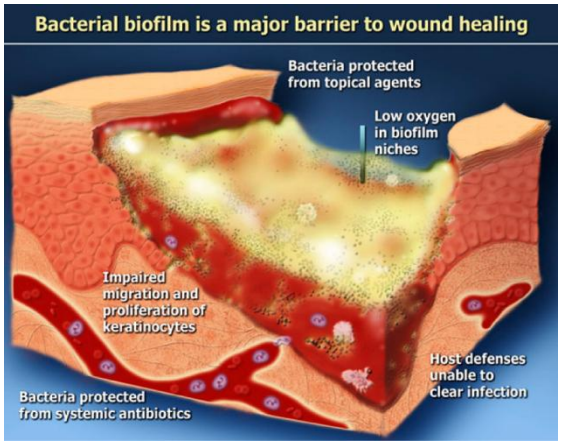

Figure 1.6. Schematic illustration of non-healing wounds caused by bacterial biofilm. Adapted from reference 18.

Bacterial infections are generally treated with antibiotics, of which the selective toxicity ensures killing (bactericidal) or inhibiting the growth and spread (bacteriostatic) of the pathogenic bacteria without harming the cells of the host. Antibiotics can be organized into six families – the penicillins, cephalosporins, tetracyclines, aminoglycosides, macrolides, and fluoroquinolones, plus other agents which include vancomycin and trimethoprim-sulfamethoxazole.[19] The mechanisms of how these antibiotics act against bacteria include (i) inhibition of bacterial cell wall synthesis (penicillins, vancomycin, etc),[20] (ii) inhibition of protein synthesis (tetracyclines, macrolides, etc),[21] (iii) alteration of cell membrane (polymycins, etc),[22] (iv) inhibition of nucleic acid synthesis (quinolones, rifampin, etc),[23] and (v) antimetabolite activity (trimethoprim, etc).[24]

1.5 Bacterial resistance to antibiotics

Antibiotics are among the most commonly prescribed drugs, and many of the prescriptions are for patients who do not need or cannot be treated effectively as prescribed.[25] Antibiotics are widely used in food animals as well to prevent, control, and treat diseases, and this practice is believed to be capable of promoting the growth and production of food.[26] The widespread use of antibiotics has caused the emergence of resistance, even multidrug resistance (MDR) in bacteria.[27] Antibiotic resistance has become a worldwide problem, as many forms of

resistance spread can cross international boundaries and even between continents with ease and remarkable speed.

Bacterial resistance to antibiotics can spread both genetically and environmentally. Genetically, antibiotic resistance transfers through bacteria population "vertically", when new generations of bacteria inherit resistance genes from parent bacteria,[28] as well as "horizontally", when bacteria share or exchange resistance-encoding genetic materials with neighboring bacteria.[29] Environmentally, antibiotic resistance spreads as bacteria travel from place to place via air, water, and hosts (human, animals, etc) contact. Among all these paths, horizontal gene transfer is the primary reason for bacterial antibiotic resistance,[30] and three mechanisms for horizontal gene transfer have been identified: transformation, transduction, and conjugation. Due to these mechanisms, horizontal gene transfer happens frequently in the general community, and particularly in healthcare setting, such as hospitals and nursing homes, where most deaths related to antibiotic resistance occur.

According to Center for Disease Control and Prevention, at least 2 million people acquire serious infections with MDR bacteria.[31] In most cases of antibiotic-resistant infections, it requires prolonged treatments, extended hospital stays, necessitate additional healthcare use, resulting in great disabilities and deaths. At least of 23,000 people die each year as a direct result from antibiotic-resistant infections, and many more from complications by an antibiotic-resistant infection. Moreover, economic cost of antibiotic resistance can be as high as $20 billion in direct healthcare, with additional costs to society for lost productivity as high as $35 billion a year.[32]

1.6 Strategies for discovery of novel antimicrobials

The ruthless spread of antibiotic resistance in bacteria, coupled with insufficient investment in antibacterial research, has led to a steady decline in the efficacy of current treatments and a lack of new drug families with which to complement their use or replace them. Hence, there is urgent and undeniable need for new antibacterial research. Perspective strategies

for discovery of novel antimicrobials usually include new antibacterials from natural products, modification of existing classes, and antimicrobial peptides.[33]

Historically, the screening of natural products obtained from microbial sources revealed many and successful antibacterial discoveries. Penicillin, for instance, was uncovered and derived from *Penicillium* fungi. However, since many of the easily accessible compounds have been explored, it become more challenging and requires technique improvement (culture the "uncultured" soil bacteria, metagenomics, etc) for future investigation in natural products.[34]

Medicinal chemistry has been adapted as a powerful tool to improve the activity or profile of existing antibiotic classes.[35] By logical and systematic modifications, the next generation can increase potency and activity spectrum. Cephalosporins, β-lactam antibiotics, belong to one class of antibiotics that has been subjected to extensive medicinal chemistry examination. In this class, first-generation agents are active primarily against Gram-positive organisms and have limited activity against Gram-negative bacilli. Second- and third generation displayed activity against some Gram-negative organisms. Fourth-generation Cefepime feature extended spectrum of activity against both Gram-positive and Gram-negative bacteria, and it is active as well against some strains producing β-lactamase enzymes that inactivates β-lactam antibiotics.[36] Due to the time-consuming and laborious synthetic requirements, the medicinal chemistry research on developing novel antibiotics is typically carried out in pharmaceutical companies, where such investigations have become exceedingly unattractive investments.[37]

Antimicrobial peptides are host-defense molecules produced by all living organisms. These evolutionary conserved peptides bear an overall positive charge and have both a hydrophobic and hydrophilic side, enabling the molecule to enter lipid-rich membrane of target bacterial cells.[38] Antimicrobial peptides possess favorable qualities as novel antibacterials, such as reduced propensity to engender resistance and anti-inflammatory and anti-endotoxin activities. Polymyxins, cationic lipopeptides, have been approved for clinical use and applied to MDR-bacterial infections.[39] Despite their attractive properties, antimicrobial peptides are costly to

synthesize, and their susceptibility to proteolytic enzymes lead to a short half-life *in vivo*.[40] These challenging difficulties need to be addressed for future development of antimicrobial peptides.[41]

Table 1.2. Summary of selected studies concerning the antimicrobial effects of nanoparticles. Adapted from reference 66.

Chemistry	Size (average)	Zeta potential	Organism tested	MIC	Proposed mechanism
ZnO	13 nm	N/A	*Staphylococcus aureus*	Reduced 95% at 80 μg/mL	ROS inhibition
ZnO	60 nm	N/A	*S. aureus*	Reduced 50% at 400 μg/mL	ROS inhibition
ZnO	40 nm	Positive (no value)	*S. aureus, Escherichia coli*	Both species reduced 99% at 400 μg/mL	Membrane disruption
ZnO	12 nm	N/A	*E. coli*	Reduced 90% at 400 μg/mL	Membrane damage due to particle abrasiveness
ZnO ions	N/A	N/A	*Pseudomonas aeruginosa, S. aureus, Candida albicans*	Reduced 100% at 1917, 9, and 39 μg/mL, respectively	ROS inhibition
Silver	21 nm	N/A	*E. coli, Vibrio cholerae, Salmonella typhi, P. aeruginosa*	All reduced 100% at 75 μg/mL	Membrane disruption, Ag ion interference with DNA replication
Silver	Triangles (50 nm)	Positive (no value, cationic surfactant)	*E. coli*	Reduced 99% with 0.1 μg/mL added to agar surface	Membrane disruption, Ag ion interference with DNA replication
Silver	12 nm	Negative (no value)	*E. coli*	Reduced 70% with 10 μg/mL in agar	Membrane disruption, Ag ion interference with DNA replication
Silver	13.5 nm	–0.33 mV	*S. aureus, E. coli*	Inhibitory concentration of 3.56 μg/L and 0.356 μg/L, respectively, added to agar surface	Membrane disruption, Ag ion interference with DNA replication
Cu	100 nm	N/A	*E. coli, Bacillus subtilis*	Reduced 90% at 33.40 μg/mL and 28.20 μg/mL, respectively	Protein inactivation via thiol interaction
Fe_3O_4	9 nm	–19.09 mV	*S. aureus*	Increased dead cells observed at 3 mg/mL	ROS, membrane disruption
Fe_3O_4	8 nm	N/A	*Staphylococcus epidermidis*	Reduced 65% at 2 mg/mL	ROS, membrane disruption
Al_2O_3	11 nm	120 mV	*E. coli*	Reduced 35%, 70%, and 68% at 10, 100, and 500 μg/mL, respectively	Dose-dependent ROS, particle penetration
Al_2O_3	60 nm	30 mV	*E. coli, B. subtilis, Pseudomonas fluorescens*	Reduced bacteria species by 36%, 57%, and 70% at 20 μg/mL	Flocculation
TiO_2	17 nm	12 mV	*E. coli*	Reduced 0%, 35%, and 80% with 10, 100, and 500 μg/mL, respectively	Membrane disruption
SiO_2	20 nm	35 mV	*E. coli, B. subtilis, P. fluorescens*	Reduced bacteria species 58%, 40%, and 70% at 20 μg/mL	Flocculation, membrane disruption
Chitosan	40 nm	51 mV	*E. coli, S. aureus*	Reduced bacteria species 100% at 4 μg/mL and 8 μg/mL, respectively	Flocculation, membrane disruption

Nanotechnology has introduced nanoparticles (NPs) as a new paradigm in therapeutic applications with their unique properties.[42] For example, NP size range is commensurate with biomolecular and bacterial cellular systems, providing additional interactions to small molecule antibiotics,[43] which can be controlled by tailoring NP interface.[44] Also, NPs being slightly larger

than drug efflux pumps, potentially reduces the efflux-mediated extrusion.[45,46] These characteristic features imply that NPs may interact with and penetrate into bacterial cells with unique bacteriostatic and bactericidal mechanisms.[47,48] Presumably, this implication allows a way to address the common mechanisms of antibiotic resistance, such as permeability regulation,[49,50] multi-drug efflux pumps,[51,52] antibiotic degradation,[53,54] and alteration of target site binding affinity.[55,56] Thus, NPs offer a new defense pathway to develop novel antibiotics to (i) combat multi-drug resistant (MDR) bacteria and (ii) lower the pace of resistance evolution by bacteria.[57,58,59] Following this strategy, photocatalytic NPs,[60,61] polycationic NPs,[62,63] and ROS-stimulating metal and metal oxide NPs[64,65] have been used to impart antimicrobial efficacy (Table 1.2).[66]

1.7 Dissertation overview

It has been shown that engineering nanoparticle surface can enhance and tailor interactions with bacterial cells. These interactions between NPs and bacteria have not yet been fully understood, but they exhibit potential pathways for application of microbial detection and treatment. In this thesis, engineered nanoparticles are used to address the urgent need of and rising challenges in rapid and sensitive detection of bacteria as well as novel antibacterials to combat MDR bacteria. The detection and treatment possibility of a higher and more complex state of microbial life, biofilms, is also explored in this thesis. First, in Chapter 2, I will describe a gold nanoparticle-based strategy for rapid colorimetric detection of bacteria using enzymatic amplification. This sensing system is proved to reach clinical and environmental-relevant sensitivity within minutes, giving colorimetric readouts. Such system is applied on a paper-based format to explore the potential of fabricating test strips for detection of bacteria in water samples.

The high sensitivity, rapid detection speed, and colorimetric readouts demonstrate promising application of the NP-enzyme biosensor. In Chapter 3, I will show the improvement based on the NP-enzyme biosensor. To address stability and shelf-life issues related to the use of natural enzymes, engineered Fe_3O_4 nanoparticles are employed as synthetic enzyme mimics. I

will show the capability and sensitivity of this synthetic enzyme mimic-based colorimetric sensor using proteins as model analytes first, and then I will discuss how this method can be used in detection of bacteria.

In Chapter 4, I will describe a gold nanoparticle-constructed multi-channel sensor for detection and identification of biofilms. This approach is the first to detect and identify biofilms based-on their overall physiological signatures using a nanobiosensor. Using this approach, I was able to identify biofilms formed by laboratory and clinical isolated uropathgenic strains. The sensor was further demonstrated to be capable of discriminating biofilms on an *in vitro* wound model.

In Chapter 5, I will demonstrate that by tailoring surface chemistry, gold nanoparticles can be used as potent antimicrobial agents against MDR bacteria. I will further discuss the found NP surface ligand structure and activity relationship, which reveals a new aspect to design and construct antimicrobial gold nanoparticles.

When a bacterial infection develops into biofilm-associated infection, it become much more difficult to treat due to raised resistance and protection from biofilm matrix. In Chapter 6 and Chapter 7, I will demonstrate how engineered NPs can be used as a probe to penetrate biofilms and how properly selected NPs can be used as promising candidates for prevention and treatment of bioflms. I will further show NP-assemble essential oil containing capsules for selective eradication of biofilms on an *in vitro* wound model. These results indicate that NPs can be used as anti-biofilm agents besides being antibacterials, making them attractive candidates in the battle between technology and evolution of bacterial resistance.

1.8 References

1. Pruss, A.; Kay, D.; Fewtrell, L.; Bartram, J. *Environ. Health Perspect.* **2002**, *110*, 537-542.

2. Allen, M. J.; Edberg, S. C.; Reasoner, D. J. *Int. J. Food Microbiol.* **2004**, *92*, 265-274.

3. Brenner, K. P.; Rankin, C. C.; Roybal, Y. R.; Stelma, G. N.; Scarpino, P. V.; Dufour, A. P. *Appl. Environ. Microbiol.* **1993**, *59*, 3534-3544.

4. Burtscher, C.; Wuertz, S. *Appl. Environ. Microbiol.* **2003**, *69*, 4618-4627.

5. Frischer, M. E.; Danforth, J. M.; Foy, T. F.; Juraske, R. *J. Environ. Qual.* **2005**, *34*, 1328-1336.

6. Van Dyck, E.; Ieven, M.; Pattyn, S.; Van Damme, L.; Laga, M. *J. Clin. Microbiol.* **2001**, *39*, 1751-1756.

7. Fenselau, C.; Demirev, P. A. *Mass Spectrom. Rev.* **2001**, *20*, 157-171.

8. Mennink-Kersten, M.; Donnelly, J. P.; Verweij, P. E. *Lancet Infect. Dis.* **2004**, *4*, 349-357.

9. Hsieh, B. Y.; Chang, Y. F.; Ng, M. Y.; Liu, W. C.; Lin, C. H.; Wu, H. T.; Chou, C. *Anal. Chem.* **2007**, *79*, 3487-3493.

10. Ju, H. X.; Zhang, X. J.; Wang, J. In *Nanobiosensing: Principles, Development and Application* 2011, p 39-84.

11. Wang, J. *Small* **2005**, *1*, 1036-1043.

12. Saha, K.; Agasti, S. S.; Kim, C.; Li, X. N.; Rotello, V. M. *Chem. Rev.* **2012**, *112*, 2739-2779.

13. Lee, J. S.; Han, M. S.; Mirkin, C. A. *Angew. Chem. Int. Ed.* **2007**, *46*, 4093-4096.

14. Euliss, L. E.; DuPont, J. A.; Gratton, S.; DeSimone, J. M. *Chem. Soc. Rev.* **2006**, *35*, 1095-1104.

15. Hacker, J.; Kaper, J. B. *Annu. Rev. Microbiol.* **2000**, *54*, 641-679.

16. Finlay, B. B.; Falkow, S. *Microbiol. Mol. Biol. Rev.* **1997**, *61*, 136-169.

17. Costerton, J. W.; Cheng, K. J.; Geesey, G. G.; Ladd, T. I.; Nickel, J. C.; Dasgupta, M.; Marrie, T. J. *Annu. Rev. Microbiol.* **1987**, *41*, 435-464.

18. CBE *Biofilms: The Hypertextbook*; National Science Foundation.

19. Strohl, W. A.; Rouse, B.; Fisher, C. D. *Microbiology*; Lippincott Williams & Wilkins, 2001.

20. Waxman, D. J.; Strominger, J. L. *Annu. Rev. Biochem* **1983**, *52*, 825-869.

21. McKee, E. E.; Ferguson, M.; Bentley, A. T.; Marks, T. A. *Antimicrob. Agents Chemother*. **2006**, *50*, 2042-2049.

22. Hancock, R. E. W. *Annu. Rev. Microbiol.* **1984**, *38*, 237-264.

23. Shen, L. L.; Mitscher, L. A.; Sharma, P. N.; Odonnell, T. J.; Chu, D. W. T.; Cooper, C. S.; Rosen, T.; Pernet, A. G. *Biochemistry* **1989**, *28*, 3886-3894.

24. Hitching.Gh *J. Infect. Dis.* **1973**, *128*, S433-S436.

25. Demerec, M. *J. Bacteriol.* **1948**, *56*, 63-74.

26. Mathur, S.; Singh, R. *Int. J. Food Microbiol.* **2005**, *105*, 281-295.

27. Grundmann, H.; Aires-De-Sousa, M.; Boyce, J.; Tiemersma, E. *Lancet* **2006**, *368*, 874-885.

28. Tenover, F. C. *Am. J. Med.* **2006**, *119*, S3-S10.

29. Ochman, H.; Lawrence, J. G.; Groisman, E. A. *Nature* **2000**, *405*, 299-304.

30. Kay, E.; Vogel, T. M.; Bertolla, F.; Nalin, R.; Simonet, P. *Appl. Environ. Microbiol.* **2002**, *68*, 3345-3351.

31. CDC *Antibiotic resistance threats in the United States*, 2013.

32. Roberts, R. R.; Hota, B.; Ahmad, I.; Scott, R. D.; Foster, S. D.; Abbasi, F.; Schabowski, S.; Kampe, L. M.; Ciavarella, G. G.; Supino, M.; Naples, J.; Cordell, R.; Levy, S. B.; Weinstein, R. A. *Clin. Infect. Dis.* **2009**, *49*, 1175-1184.

33. O'Connell, K. M. G.; Hodgkinson, J. T.; Sore, H. F.; Welch, M.; Salmond, G. P. C.; Spring, D. R. *Angew. Chem. Int. Ed.* **2013**, *52*, 10706-10733.

34. Bull, A. T.; Ward, A. C.; Goodfellow, M. *Microbiol. Mol. Biol. Rev.* **2000**, *64*, 573-606.

35. von Nussbaum, F.; Brands, M.; Hinzen, B.; Weigand, S.; Habich, D. *Angew. Chem. Int. Ed.* **2006**, *45*, 5072-5129.

36. Barradell, L. B.; Bryson, H. M. *Drugs* **1994**, *47*, 471-505.

37. Kresse, H.; Belsey, M. J.; Rovini, H. *Nat. Rev. Drug Discovery* **2007**, *6*, 19-20.

38. Zasloff, M. *Nature* **2002**, *415*, 389-395.

39. Falagas, M. E.; Grammatikos, A. P.; Michalopoulos, A. *Expert Rev. Anti. Infect. Ther.* **2008**, *6*, 593-600.

40. Giuliani, A.; Rinaldi, A. C. *Cell. Mol. Life Sci.* **2011**, *68*, 2255-2266.

41. Rotem, S.; Mor, A. *Biochim. Biophys. Acta Biomembr.* **2009**, *1788*, 1582-1592.

42. Davis, M. E.; Chen, Z.; Shin, D. M. *Nat. Rev. Drug Discov.* **2008,** 7, 771-782.

43. Redl, F. X.; Black, C. T.; Papaefthymiou, G. C.; Sandstrom, R. L.; Yin, M.; Zeng, H.; Murray, C. B.; O'Brien, S. P. *J. Am. Chem. Soc.* **2004,** 126, 14583-14599.

44. Mout, R.; Moyano, D. F.; Rana, S.; Rotello, V. M. *Chem. Soc. Rev.* **2012,** 41, 2539-2544.

45. Bresee, J.; Bond, C. M.; Worthington, R. J.; Smith, C. A.; Gifford, J. C.; Simpson, C. A.; Carter, C. J.; Wang, G.; Hartman, J.; Osbaugh, N. A.; Shoemaker, R. K.; Melander, C.; Feldheim, D. L. *J. Am. Chem. Soc.* **2014,** 136, 5295–5300.

46. Higgins, M. K.; Bokma, E.; Koronakis, E.; Hughes, C.; Koronakis, V. *Proc. Natl. Acad. Sci. U.S.A.* **2004,** 101, 9994-9999.

47. Seil, J. T.; Webster, T. J. *Int. J. Nanomedicine* **2012,** 7, 2767-2781.

48. Blecher, K.; Nasir, A.; Friedman, A. *Virulence* **2011,** 2, 395-401.

49. Falagas, M. E.; Kasiakou, S. K. *Clin. Infect. Dis.* **2005,** 40, 1333-1341.

50. Cui, L. Z.; Iwamoto, A.; Lian, J. Q.; Neoh, H. M.; Maruyama, T.; Horikawa, Y.; Hiramatsu, K. *Antimicrob. Agents Chemother.* **2006,** 50, 428-438.

51. McMurry, L.; Petrucci, R. E. J.; Levy, S. B. *Proc. Natl. Acad. Sci. U.S.A.* **1980,** 77, 3974-3977.

52. Li, X. Z.; Nikaido, H. *Drugs* **2004,** 64, 159-204.

53. Davies, J.; Wright, G. D. *Trends. Microbiol.* **1997,** 5, 234-240.

54. Livermore, D. M. *Clin. Microbiol. Rev.* **1995,** 8, 557-584.

55. Courvalin, P. *Clin. Infect. Dis.* **2006,** 42, S25-S34.

56. Mulligan, M. E.; Murrayleisure, K. A.; Ribner, B. S.; Standiford, H. C.; John, J. F.; Korvick, J. A.; Kauffman, C. A.; Yu, V. L. *Am. J. Med.* **1993,** 94, 313-328.

57. Taylor, E.; Webster, T. J. *Int. J. Nanomedicine* **2011,** 6, 1463-14]73.

58. Hajipour, M. J.; Fromm, K. M.; Ashkarran, A. A.; de Aberasturi, D. J.; de Larramendi, I. R.; Rojo, T.; Serpooshan, V.; Parak, W. J.; Mahmoudi, M. *Trends Biotechnol.* **2012,** 30, 499-511.

59. Huh, A. J.; Kwon, Y. J. *J. Control. Release* **2011,** 156, 128-145.

60. Elahifard, M. R.; Rahimnejad, S.; Haghighi, S.; Gholami, M. R. *J. Am. Chem. Soc.* **2007,** 129, 9552-9553.

61. Wang, P.; Huang, B. B.; Zhang, X. Y.; Qin, X. Y.; Jin, H.; Dai, Y.; Wang, Z. Y.; Wei, J. Y.; Zhan, J.; Wang, S. Y.; Wang, J. P.; Whangbo, M. H. *Chem. Eur. J.* **2009,** 15, 1821-1824.

62. Lin, J.; Qiu, S. Y.; Lewis, K.; Klibanov, A. M. *Biotechnol. Progr.* **2002,** 18, 1082-1086.

63. Murata, H.; Koepsel, R. R.; Matyjaszewski, K.; Russell, A. J. *Biomaterials* **2007,** 28, 4870-4879.

64. Schwartz, V. B.; Thetiot, F.; Ritz, S.; Putz, S.; Choritz, L.; Lappas, A.; Forch, R.; Landfester, K.; Jonas, U. *Adv. Funct. Mater.* **2012,** 22, 2376-2386.

65. Kim, J. S.; Kuk, E.; Yu, K. N.; Kim, J. H.; Park, S. J.; Lee, H. J.; Kim, S. H.; Park, Y. K.; Park, Y. H.; Hwang, C. Y.; Kim, Y. K.; Lee, Y. S.; Jeong, D. H.; Cho, M. H. *Nanomed-Nanotechnol.* **2007,** 3, 95-101.

66. Seil, J. T.; Webster, T. J. *Int. J. Nanomedicine* **2012**, *7*, 2767-2781.

CHAPTER 2

COLORIMETRIC DETECTION OF BACTERIA USING A HYBRID ENZYMATIC NANOCOMPOSITE SENSOR

2.1 Introduction

Bacterial infection causes millions of severe illnesses each year,[1] and is estimated to kill over 2 million children every year.[2] The great majority of these illnesses and deaths occur in developing countries where drinking water and food are frequently contaminated with bacteria.[3] Several techniques[4] are available for bacteria detection and identification, including i) plating and culturing, [5] ii) luminescence, [6] iii) immunological approaches, [7] iv) nucleic acid probe-based methods (PCR, LCR),[8] v) mass spectrometry, [9] vi) microarrays,[10] and vii) biosensors.[11] Each of these systems has its own advantages; however the utility of these methods is generally limited by high cost for use and requirement for trained personnel.

Recent advances in nanotechnology have enabled the development of new diagnostic platforms for sensitive and rapid bacteria detection. For example, Ji *et.al.*[12] used positively-charged amine-terminated polyamidoamine dendrimers to capture bacteria, reporting a sensitivity as low as 1 x 10^4 cfu/mL.[13] Gold nanoparticles (AuNPs) have likewise been employed for detection of bacteria,[14] virus,[15] cancer cells,[16] and proteins.[17] In 2005, Murphy *et al.*[18] showed that CTAB (cetyltrimethylammonium bromide)-functionalized gold nanorods or nanospheres can conformally deposit to form monolayer on *Bacillus cereus* by strong electrostatic interaction. More recently, our group has demonstrated how electrostatic assembly can be used for bacteria sensing through a nanoparticle-fluorescent polymer conjugate system at 2×10^5 cfu/mL.

There are two key issues in designing effective sensors for pathogen detection in the field. First, the limits of detection (LOD) required for application in either environmental testing[19] or clinical applications [20] is 10^4-10^2 cfu/mL, Second, readout should not require expensive instrumentation. Therefore, in this chapter, we developed a hybrid colorimetric enzymatic

nanocomposite biosensor to address these issues. This biosensor uses enzyme amplification to provide high sensitivity for the detection of pathogens in aqueous solutions. The efficacy of this system was demonstrated in both solution and test strip format.

The sensor design features three main components: a) β-Galactosidase (β-Gal),[21] an anionic enzyme (pI 4.6) for signal amplification, b) a chromogenic substrate for color readout (chlorophenol-red-β-D-galactopyranside, CPRG), and c) a cationic gold nanoparticle that binds reversibly to β-Gal, inhibiting the enzyme (Figure 1a). The anionic surface of analyte bacteria introduces competitive binding between NP-β-Gal and NP-bacteria,[22] displaceing the β-Gal with concomitant restoration of activity. The released and active enzyme converts the pale yellow substrate into the red product, providing a colorimetric readout (Figure 2.1). Part of these results have been published in the Journal of the American Chemical Society (**2011**, *133*, 9650-9653).[23]

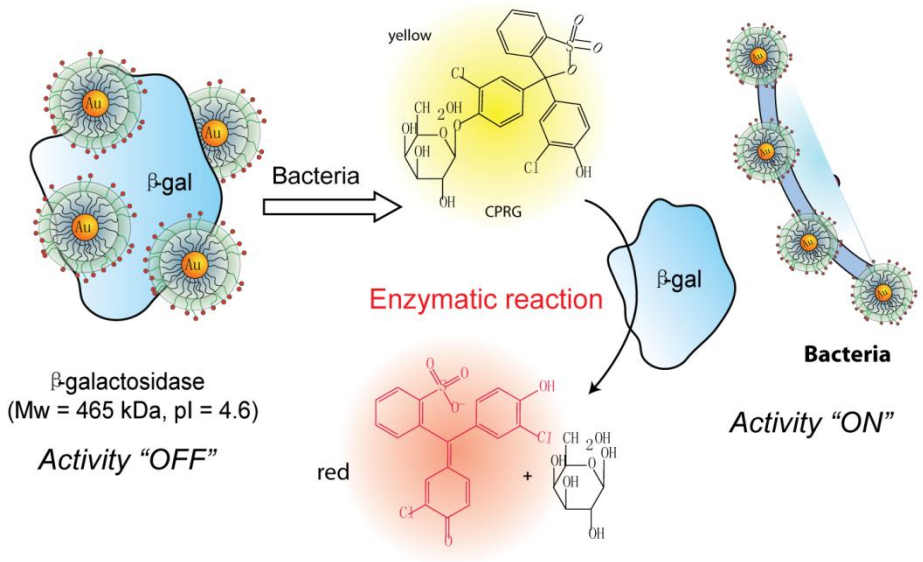

Figure 2.1. Schematic illustration of the enzyme-amplified sensing of bacteria, showing the relative sizes of 2 nm core diameter particles and β-Gal.

2.2 Results and Discussions

Prior to sensing studies, we conducted activity titrations of β-Gal-catalyzed hydrolysis of the CPRG substrate using different functionalized NPs, **NP1**-**NP4** (Figure 2.2). The purpose of

these studies is to screen the best candidate that inhibits enzyme activity most and binds to bacterial cell surface most as well.

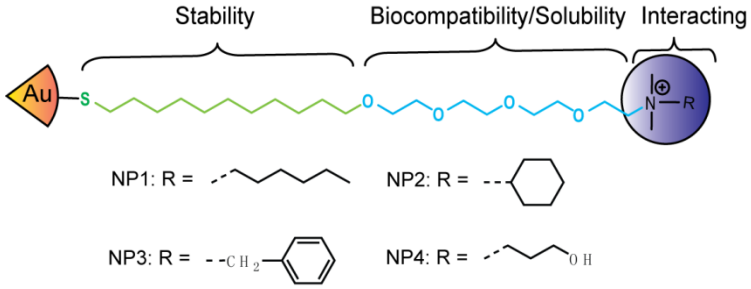

Figure 2.2. Molecular structure of ligands on the selected cationic functionalized gold nanoparticles.

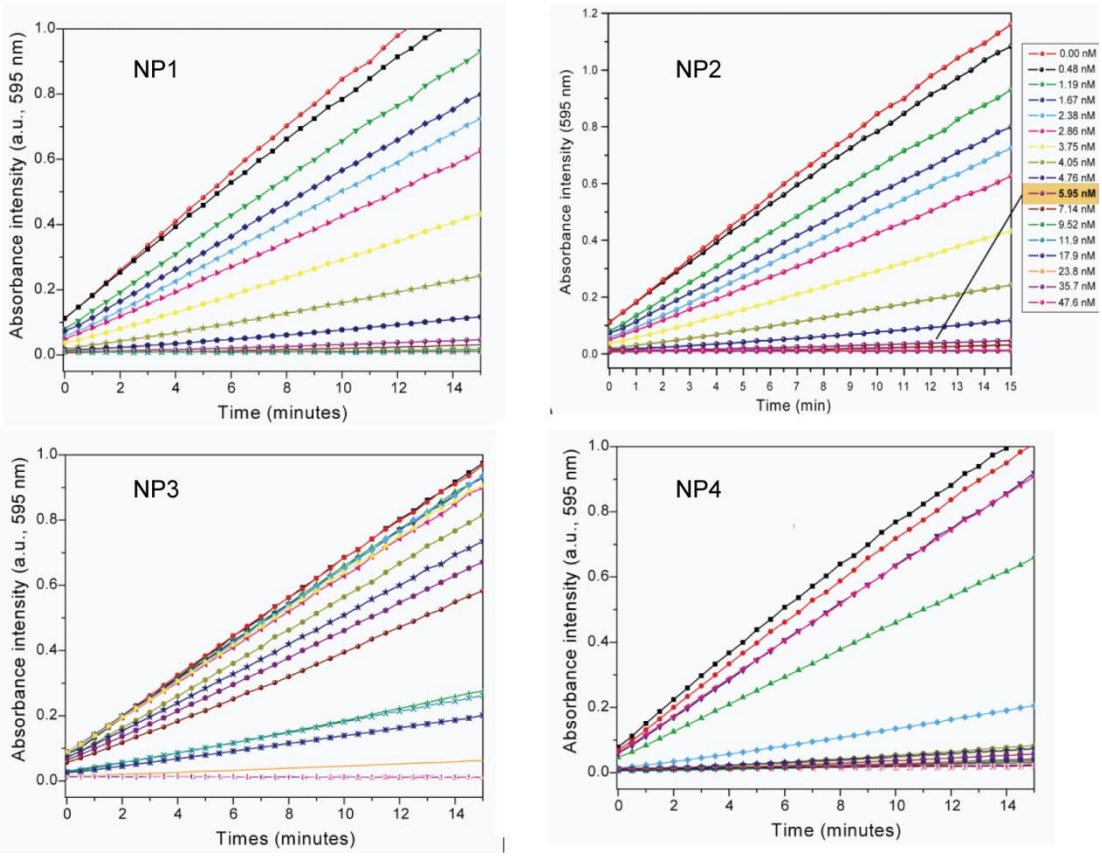

Figure 2.3. Inhibition of activity assay of β-Gal (0.5 nM) with 5 mM substrate CPRG upon addition of **NP1-NP4**.

The titration studies were performed at 0.5 nM of β-Gal, a concentration that provided a reasonable time course (~10 min) for the colorimetric event. The normalized first-order rate of

chromogenic substrate (CPRG, λ_{max} = 595 nm) hydrolysis was plotted versus the molar ratio of nanoparticles to β-Gal, and decreased upon addition of nanoparticles, and this trend was similar for all four cationic AuNPs (Figure 2.3). The decrease hydrolysis rate proved that interactions between enzyme and NPs resulted in inhibition of enzymatic reaction. As a control, the enzyme inhibition was also studied with neutral tetraethylene glycol (**NP_{TEG}**) and carboxylate (**NP_{CO2}**) functionalized nanoparticles, with no inhibition observed with these particles, indicating the interaction between enzyme and cationic AuNPs was mainly electrostatic interaction. The concentrations at which the enzyme was completely inhibited differed for different NPs. For example, **NP1** and **NP2** inhibited the enzyme completely at 5.95 nM while it was 23.5 nM for **NP3** and 3.75 nM for **NP4**. We assumed that the various inhibiting rate and concentration result from the difference in NP-enzyme binding affinity. The similar inhibiting capability of **NP1** with a hexyl-end group and **NP2** with a cyclo-hexyl-end group indicated that similar carbon chain length end groups possess similar interaction affinity to the enzyme, and **NP1**'s hexyl group was mostly like folded, making it behave more similarly to **NP2**. The presence of an aromatic group, however, decreased interaction affinity with the enzyme.

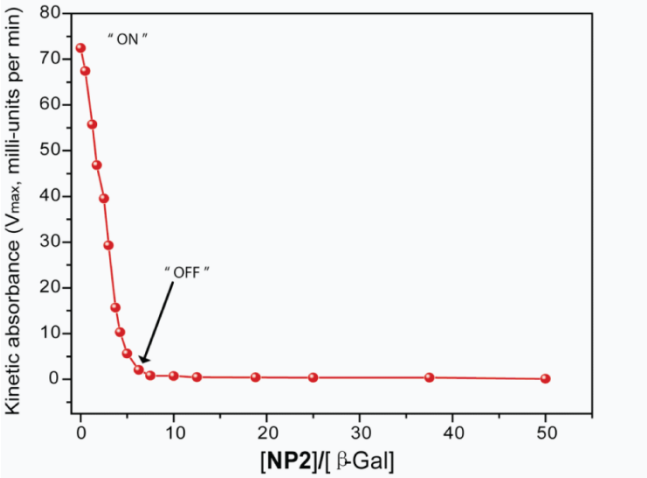

Figure 2.4. Inhibition of β-Gal before ("ON") and after ("OFF") addition of **NP2**. And the "OFF" state is the concentration chosen to construct the colorimetric biosensor.

After preliminary activity studies, **NP2** was chosen as the best candidate, (Figure 2.3), inhibiting the β-Gal activity at very low concentrations as well as restoring the β-Gal activity when interacted with bacteria. The sensor was constructed with **NP2** concentration that gave "OFF" activity state of the enzyme (Figure 2.4). The best performance from NP2 was proposed to be a balance of binding affinities towards both the enzyme and bacterial cells.

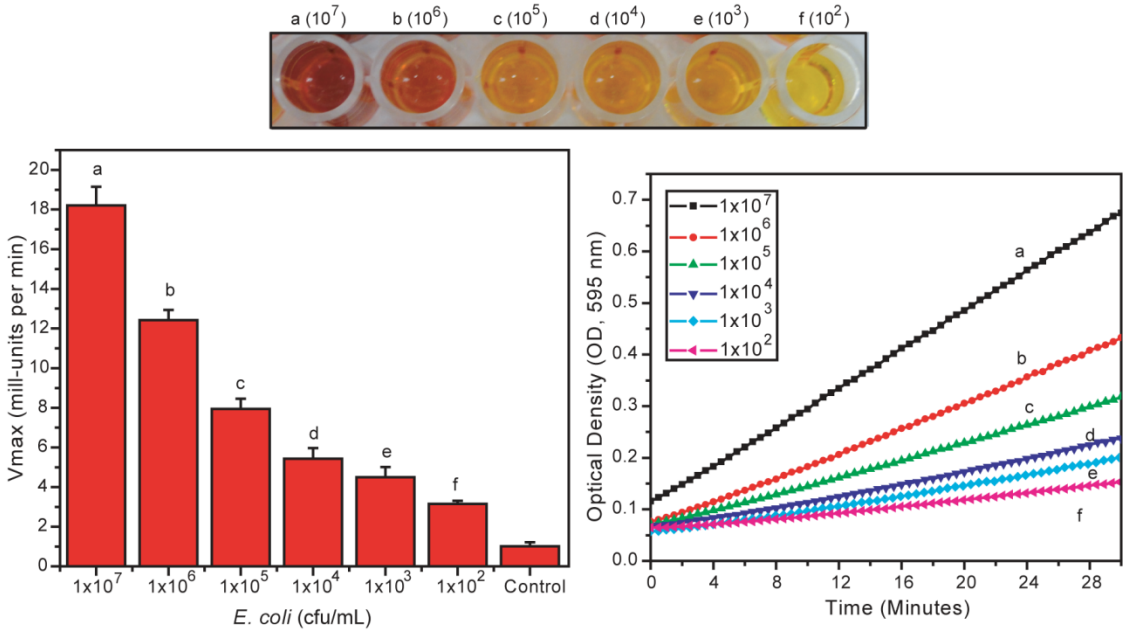

Figure 2.5. Limit of detection of *E. coli* using β-Gal/**NP2** nanocomposite. Kinetic absorbance response upon addition of different bacteria concentrations, as control β-Gal/**NP2** nanocomposite was used without bacteria. At the top, microplate wells showing the color change upon variation of bacteria concentrations.

For our initial sensing studies, *E. coli* was employed as a model analyte (Figure 2.5). Solutions containing different bacteria concentrations were used to investigate the limit of detection (LOD) of this sensing system. From these studies, we can reproducibly differentiate bacterial levels as low as 100 cfu/mL (three replicates were carried out for each sample). Each concentration can be discerned not only by intensity curves and the V_{max} histogram but also by visible color changes: images taken immediately after reading (10 min) by an LCD camera demonstrate this colorimetric effect (Figure 2.5 top).

I next investigated the application of our design to a test strip format suitable for potential portable use,[24] featuring visual read-out of the originated color in comparison to a reference color scale.[25] A key issue in this format is how to generate rapid and reproducible response times. Rapid bacterial penetration occurs on highly porous papers, while restriction of particle/enzyme conjugates to the surface occurs on less porous materials. Considering these issues, a wide range of materials available were explored to maintain the enzyme activity, the efficiency of enzyme inhibition, and activity recovery process. Of the materials tested, GF/B binder-free microfiber filter (Whatman, cat. No. 1821021) was selected as the ideal platform due to its high wet strength, high loading capacity and rapid response.

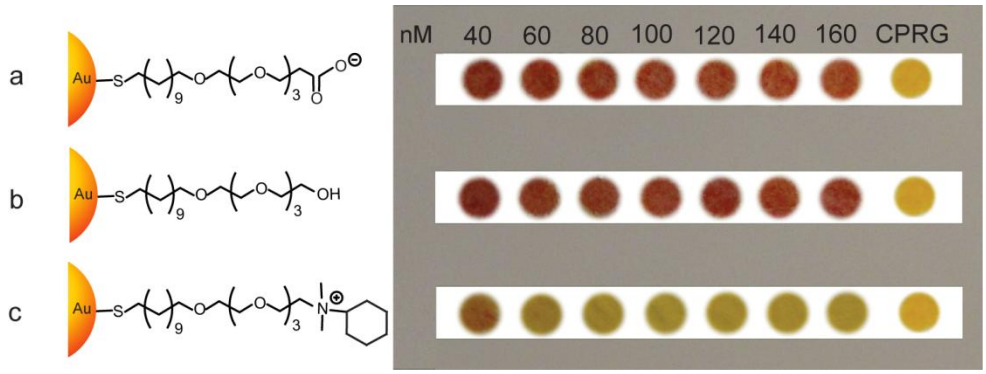

Figure 2.6. Enzymatic inhibition-colorimetric assay of β-Gal (15 nM) against 25 mM substrate CPRG upon addition of cationic, anionic and neutral nanoparticles. **a.** carboxylate ($\mathbf{NP_{CO2}}$), **b.** hydroxyl ($\mathbf{NP_{TEG}}$), and **c.** quaternary amine functionalized gold nanoparticles on a platform testing. Inset shows total inhibition for the positive nanoparticle **NP2** at 80 nM, while no inhibition was observed for both the anionic and neutral AuNPs even at 160 nM.

The formulation of the strip sensor featured 25 mM CPRG and 15 nM β-Gal, providing conversion from yellow to dark red within 10 minutes with uninhibited enzyme. Due to the difference in reaction rates in aqueous solution and on paper format, inhibition studies were carried out again to determine the optimal concentration of cationic particle **NP2** and β-Gal to form the hybrid enzymatic nanocomposite sensor [(β-Gal/**NP2**) complex]. $\mathbf{NP_{TEG}}$ and $\mathbf{NP_{CO2}}$ were also used as controls with no inhibition observed (Figure 2.6). The β-Gal/**NP2** complex was

ultimately generated by mixing β-Gal (15 nM) and **NP2** (80 nM) and allowing the composite to dry for 15 minutes.

To test the performance of our system on a paper strip, 3 μL of CPRG (25 mM), complex solution and solutions from 1×10^8 to 1×10^4 cfu/mL of *E. coli* were spotted onto GF/B filter paper. Images were obtained after 10 min with an LCD digital camera and appropriate lighting. As shown in Figure 5, clear visual differences were observed for concentrations ranging from 10^8-10^4 cfu/mL. To provide quantitative assessment of the test strips, the RGB profile of the images were analyzed. The plots of RGB colorimetric channels (all values were taken at least three times) in Figure 2.7 established the effectiveness of the chromogenic platform, demonstrating that 1×10^4 cfu/mL can be distinguished using this method.

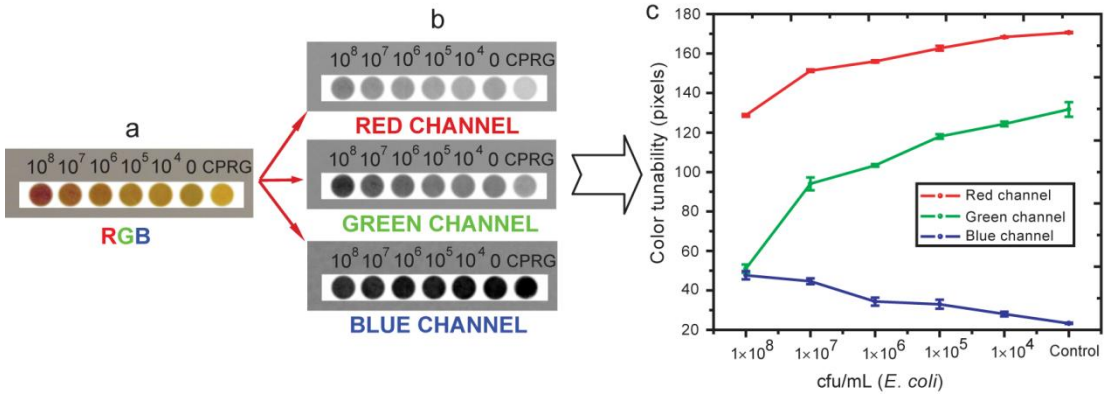

Figure 2.7. Schematic illustration of the RGB colorimetric analysis to monitor color changes on the GF/B filter paper spot at pH 7.4. **a.** image of the enzymatic activity response-colorimetric assay of the β-Gal-**NP2** complex upon addition of *E. coli* at different concentration, CPRG substrate was used as a control. **b.** red, green, and blue channels obtained from the original sample **a** to differentiate between bacteria concentration. **c.** the extracted values of red, green, and blue channel from the original data **a**. This process is repeated three times for each measurement in a series of images.

For field application, implementation of enzymatic amplified test strips is challenging. Both enzyme and enzyme substrate should be incorporated on the same strip for simple and direct detection purpose. But contact of these two elements should be prevented during fabrication process to avoid pre-test reaction. Therefore, we investigated the possibility of using inkjet printing technique for fabrication of this enzyme-NP hybrid sensor. In the fabrication process, the

enzyme and NPs were pre-mixed in water (50 nM β-Gal and 500 nM nanoparticles) and put into a clean unused inkjet cartridge. And the colorimetric enzyme substrate CPRG solution in water (2.5 mM CPRG) was put into another clean unused inkjet cartridge. Utilizing the inkjet printers CMYK color model, four separate printing channels are available and here we used two channels for sensor fabrication.

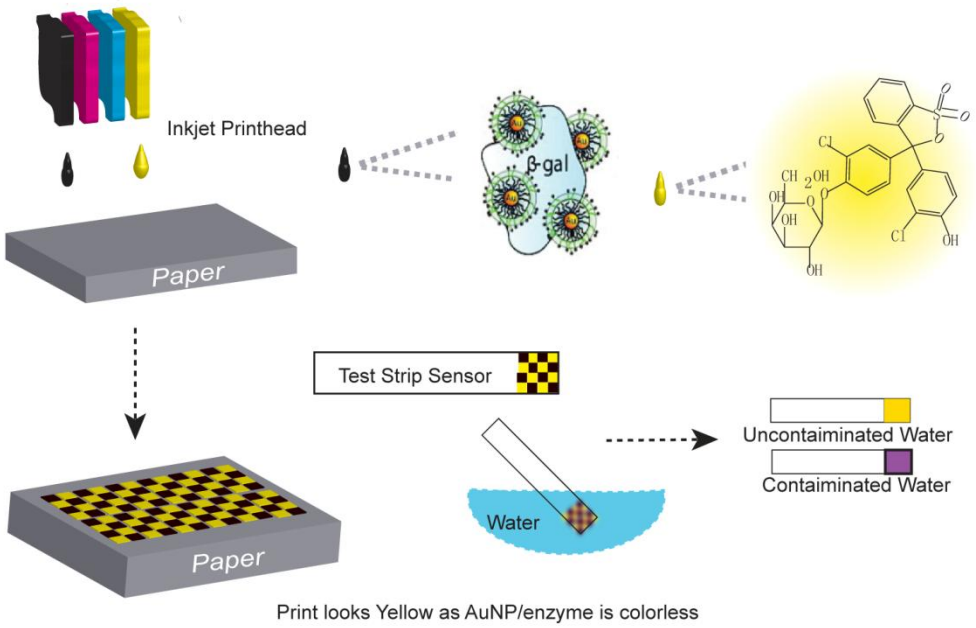

Figure 2.8. Schematic illustration of inkjet printing of the NP-based enzymatic amplified bacteria test strips. Inks were printing in a checker pattern to ensure no interaction before use.

As illustrated in Figure 2.8, the enzyme-NP conjugate solution was represented by the black (key) ink, and the solution was dispersed onto the paper from the key channel. The enzyme substrate, CPRG solution, as represented by the yellow ink, was casted onto the paper from the yellow channel. The printing was done in such separation manner in order to avoid interactions between the materials before use. After immersed in water, if the water is clean without bacteria, enzyme remains restricted by NP and the strip shows a light yellow color, whereas if the water is contaminated by bacteria, enzyme is replace by bacteria and mixes and interacts with the substrate for reaction, giving out a red to purple color depending on the actual bacteria concentration in the sample.

For fabrication of these strip sensors, the activity of β-Gal after printing process was tested first. And the result confirmed that β-Gal survived the printing process and reserved its activity. The sensor strips were then printed, cut, and tested with solutions containing different *E.coli* bacteria concentrations. These strips turned purple upon immersion in the bacteria containing solution (Figure 2.9) and the limit of detection was demonstrated by the photos as 10^2 cfu/mL. The increased sensitivity on the strips compared to spotted filter paper format could result from the more uniform dispersion of the enzyme-NP conjugates and substrate solutions. Besides in the case of the spotted filter paper, more materials could penetration inside the filter paper, whereas the printing process shortens the drying time and creates a thin film on top of the paper, preserving more materials on the surface for interaction and detection.

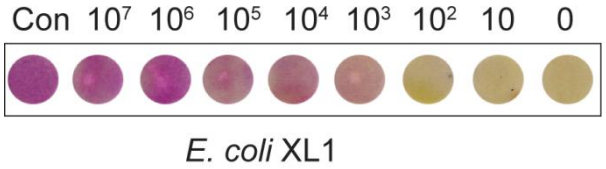

Figure 2.9. Sensitivity of the colorimetric sensor printed by an inkjet printer. The unit of the concentrations above the strips is cfu/mL.

2.3 Conclusions

In this work, enzyme-nanoparticle assemblies have been used to provide rapid and sensitive colorimetric sensing of bacteria. The use of enzyme enabled not only signal amplification but also colorimetric readout generation, allowing future application for portable devices. Using this system in a solution platform, bacteria concentrations as low as 100 cfu/mL could be determined in a matter of minutes. Transfer of this methodology to a test strip format provided a potential tool for field applications with a visual sensitivity of 10^4 cfu/mL. The selective instead of specific detection principle adapted in this system provides a great potential for detection of total bacterial count in water sample, which is an important factor considered for water quality. Finally, the feasibility of this system was demonstrated by inkjet printing technique.

Test strips composed of this enzyme-nanoparticle hybrid colorimetric bacteria sensor were printed by an inkjet printer. Success in this work and the inkjet printing work confirmed that nanoparticles are great candidates for rapid and sensitive detection of bacteria.

The rapid detection (within 15 minutes) and visual readout provided by the studies revealed here can enable real-time bacteria detection, which is critical for determination of water quality, potentially preventing many people from getting ill by drinking or swimming in contaminated water. Besides, the high sensitivity showed a great potential to match certain detection standard level. The easy and fast fabrication demonstrated by the inkjet printing technique suggests a great commercialization potential. All together, our studies not only showed that nanoparticles offer a great platform for bacteria detection, but also present a system that could be manufactured in mass production and used for on-site real time bacteria detection.

2.4 Experimental methods

Synthesis of AuNPs 1-4 Pentanethiol-coated AuNPs with core diameter ~2 nm were synthesized using the Brust-Schiffrin two-phase synthesis method.[26] Murray place-exchange method[27] was used to obtain the quaternary ammonium functionalized **AuNPs 1-4**. The cationic AuNPs were very stable in aqueous solution.

Activity assays β-galactosidase (β-Gal) and the colorgenic substrate chlorophenol-red-*β*-D-galactopyranside, CPRG were purchased from Sigma-Aldrich. In this study, nanoparticle and β-Gal solutions were prepared in sodium phosphate buffer solution (5 mM, pH 7.4). In the activity assay studies, β-Gal (0.5 nM) was incubated with various concentrations of **NP1**-**NP4** for 30 minutes and 1.5 mM of the colorgenic substrate (CPRG) was added. As control experiments, the enzymatic activity of β-Gal was also monitored in the presence of neutral tetraethylene glycol and carboxylate functionalized nanoparticles as well as an enzymatic protein (α-Gal). The β-Gal stock concentration was 314 nM, while the stock concentrations of **NP1**-**NP4** were prepared at

100 nM. The inhibition studies in solution were carried out at pre-determined times by adding 5 μL of CPRG (1.5 mM in PB buffer) and 5 μL of PB buffer into 200 μL β-Gal/**AuNP** solution. The enzymatic activity was followed by monitoring product formation every 22 s for 15 minutes at 595 nm using a microplate reader (SpetraMax, Molecular Devices). The samples were measured in triplicates. From the activity/inhibition studies, optimal concentrations of β-Gal/**AuNP** complexes were obtained. Once the different inhibiting characteristics of the β-Gal/**AuNP** complexes were established, stoichiometric amounts of β-Gal and **NP1**-**NP4** were used to the bacteria detection.

In the case of the test strip platform, 25 mM CPRG and 15 nM β-Gal was set up in a way to make the reaction take place at an appropriate speed for tuning the color of the substrate from yellow to dark red within a pre-determined time i.e. 10 minutes. Once the different inhibiting characteristics of the β-Gal/**NP2** complexes were established, stoichiometric amounts of β-Gal and **NP2** was used on the bacteria detection. $\mathbf{NP_{TEG}}$ and $\mathbf{NP_{CO2}}$ were also used, as control experiment and no inhibition was observed as expected. The samples were measured in triplicate.

Bacterial culture *E. coli* was inoculated in LB broth and incubated over night at 37 ℃ till stationary phase. The overnight culture was then centrifuged and washed with 5 mM phosphate buffer (pH 7.4) for three times. Bacteria were resuspended in 5 mM phosphate buffer and the concentration was determined by measurement of optical density at 600 nm (OD_{600}).

2.5 References

1. a) Inglesby, T. V.; O'Toole, T.; Henderson, D. A.; Bartlett, J. G.; Ascher, M. S.; Eitzen, E.; Friedlander, A. M.; Gerberding, J.; Hauer, J.; Hughes, J; McDade, J.; Osterholm, M. T.; Parker, G.; Perl, T. M.; Russell, P. K.; Tonat, K. ; Biodef, W. G. C. *J. Am. Med. Assoc.* **2002**, *287*, 2236-2252. b) Brecher, M. E.; Hay, S. N. *Clin. Microbiol. Rev.* **2005**, *18*, 195-204. c) Shorten, P.R.; Pleasants, A. B.; Soboleva, T. K. *Int. J. Food Microbiol.* **2006**, *108*, 369-375.

2. Ford, E. E.; Colwell, R. R. *A global decline in microbiological safety: a call for action. A report from The American Academy of Microbiology*, Washington, D.C., **1996**, pp. 1-40.

3. Pedley, S.; Bartram, J.; Rees, G.; Dufour, A.; Cotruvo, J. A. *Pathogenic mycobacteria in Water*; World Health Organization (WHO): London, **2004**.

4. a) Deisingh, A. K.; Thompson, M. *Analyst* **2002**, *127*, 567-581. b) Deisingh, A. M; Thompson, M. *Can. J. Microbiol*. **2004**, *50*, 69-77. c) Cole, L. A. *Sci. Am.* **1996**, *275*, 60-65.

5. a) Hugo, W. B.; Russell, A. D. *Pharmaceutical Microbiology*; 6th ed.; Blackwell: Oxford, **1998**. b) Adams, M. R.; Moss, M. O. *Food Microbiology*, 2nd ed.; Royal Society of Chemistry: Guildford, **2000**.

6. Hilpert, K.; Hancock, R. E. W. *Nat. Protoc*, **2007**, *2*, 1652-1660.

7. Safarik, I.; Safarikova, M.; Forsythe, S. J. *J. Appl. Bacteriol.* **1995**, *78*, 575-585.

8. Newton, C. R.; Graham, A. *PCR, 2nd ed.* ; Bios Scientific: Oxford, **1997**.

9. Strachan, N. J. C.; Nicholson, F. J.; Ogden, I. D. *Anal. Chim. Acta* **1995**, *313*, 63-67.

10. Maughan, N. J.; Lewis, F. A.; Smith, V. *J. Pathol.* **2001**, *195*, 3-6.

11. Haa, E. A. H. *Biosensors*; Open University Press: Buckinghan, **1990**.

12. J. Ji, A. Schanzle, M. B. Tabacco, *Anal. Chem.* **2004**, *76*, 1411-1418.

13. a) Heal, J. S.; Blom, A.W.; Titcomb, D.; Taylor, A.; Bowker K.; Hardy, J. R. W. *J. Hosp. Infect.* **2003**, *53*, 136-139. b) Perkins, S. D.; Mayfield, J.; Fraser, V.; Angenent, L. T. *Appl. Environ. Microbiol.* **2009**, *75*, 5363-5372. d) Chen, C. L.; Yu, J-C.; Holme, S.; Jacobs, M. R.; Yomtovian, R.; McDonald, C. P. *Transfusion*, **2008**, *48*, 1550-1557.

14. a) Phillips, R.; Miranda, O.; You, C.; Rotello, V.; Bunz, U. *Angew. Chem. Int. Ed.* **2008**, *47*, 2590-2594; b) Grossman, H.; Myers, W.; Vreeland, V.; Bruehl, R.; Alper, M.; Bertozzi, C.; Clarke, J. *P. Natl. Acad. Sci. USA.* **2004**, *101*, 129-134.

15. Yang, S. Y.; Wang, W. C.; Lan, C. B.; Chen, C. H.; Chieh, J. J.; Horng, H. E.; Hong, C. Y.; Yang, H. C.; Tsai, C. P.; Yang, C.Y.; Cheng, I. C.; Chung, W. C. *J. Virol. Methods* **2010**, *164*, 14-18.

16. a) Bajaj, A.; R Miranda, O.; Kim, I. B.; Phillips, R. L.; Jerry, D. J.; Bunz, U. H. F.; Rotello, V. M. *P. Natl. Acad. Sci. U.S.A* **2009**, *106*, 10912–10916. b) Bajaj, A.; Rana, S.; Miranda, O. R.; Yawe, J. C.; Jerry, D. J.; Bunz, U. H. F.; Rotello, V. M. *Chem. Sci*. **2010**, *1*, 134-138.

17. a) You, C. C.; Miranda, O. R.; Gider, B.; Ghosh, P. S.; Kim, I. B.; Erdogan, B.; Krovi, S. A.; Bunz, U. H. F.; Rotello, V. M. *Nat. Nanotechnol.* **2007,** *2*, 318-323. b) Miranda, O. R.; Chen, H. T.; You, C. C.; Mortenson, D. E.; Yang, X. C.; Bunz, U. H. F.; Rotello, V. M. *J. Am. Chem. Soc.* **2010**, *132*, 5285-5289.

18. Berry, V.; Gole, A.; Kundu, S.; Murphy, C. J.; Saraf, R.F. *J. Am. Chem. Soc.* **2005**, *127*, 17600-17601.

19. a) *Guidelines for Drinking Water*, 3rd ed.; World Health Organization (WHO): Geneva, **2004**. b) Gerba, C. P. *Pathogens in the environment* Academic press: New York, **1996**, 279-299. c) Chandler, D. P.; Straub, T. M. *J. Microbiol. Meth.* **2003**, *53*, 185-197. d) McFeters, G. A. *Drinking water microbiology*, Springer: New York, **1990**.

20. a) Holme, S.; McAlister, M. B.; Ortolano, G. A.; Chong, C.; Cortus, M. A.; Jacobs, M. R.; Yomtovian, R.; Freundlich, L. F.; Wenz, B. *Transfusion* **2005**, *45*, 984-993. b) Hoffmann, O.; Keilwerth, N.; Bille, M.; Reuter, U.; Angstwurm, K.; Schumann, R. R.; Dirnagl, U.; Weber, J. R. *J. Cerebr. Blood F. Met.* **2002**, *22*, 988–996.

21. a) Jacobson, R. H.; Zhang, X. J.; Dubose, R. F.; Matthews, B. W.; *Nature* **1994**, *369*, 761-766. b) Verma, A.; Simard, J. M.; Worrall, J. W. E.; Rotello, V. M. *J. Am. Chem. Soc.* **2004**, *126*, 13987-13991. c) Fowler, A. V.; Zabin, I. *J. Biol. Chem.* **1978**, *253*, 5521-5525.

22. a) Dmitriev, B.; Toukach, F.; Ehlers, S. *Trends Microbiol.* **2005**, *13*, 569-574. b) Koch, A. L.; *Clin. Microbiol. Rev.* **2003**, *16*, 673-687. c) Schaffer, C.; Messner, P. *Microbiology* **2005**, *151*,

643-651. d) Bos, M. P.; Tefsen, B.; Geurtsen, J.; Tommassen, J. *P. Natl. Acad. Sci. USA* **2004**, *101*, 9417-9422.

23. Miranda, O. R.; Li, X. N.; Garcia-Gonzalez, L.; Zhu, Z. J.; Yan, B.; Bunz, U. H. F.; Rotello, V. M. *J. Am. Chem. Soc.* **2011**, *133*, 9650-9653.

24. a) Hall, M.; Eldridge, D. B.; Saunders, R. D.; Fairclough, D. L.; Bateman, R. C. *Food Biotechnol.* **1995**, *9*, 39-57. b) Patange, S. B.; Mukundan, M. K.; Kumar, K. A. *Food Control* **2005**, 16, 465-472.

25. a) Steiner, M. S.; Meier, R. J.; Duerkop, A.; Wolfbeis, O. S. *Anal. Chem.* **2010**, 82, 8402-8405. b) Bonifacio, L. D.; Puzzo, D. P.; Breslav, S.; Ozin, G. A. *Adv. Mater.* **2010**, 22, 1351.

26. a) A. G. Kanaras, F. S. Kamounah, K. Schaumburg, C. J. Kiely, M. Brust, *Chem. Commun.* **2002**, 2294. b) M. Brust, M. Walker, D. Bethell, D. J. Schiffrin, R. Whyman, *J. Chem. Soc. Chem. Commun.* **1994**, 801.

27. A. C. Templeton, M. P. Wuelfing, R. W. Murray, *Acc. Chem. Res.* **2000**, *33*, 27.

CHAPTER 3

ARTIFICIAL ENZYME MIMIC-BASED COLORIMETRIC SENSOR

3.1 Introduction

Detection of bacteria requires development of fast, sensitive, and cost-effective sensors aimed at point-of-care applications. Among these sensors, colorimetric methods provide both enhanced instrumental transduction as well as the potential for direct visual readout.[1] For example, the clearly distinguished color shifts resulting from controllable aggregation of gold nanoparticles have facilitated simple color readout for biosensor applications.[2]

Array-based sensing uses differential binding interactions with an array of selective receptors, providing an alternative to biomarker detection[3]. This alternative is based on the mammalian olfaction and gestation process, utilizing sensors biased toward classes of analytes. In this approach, an array composed of selective rather than specific receptors that bind to analytes by different binding characteristics. This cross-reactive sensor array is composed of multiple sensors, most of which respond to each analyte, but generating a level of variance. This variance produced by each sensor element results in a fingerprint pattern corresponding to each analyte, serving as guidance for identification of these analytes.

Colorimetric implementation of the array-based sensing methodology has created highly effective small molecule sensors that have been applied to a variety of important analytes.[4] Application of colorimetric methods to array-based sensing of bacteria is challenging, however, due to the low concentrations of these materials relative to the amount of signal required for colorimetric transduction. In recent studies we have used enzyme amplification for colorimetric detection of bacteria.[5] While enzyme-based amplification processes are attractive, the protein nature of enzyme stability under transport and storage conditions may limit the application of this strategy to highly controlled environments.[6]

Synthetic enzyme mimics [7] such as macromolecular complexes, [8] iron oxide nanoparticles,[9] and cerium oxide nanoparticles[10,11] feature higher stability than enzymes over a wide range of pH levels and temperatures. The ability of these mimics to catalytically amplify responses has made them useful for biosensing. For instance, Fe_3O_4 NPs that mimic horseradish peroxidase (HRP) activity have been used to replace HRP in traditional immunoassay techniques[9, 12] and to achieve label-free detection of nucleic acids.[13]

In this chapter, I investigate the potential of artificial enzyme mimic, Fe_3O_4 NPs, to replace natural protein enzyme for colorimetric amplification biosensing. Due to the NP nature, I propose that Fe_3O_4 NPs can serve as both recognition and transduction elements, which will simply the fabrication of biosensor. First, I investigate if Fe_3O_4 NPs can be used for amplified colorimetric sensing using proteins as model analytes. The size, charge, and structure variation of different proteins serve as an excellent test bed, providing insights into the sensor principle and sensitivity. I then further test if Fe_3O_4 NPs can be used for colorimetric detection of bacteria and the possibility of constructing test strips with these NPs. Part of these results have been published in the journal Small (**2012**, *8*, 3589-3592)[14].

3.2 Results and discussion

a

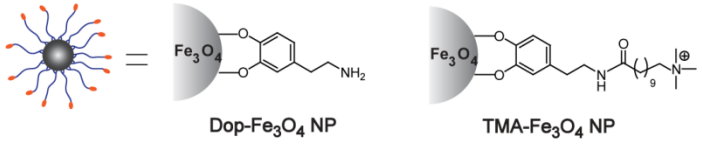

b

	Dop-Fe_3O_4	TMA-Fe_3O_4
Hydrodynamic diameter (nm)	18.4 ± 0.5	25.2 ± 0.1
Zeta potential (mV)	57.4 ± 1.6	6.0 ± 0.9

Figure 3.1. a. Structures of Dop-Fe_3O_4 and TMA-Fe_3O_4. **b.** Hydrodynamic diameter and zeta potential of Fe_3O_4 NPs in 5 mM CH_3COONa buffer at pH 5.0.

For our sensing studies, two NPs, dopamine functionalized Fe_3O_4 NP (Dop-Fe_3O_4 NP) and trimethylammonium functionalized Fe_3O_4 NP (TMA-Fe_3O_4 NP) were fabricated (Figure 3.1).

The different surface functionalization is designed to provide differential interactions to analytes. The hydrodynamic diameter and charges were listed in Figure 3.1 as well. Both NPs displayed positive charge when measure in sodium acetate buffer at pH 5.0. TMA-Fe_3O_4 NP possesses a larger diameter due to the longer surface ligand compared to Dop-Fe_3O_4 NP.

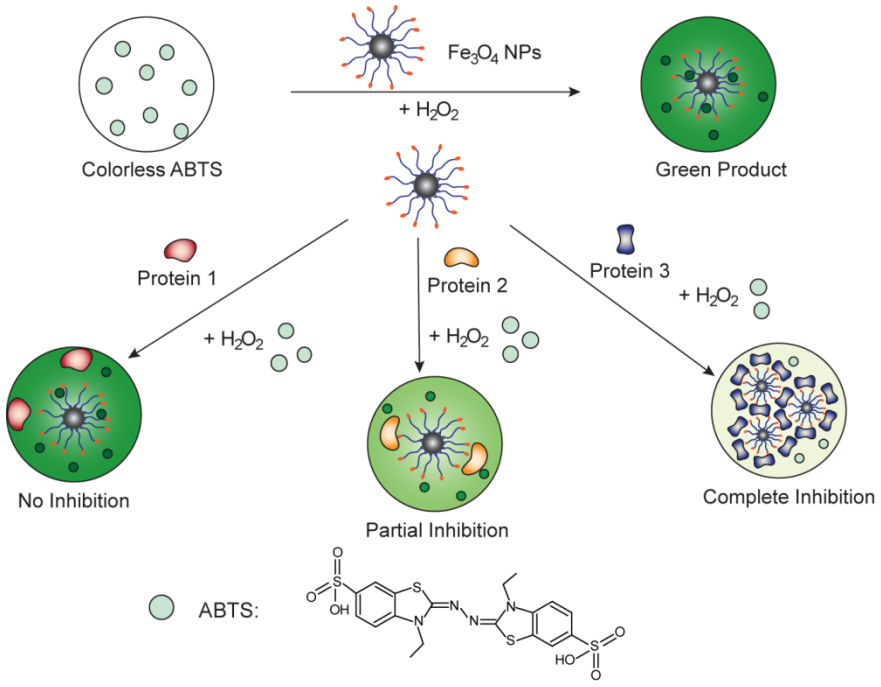

Figure 3.2. Schematic illustration of the Fe_3O_4 NP enzyme mimetic amplified colorimetric sensing of proteins.

The sensing principle originates from the catalytic property of Fe_3O_4 NP, which mimics the HRP activity. In general, similar to HRP, Fe_3O_4 NP can catalyze oxidation of colorless 2,2'-azino-bis(3-ethylbenzothiazoline-6-sulfonic acid) (ABTS), generating a green product in the presence of hydrogen peroxide (H_2O_2). In the presence of analytes, in this case, model analyte – protein, I propose there could be three possibilities. As illustrated in Figure 3.2, one possibility is when analyte, protein 1, has no interaction with Fe_3O_4 NPs, therefore the catalytic reaction occur without impact, yielding the dark green color in solution; another possibility is when analyte, protein 2, has moderate interaction with Fe_3O_4 NP and attaches on NP surface, leading to partial coverage of NP surface, and hence, to some extent blocks the access of substrate, ABTS, to the

NP core where the oxidation reaction is catalyzed, resulting to partial inhibition of NP catalytic activity and a lighter green color in solution; the third possibility is when analyte, protein 3, has strong interaction with Fe_3O_4 NP and forms protein-NP conjugate aggregation, in which case, the access to the NP is entirely blocked and NP catalytic activity is completely inhibited, giving a colorless solution. According to this hypothesis, analyte profile generation with these particles arises from differential interactions of these particles with analyte proteins with concomitant alteration in catalytic efficiency.

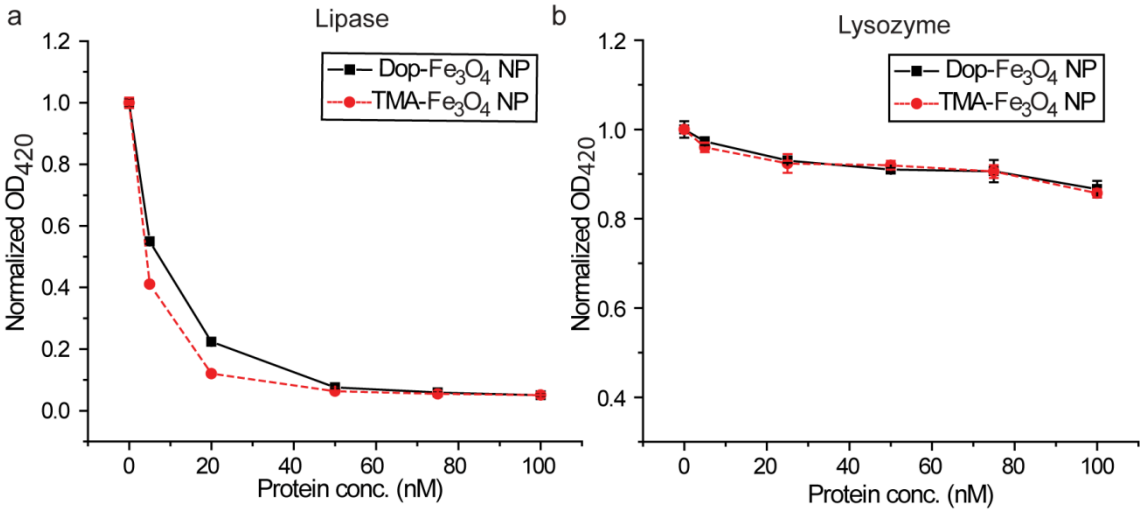

Figure 3.3. Normalized OD at 420 nm upon protein addition with fixed NPs concentration (25 µg/mL). **a.** Concentration dependent OD curve of lipase. **b.** Normalized OD curve of lysozyme with modest permutation. Results are average of three measurements and error bars are standard deviation.

Initial studies focused on optimizing the sensor response. An effective chromogenic response was observed using 25 µg/mL Fe_3O_4 NP with 2.5 mM H_2O_2 and 1 mM ABTS in 5 mM sodium acetate (CH_3COONa) buffer (pH 5.0). Changes in NP activity were then determined using two model proteins, lipase and lysozyme. With NP concentration fixed and protein solutions varied, NP activity titration studies were carried out by monitoring the absorption of the oxidized product at 420 nm. In the case of lipase, a dramatic drop in reaction rate was observed, with complete inhibition observed at higher concentrations (50 nM, Figure 3.3 a), indicating that lipase was able to affect NP's catalytic activity in a concentration-dependent manner and was able

to completely prevent the colorimetric reaction from taking place, which fitted the third proposed case of analyte-NP interactions where analytes display strong interaction towards NPs. By contrast, lysozyme did not significantly affect the colorimetric reaction up to a concentration of 100 nM (Figure 3.3 b), indicating that lysozyme was not able to affect NP's catalytic activity, which matched the first proposed case of analyte-NP interactions where analytes do not exhibit binding affinity towards NPs.

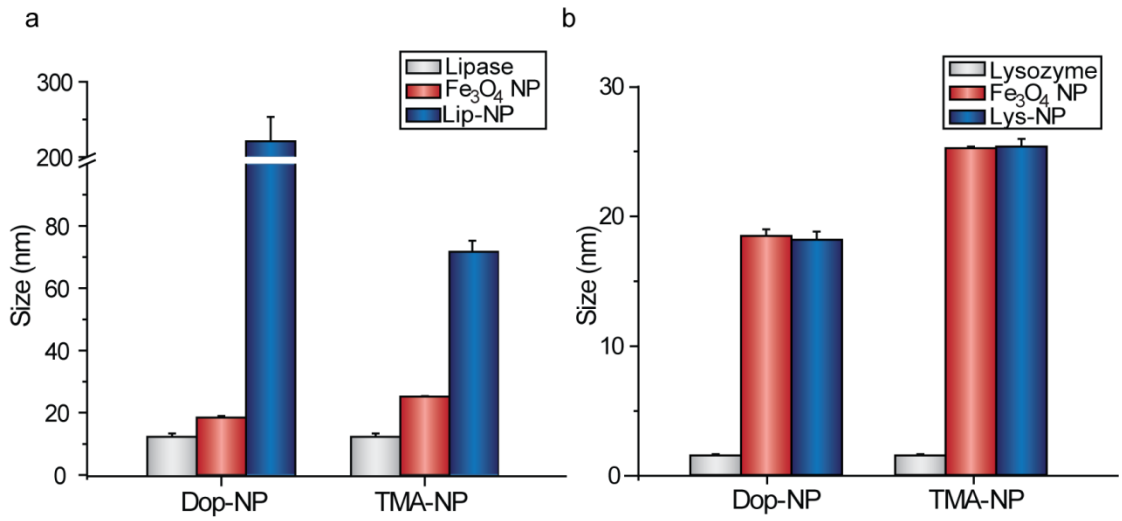

Figure 3.4. Hydrodynamic diameters of **a.** lipase, functionalized Fe_3O_4 NP, and lipase-NP complex, and **b.** lysozyme, functionalized Fe_3O_4 NP, lysozyme-NP complex. Results are average of three measurements and error bars are standard deviation. The NP concentration used in the size measurement is 250 μg/mL and the protein is at a concentration of 500 nM.

The different behaviors towards NP catalytic activity observed above can be used to differentiate the two proteins. The mechanism for this protein differentiation was probed by dynamic light scattering (DLS) measurements of the protein-NP complexes. For the DLS studies, 10-fold higher concentrations of particle and protein were used to provide reliable DLS signals. According to the size measurements from DLS, Lipase-NP complexes formed large aggregates with both Dop-Fe_3O_4 NP and TMA-Fe_3O_4 NPs (Figure 3.4 a), consistent with the large change in activity observed. In contrast, no significant changes in particle size were observed after incubation with lysozyme (Figure 3.4 b), consistent with the modest permutation in activity

observed. The NP activity titration studies and the DLS experiments supported the two extreme cases, complete inhibition and no inhibition, in the initial hypothesis.

Sensing of individual analytes in isolation provides a testbed for array-based sensors, providing insight into their ability to detect small changes in analyte structure and property. The ability of our sensor to discriminate proteins was tested using ten proteins featuring varying size and charge (Table 3.1). In the procedure, each protein solution was first mixed with NP (25 μg/mL) to a final protein concentration of 50 nM and incubated at room temperature for 30 minutes. This was followed by the addition of H_2O_2 (2.5 mM) and ABTS (1 mM) into each solution. After 15 minutes of incubation at room temperature, OD responses (OD/OD_0, where OD_0 is a control without addition of protein) at 420 nm were monitored.

Table 3.1. Physical properties of analyte proteins.

Protein	MW (kDa)	pI
α-amylase (α-Am)	50	5.0
bovine serum albumin (BSA)	66.3	4.8
α-chymotrypsin (ChT)	25	8.7
cytochrome c (CytC)	12.3	10.7
transferrin (Tf)	76	5.9
human serum albumin (HSA)	69.4	5.2
lipase (Lip)	58	5.6
lysozyme (Lys)	14.4	11.0
myoglobin (Myo)	17	7.2
alkaline phosphatase (PhosB)	140	5.7

As displayed in Figure 3.5 b, the two particle sensor array generated a range of outputs.[15] As a general trend, proteins possessing lower pIs (α-Am, BSA, HSA, Lip) exhibited relatively stronger inhibition of the NP activity than those with higher pIs (Lys, CytC, ChT, Myo), indicating surface charge plays an important role in discrimination. Proteins with similar pIs such as Lip (pI 5.6) and PhosB (pI 5.7), also gave different signal patterns, however, indicating that protein size also plays a role in protein-NP interactions. The sensor was even able to distinguish BSA and HSA, two very similar proteins with close pI and size, showing that protein surface functionality, hydrophobicity for example, is also a factor in the detection process. Comparison

between these protein pairs revealed that this two-NP sensor array detects analyte protein based on charge, size, and surface functionality, differentiating analytes from many physical and chemical properties. Each protein can be reproducibly discerned by the OD response patterns. The pattern differences among analytes can be easily detected even by the naked eye (Figure 3.5 a).

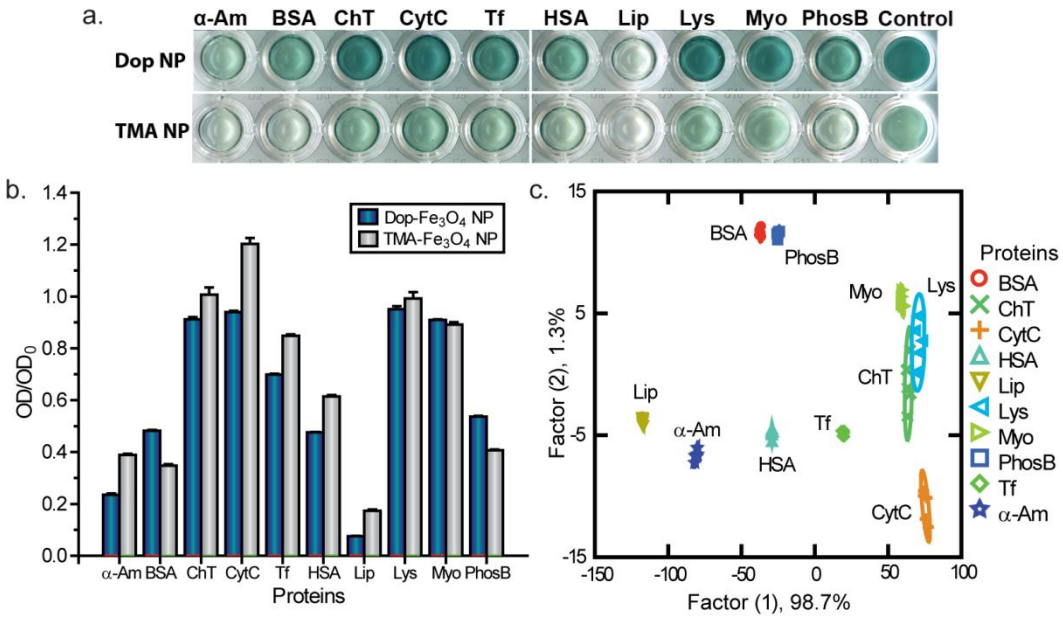

Figure 3.5. Array-based sensing of ten proteins. **a.** Photograph of the color change upon addition of protein solutions at 50 nM. **b.** OD response (OD/OD_0 at 420 nm) patterns in the presence of proteins at 50 nM (responses are an average of five measurements and the error bars are the standard deviation). **c.** Canonical score plot for the OD response patterns as obtained from LDA with 95% confidence ellipses.

Linear discriminant analysis (LDA) was employed to quantitatively differentiate the OD response patterns of the Fe_3O_4 NPs with proteins. All five replicates of the ten proteins are grouped with 100% accuracy according to the jackknifed classification matrix, and scores of the two factors are plotted with 95% confidence ellipses (Figure 3.5 c). In the canonical score plot, the distribution of analyte clusters along the factor 1 axis primarily reflects the OD/OD_0 value. And proteins with lower pIs were primarily located on the left side of the plot, below value of 0, while proteins with higher pIs clustered mostly on the right side of the plot. In the LDA score plot, six replicates from each sample were closely overlapped with each other, indicating the sensor

works in a precise manner, which is an important attribute for biosensor development. The individual response from each of the elements provides reasonable differentiation: TMA-Fe_3O_4 NP itself can differentiate the ten proteins with 90% accuracy and Dop-Fe_3O_4 NP with 78%. This result also demonstrated that necessity of using both NP to compose an array to improve sensitivity. It is noteworthy that by the use of only two modified Fe_3O_4 NPs, the sensor can detect and identify ten proteins rapidly and effectively.

The detection efficiency was further validated by the identification of unknown samples. 80 protein samples were generated and randomly assigned with a number by one person. The OD response of each sample was collected by another person and put into the training set shown in Figure 3.5 c for classification and identification. The blind tests outcome was then verified with the person who prepared the samples. The results were displayed in Table 3.2, 76 out of 80 unknown samples were correctly identified, giving 95% accuracy, which showed that the sensor's performance was not only precise but also accurate.

Table 3.2. Identifiation of 80 unknown protein samples with LDA using Fe_3O_4 NP sensor array.

Entry	Absorbance response pattern (OD/OD_0)		Identification	Accuracy
	Dop-NP	TMA-NP	Proteins	YES/NO
1	0.211908	0.399919	α-Am	Yes
2	0.479546	0.621516	HSA	Yes
3	0.462776	0.318205	BSA	Yes
4	0.94571	1.057261	Lys	Yes
5	0.916518	1.255711	CytC	Yes
6	0.926287	1.357754	CytC	NO
7	0.899918	1.056053	ChT	Yes
8	0.541769	0.437557	PhosB	Yes
9	0.075944	0.17772	Lip	Yes
10	0.711499	0.872295	Tf	Yes
11	0.547641	0.429305	PhosB	Yes
12	0.893312	1.037939	ChT	Yes
13	0.912566	0.843313	Myo	Yes
14	0.697439	0.909731	Tf	Yes
15	0.221394	0.390661	α-Am	Yes
16	0.477796	0.633592	HSA	Yes
17	0.967675	1.047197	Lys	Yes
18	0.458824	0.32545	BSA	Yes
19	0.952429	1.281071	CytC	Yes
20	0.07871	0.174298	Lip	Yes
21	0.965134	1.35715	CytC	Yes
22	0.081025	0.172688	Lip	Yes
23	0.465938	0.368723	BSA	Yes

24	0.526919	0.430311	PhosB	Yes
25	0.882245	1.013988	ChT	Yes
26	0.683832	0.873302	Tf	Yes
27	0.210779	0.400523	α-Am	Yes
28	0.456396	0.612458	HSA	Yes
29	0.855368	0.824796	Myo	Yes
30	0.928489	1.041763	ChT	NO
31	0.704328	0.870484	Tf	Yes
32	0.969651	0.96991	Lys	Yes
33	0.470286	0.629365	HSA	Yes
34	0.864741	1.030291	ChT	Yes
35	0.910251	1.273624	CytC	Yes
36	0.468253	0.336118	BSA	Yes
37	0.900031	0.889001	Myo	Yes
38	0.077638	0.170675	Lip	Yes
39	0.206601	0.384019	α-Am	Yes
40	0.52387	0.415618	PhosB	Yes
41	0.20677	0.391668	α-Am	Yes
42	0.917365	0.855791	Myo	Yes
43	0.078202	0.171279	Lip	Yes
44	0.702747	0.853779	Tf	Yes
45	0.950566	1.019221	Lys	Yes
46	0.434996	0.629365	HSA	Yes
47	0.94108	1.252893	CytC	Yes
48	0.494678	0.410989	BSA	NO
49	0.463002	0.378585	BSA	Yes
50	0.863273	1.00473	ChT	Yes
51	0.076452	0.174499	Lip	Yes
52	0.937579	1.038945	Lys	Yes
53	0.21044	0.373956	α-Am	Yes
54	0.525959	0.414612	PhosB	Yes
55	0.453347	0.358861	BSA	Yes
56	0.887948	1.011975	ChT	Yes
57	0.914655	0.821978	Myo	Yes
58	0.669603	0.845728	Tf	Yes
59	0.914768	1.245245	CytC	Yes
60	0.460405	0.613264	HSA	Yes
61	0.480845	0.60642	HSA	Yes
62	0.410491	0.312569	BSA	Yes
63	0.911154	0.854986	Myo	Yes
64	0.678863	0.853578	Tf	Yes
65	0.886367	0.988427	ChT	Yes
66	0.516586	0.41582	PhosB	Yes
67	0.20502	0.378183	α-Am	Yes
68	0.072217	0.168663	Lip	Yes
69	0.92352	1.033712	ChT	NO
70	0.921882	1.243232	CytC	Yes
71	0.994608	1.264366	CytC	Yes
72	0.859603	0.838281	Myo	Yes
73	0.209537	0.380396	α-Am	Yes
74	0.477739	0.618698	HSA	Yes
75	0.919455	1.038744	ChT	Yes
76	0.073911	0.177921	Lip	Yes
77	0.542672	0.429707	PhosB	Yes
78	0.460405	0.364698	BSA	Yes
79	0.677451	0.852571	Tf	Yes

80	0.946049	1.073563	Lys	Yes

The initial experiments showed success of using Fe_3O_4 NPs for colorimetric sensing, and the amplification efficiency was demonstrated by the high sensitivity of differentiation ten proteins at 50 nM concentration. We were then interested to know if the artificial enzyme, Fe_3O_4 NPs, can be used for detection of bacteria. The sensing principle remains the same for analyte bacteria with analyte proteins. Considering the real-world application, the fact that the sensor would remain colorless when tested with sample containing high bacteria concentration might bring confusion to users, we decided replace the substrate ABTS with pyrogallol, which changes color from light yellow to red upon reaction. In this way, sensor remains yellow when tested with high bacteria concentrations. One NP, Dop-Fe_3O_4 NP, was first tested with bacteria *E. coli* at different concentrations to explore the limit of detection. As shown in Figure 3.6, Dop-Fe_3O_4 NP catalytic activity was inhibited at high bacteria concentrations, and solutions remained light yellow, meanwhile NP activity was not affected at low bacteria concentrations, and solutions turned into red color after a few minutes. The difference of the clear color in response was evident from the red color of the standard reference (uninhibited conditions), providing readouts that can be easily interpreted visually. The limit of detection using Dop-Fe_3O_4 NP alone was 10^5 cfu/mL. This resuls indicated that synthetic Fe_3O_4 NPs could be indeed used for amplified colorimetric detection of bacteria.

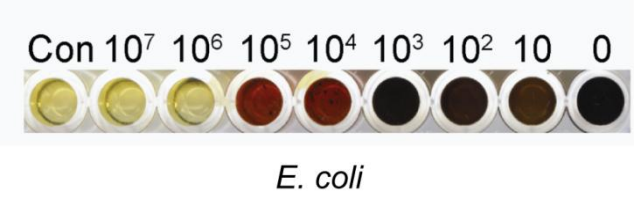

Figure 3.6. Sensitivity of the Fe3O4 NP colorimetric in solution. The unit of the concentrations above the strips is cfu/mL.

Effective implementation of our sensing strategy requires higher throughput fabrication of substrates to realize a low cost of production. Likewise, accurate printing of both the

colorimetric substrate and nanoparticle must be done quickly and accurately. To provide the reagent H_2O_2 in reaction, we will first explore urea hydrogen peroxide (UHP, $CH_6N_2O_3$), a widely available and stable chemical when stored cool and dry,[16] as peroxide generator. In our sensor design, NPs were spatially deposited next to the colorimetric substrates and the peroxide generator (Figure 3.7). This process assured that all elements were intact without interaction. Upon immersion into the water sample, the substrate and peroxide were carried over the Fe_3O_4 NPs, allowing oxidation to give color readout. In the presence of bacteria, however, Fe_3O_4 NP-catalyzed reaction will be modulated, giving a lighter yellow color depending on the bacteria concentration.

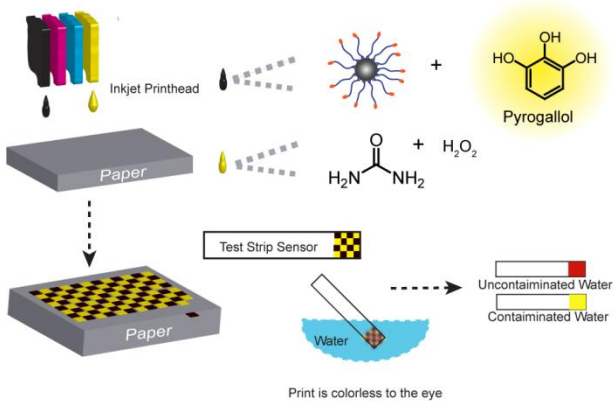

Figure 3.7. Schematic illustration of Fe_3O_4 NP-based inkjet printed test strip fabrication.

Strips were then printed with Fe_3O_4 NPs, substrate pyrogallol, and urea hydrogen peroxide and these strips were tested with *E. coli* bacteria with different concentrations to probe the limit of detection. Photos of tested strips showed a sensitivity of 10^5 cfu/mL (Figure 3.8), which was similar to the limit of detection obtained in sensing in aqueous solution. The dark brown color showed on strips was different from the red color in solution due to the solid state of substrate product.

Figure 3.8. Inkjet printed test strip sensitivity against *E. coli*. The unit of concentrations above strips is cfu/mL.

The implementation of artificial enzyme mimic Fe_3O_4 NP in biosensor can potentially improve the stability as well as reduce cost. With an initial estimate of materials, labor, and machinery, it cost around only 42 cents per strip/test. The stability of these inkjet printed strip lies in two possible portions, including receptor/amplifier and the oxidant H_2O_2 source. Using synthetic enzyme mimic helped to increase stability of the receptor/amplifier, however, the robustness related to H_2O_2 source needs to be tested at different conditions such as different temperatures and pHs. The urea hydrogen peroxide can be further stabilized by addition of stabilizer such as NaH_2PO_4 or $Na_2H_2P_2O_7$ and a coating layer to prevent the release of H_2O_2 in moist conditions. If urea hydrogen peroxide still cannot serve as a stable peroxide generator, more expensive hydrogen peroxide/polymer[17] or UHP/polymer complexes[18] could also be used that are more stable to decomposition.

The sensitivity of current system, however, is not high enough to reach environmental quality cutoff. In ongoing and future work which is conducted by my colleagues, plans have been made to further optimize and improve the sensitivity by altering the NP surface ligand. The chemical functionality of these ligands can provide various binding profiles towards analytes and therefore can regulate the sensitivity of the system as seen in our previous work. We also believe that adjusting the Fe_3O_4 NP size can change the volume ratio of NPs to bacteria cells, and this change will affect the capability of bacteria to shield substrates from the nanoparticle surface, consequently modifying the sensitivity.

3.3 Conclusions

In summary, a new platform has been developed for sensitive, fast, and effective colorimetric biosensor that uses a catalytically active particle for both recognition and signal transduction/amplification. By tuning the surface functionalities, The Fe_3O_4 NPs were able to differentiate ten proteins at a concentration of 50 nM, substantially lower concentrations than prior array-based protein sensors (1–350 μM). The robust nature of these synthetic enzyme mimics gives this strategy the potential to provide real-world sensors for both clinical and non-clinical health applications.

Further, I investigate with my colleagues the possibility of using the catalytic NP-based biosensor for detection of bacteria. An iron oxide NP-composed test strip sensor was fabricated that gave color response upon bacteria as indication for water quality. This sensing system was integrated with inkjet printing approach to probe the feasibility of fast and precise fabrication of nano-sensors. The initial studies explored the sensitivity of the Fe_3O_4 NP based sensing system with model bacteria strains. The system was then transferred to a field friendly strip platform by inkjet printing strategy and was tested for bacteria detection in water. Data shown in this chapter demonstrated the successful proof-of-concept of this system. This system was also filed for patent for its great commercial potential. Our test strip-based colorimetric sensor can provide easy and rapid (within minutes) detection of bacteria in water without additional equipment. This type of technology has not been commercialized in current market. There should be a large market for our test strip, considering the breadth of the recreational water market segment as well as the desperate need for rapid detection of bacteria-contaminated drinking water in emerging nations.

3.4 Experimental methods

Synthesis of dopamine functionalized Fe_3O_4 NP (Dop-Fe_3O_4 NP) Water-dispersible Dop-Fe_3O_4 NPs were synthesized and purified according to literature.[19] In the general process, $FeCl_2$•$4H_2O$ (99.4 mg, 0.5 mmol), $FeCl_3$•$6H_2O$ (270.3 mg, 1mmol), and 20 g of diethylene glycol (DEG) were added to a nitrogen-protected three-necked flask. A solution of NaOH (160 mg, 4 mmol) in 20 g DEG was then added to the flask. The mixture was heated for 2 h at 220 ℃. At the end of heating, a mixture of 3-hydroxytyramine hydrochloride (189 mg, 1 mmol) in 400 μL of H_2O and 5 g of DEG was injected into the flask. After cooling to room temperature (r.t.), the solid product was isolated by centrifugation and washed five times with ethanol and finally redispersed in water.

Synthesis of dopamine trimethyl ammonium (DTMA) ligand

Step 1.

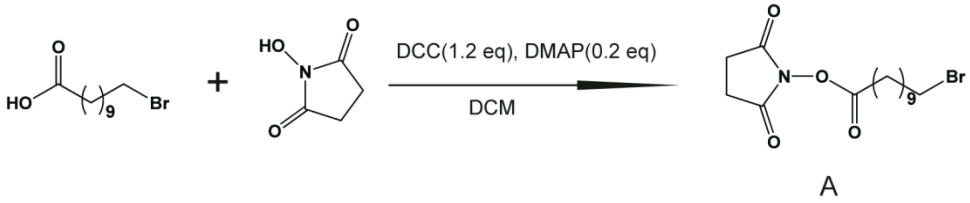

A

1-Bromoundecanoic acid (500 mg, 1.88 mmol) was dissolved in dry DCM. To this solution N-hydroxysuccinimide (216 mg, 1.88 mmol) was added followed by a solution of DCC (456 mg, 2.26 mmol) in 5 mL of dry DCM at 0 ℃. The mixture was stirred for 15 min, and then DMAP (46 mg, 0.38 mmol) was added. After 1 h the reaction was allowed to reach r.t.. A white precipitate formed indicating the advancement of the reaction. The reaction was continued for 24 h. The white precipitate was filtered and the solvent was removed from the filtrate to give a residue that was then re-dissolved in DCM and washed with water. The organic layer was dried over Na_2SO_4, filtered and evaporated and the crude product obtained was purified by flash chromatography with 3:1 hexanes:EtOAc as eluent to give the activated acid in 90 % yield.

^{1}H NMR_(400 MHz, $CDCl_3$): 1.24-1.42 (m, 12H, CH_2); 1.56 (m, 2H, CH_2); 1.77 (m, 2H, CH_2); 2.25 (t, 2H, CH_2); 2.72 (t, 4H, CH_2); 3.31(t, 2H, CH_2)

Step 2.

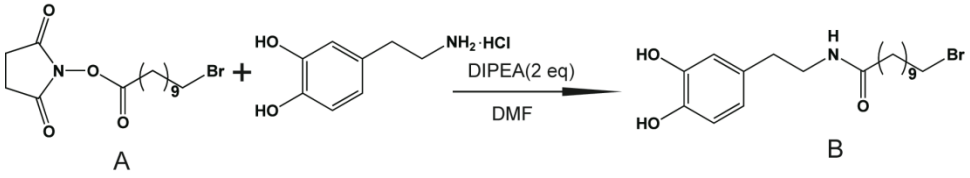

A B

3-Hydroxytyramine hydrochloride (356mg, 1.88mmol) was dissolved in dry DMF and the solution was purged for 10 min with nitrogen gas. DIPEA (507mg, 3.76 mmol) was slowly added to the reaction mixture. The mixture was stirred for another 5 min and then compound A (670mg, 1.18 mmol) was added to the reaction mixture. The mixture was stirred at r.t. for 64 h. After that the DMF was evaporated under reduced pressure. The residue was dissolved in ethyl acetate. The soluble part was taken out and washed with 1M HCl and brine water. The organic component was dried over Na_2SO_4 and evaporated to get the crude product. The crude product obtained was purified by flash chromatography with 3:1 EtOAc:hexanes as eluent to give the activated acid in 55 % yield.

^{1}H NMR_(400 MHz, $CDCl_3$): 1.24-1.42 (m, 12H, CH_2); 1.56 (m, 2H, CH_2); 1.81 (m, 2H, CH_2); 2.18 (t, 2H, CH_2); 2.65 (t, 2H, CH_2); 3.31 (t, 2H, CH_2); 3.55 (t, 2H, CH_2); 6.42 (d, 1H, H_{arom}); 6.66-6.74 (m, 2H, H_{arom})

Step 3.

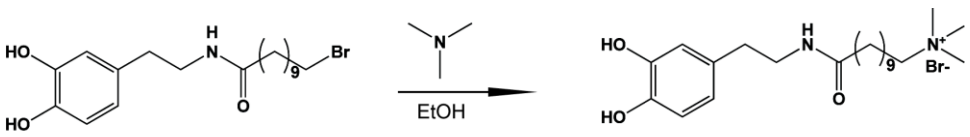

B C

Compound B (230 mg, 0.59 mmol) and trimethylamine (696 mg, 11.8 mmol) were dissolved in 1mL of EtOH. The solution was degassed with nitrogen gas. The reaction mixture

was stirred at r.t. for 64 h and then the solvent was evaporated under vacuum. The residue was purified by washing with hexane and ether several times to obtain C in 99% yield.

^{1}H NMR_(400 MHz, MeOD): 1.24-1.42 (m, 12H, CH_2); 1.56 (m, 2H, CH_2); 1.81 (m, 2H, CH_2); 2.18 (t, 2H, CH_2); 2.78 (t, 2H, CH_2); 3.19 (s, 9H, CH_3); 3.31 (t, 2H, CH_2); 3.55 (t, 2H, CH_2); 6.42 (d, 1H, H_{arom}); 6.66-6.74 (m, 2H, H_{arom})

Synthesis of trimethyl ammonium functionalized Fe_3O_4 NP (TMA-Fe_3O_4 NP) Sun's method[20] was used to obtain 4-nm Fe_3O_4 NPs. $Fe(acac)_3$ (2 mmol) was mixed in phenyl ether (20 mL) with 1,2-hexadecanediol (10 mmol), oleic acid (6 mmol), and oleylamine (6 mmol) under nitrogen and was heated to reflux for 30 min. After cooled to room temperature, the dark-brown mixture was treated with ethanol under air, and a dark-brown material was precipitated from the solution. The product was dissolved in hexane in the presence of oleic acid and oleylamine and reprecipitated with ethanol to give 4-nm Fe_3O_4 nanoparticles. A place-exchange reaction[21] of DTMA dissolved in DCM with the obtained 4-nm Fe_3O_4 NPs was carried out for 2 days at 40 ℃. DCM was then evaporated under reduced pressure. The residue was dissolved in a small amount of distilled water and dialyzed (membrane MWCO = 10,000) to remove excess ligands.

Protein sensing Protein solutions were prepared freshly before use and concentrations were determined by UV absorbance at 280 nm and calculated using the theoretical extinction coefficient at 280nm (ε_{280}). The extinction coefficients of different proteins are list in the table below.

Table 3.3. Protein extinction coefficient.

Protein	ε_{280} (M^{-1} cm^{-1})
α-amylase (α-Am)	130000
bovine serum albumin (BSA)	46860
α-chymotrypsin (ChT)	51000
cytochrome c (CytC)	23200
transferrin (Tf)	92300
human serum albumin (HSA)	37800
lipase (Lip)	54350
lysozyme (Lys)	38000
myoglobin (Myo)	13940
alkaline phosphatase (PhosB)	62780

Bacterial culture *E. coli* was inoculated in LB broth and incubated over night at 37 ℃ till stationary phase. The overnight culture was then centrifuged and washed with 5 mM phosphate buffer (pH 7.4) for three times. Bacteria were resuspended in 5 mM phosphate buffer and the concentration was determined by measurement of optical density at 600 nm (OD_{600}).

3.5 Supplementary information

In our study, we found that hemoglobin had an enhancement in OD response instead of inhibition. We believe this is due to the peroxidatic activity of the heme group in hemoglobin (as noted in reference 15).

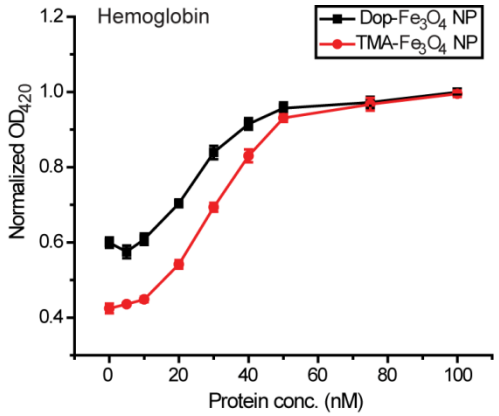

Figure 3.S1. Normalized OD upon different hemoglobin concentrations with the fixed NPs concentration (25 μg/mL). OD curve of hemoglobin is concentration dependant in an increasing fashion till a saturated point.

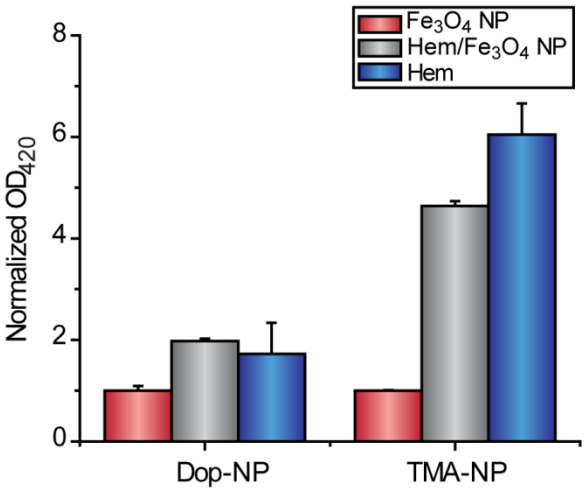

Figure 3.S2. Normalized OD at 420 nm of Fe_3O_4 NPs (25 μg/mL), hemoglobin (50 nM), and hemoglobin-Fe_3O_4 NP complex. The catalytic activity of Hem-Fe_3O_4 NP complex is higher than that of Fe_3O_4 NPs but is lower than the sum of Fe_3O_4 NP and hemoglobin.

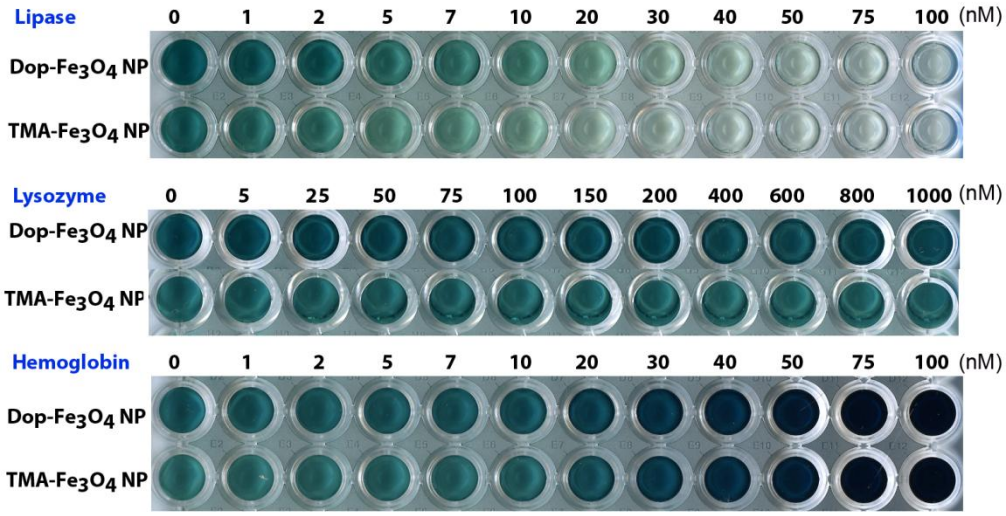

Figure 3.S3. Photographs of color changes in the titration studies of lipase, lysozyme, and hemoglobin. Images were obtained by scanning right after reading OD at 420 nm. The peroxidase-like activity of both NPs (Dop- and TMA-Fe_3O_4) is inhibited by lipase and the green color intensity of the product from the catalyzed hydrolysis of substrate ABTS decreases as lipase concentration increases. The colorimetric signals have no significant differences in a wide range of lysozyme concentrations. The catalyzed colorimetric reaction rate is increased in the presence of hemoglobin, giving increased intensity of the green color in higher concentrations of hemoglobin.

3.6 References

1. (a) Charych, D. H.; Nagy, J. O.; Spevak, W.; Bednarski, M. D. *Science* **1993**, *261*, 585-588. (b) Thanh, N. T. K.; Rosenzweig, Z. *Anal. Chem.* **2002**, *74*, 1624-1628. (c) Sastry, M.; Lala, N.; Patil, V.; Chavan, S. P.; Chittiboyina, A. G. *Langmuir* **1998**, *14*, 4138-4142. (d) Ho, H. A.; Najari, A.; Leclerc, M. *Acc. Chem. Res.* **2008**, *41*, 168-178.

2. (a) Elghanian, R.; Storhoff, J. J.; Mucic, R. C.; Letsinger, R. L.; Mirkin, C. A. *Science* **1997**, *277*, 1078-1081. (b) Storhoff, J. J.; Elghanian, R.; Mucic, R. C.; Mirkin, C. A.; Letsinger, R. L. *J. Am. Chem. Soc.* **1998**, *120*, 1959-1964. (c) Aili, D.; Selegard, R.; Baltzer, L.; Enander, K.;

Liedberg B. *Small*, **2009**, *5*, 2445-2452. (d) Huang, C. C.; Huang, Y. F.; Cao, Z. H.; Tan, W. H.; Chang, H. T. *Anal. Chem.* **2005**, *77*, 5735-5741.

3. (a) You, C. C.; Miranda, O. R.; Gider, B.; Ghosh, P. S.; Kim, I. B.; Erdogan, B.; Krovi, S. A.; Bunz, U. H. F.; Rotello, V. M. *Nat. Nanotech*. **2007**, *2*, 318-323. (b) De, M.; Rana, S.; Akpinar, H.; Miranda, O. R.; Arvizo, R. R.; Bunz, U. H. F.; Rotello, V. M. *Nat. Chem.* **2009**, *1*, 461-465. (c) Albert, K. J.; Lewis, N. S; Schauer, C. L.; Sotzing, G.A.; Stitzel, S. E.; Vaid, T. P.; Walt, D. R. *Chem. Rev*. **2000**, *100*, 2595–2626.

4. (a) Folmer-Andersen, J. F.; Kitamura, M.; Anslyn, E. V. *J. Am. Chem. Soc.* **2006**, *128*, 5652-5653. (b) Greene, N. T. and Shimizu, K. D. *J. Am. Chem. Soc.* **2005**, *15*, 5695– 5700. (c) Zhang, C.; Suslick, K. S. *J. Am. Chem. Soc.* **2005**, *127*, 11548-11549. (d) Miranda, O. R.; Chen, H. T.; You, C. C.; Mortenson, D. E.; Yang, X. C.; Bunz, U. H. F.; Rotello, V. M. *J. Am. Chem. Soc*. **2010**, *132*, 5285-5289.

5. Miranda, O. R.; Li, X.; Garcia-Gonzalez, L.; Zhu, Z.-J.; Yan, B.; Bunz, U. H. F.; Rotello, V. M. *J. Am. Chem. Soc.* **2011**, *133*, 9650– 9653.

6. (a) Shoji, E. and Freund, M. S. *J. Am. Chem. Soc.* **2001**, *123*, 3383-3384. (b) Wei, H.; Wang, E. *Anal. Chem*. **2008**, *80*, 2250-2254.

7. (a) Jv, Y.; Li, B. X.; Cao, R. *Chem. Commun*. **2010**, *46*, 8017-8019. (b) Song, Y. J.; Qu, K. G.; Zhao, C.; Ren, J. S.; Qu, X. G. *Adv. Mater*. **2010**, *22*, 2206-2210. (c) Guo, Y. J.; Deng, L.; Li, J.; Guo, S. J.; Wang, E. K.; Dong, S. J. *ACS Nano* **2011**, *5*, 1282-1290. (d) Pelossof, G.; Tel-Vered, R.; Elbaz, J.; Willner, I. *Anal. Chem*. **2010**, *82*, 4396-4402.

8. Wiester, M. J.; Ulmann, P. A.; Mirkin, C. A. *Angew. Chem. Int. Ed.* **2011**, *50*, 114-137.

9. Gao, L. Z.; Zhuang, J.; Nie, L.; Zhang, J. B.; Zhang, Y.; Gu, N.; Wang, T. H.; Feng, J.; Yang, D. L.; Perrett, S.; Yan, X. *Nat. Nanotech*. **2007**, *2*, 577-583.

10. Asati, A.; Santra, S.; Kaittanis, C.; Nath, S.; Perez, J. M. *Angew. Chem. Int. Ed.* **2009**, *48*, 2308-2312.

11. Ornatska, M.; Sharpe, E.; Andreescu, D.; Andreescu, S. *Anal. Chem.* **2011**, *83*, 4273-4280.

12 . Gao, L. Z.; Wu, J. M.; Lyle, S.; Zehr, K.; Cao, L. L.; Gao, D. *J. Phys. Chem. C* **2008**, *112*, 17357-17361.

13. Park, K. S.; Kim, M. I.; Cho, D. Y.; Park, H. G. *Small* **2011**, *7*, 1521–1525.

14 Li, X. N.; Wen, F.; Creran, B.; Jeong, Y. D.; Zhang, X. R.; Rotello, V. M. *Small* **2012**, *8*, 3589-3592.

15. In our study, we found that hemoglobin had an enhancement in OD response instead of inhibition. We believe this is due to the peroxidatic activity of the heme group in hemoglobin. Reference: (a) Bunn H.F.; Jandl J.H. *J. Biol. Chem*. **1968**, *243*, 465–475. (b) Karnovsky M. J. *J. Cell. Biol*. **1967**, *35*, 213–236.

16 . Jakob, H.; Leininger, S.; Lehmann, T.; Jacobi, S.; Gutewort, S. "Peroxo compounds, inorganic" *Ullmann's Encyclopedia of Industrial Chemistry*, 6th ed., Wiley-VCH:Weinheim, **2003**.

17 . Shih, J. S.; Merianos, J. J.; Smith, T. E.; Chuang, J-C. "Aqueous Stable Complex of a Strongly Swellable, Moderately Crosslinked Polyvinylpyrrolidone and Hydrogen Peroxide" U.S. Patent 5312619, **1992.**

18 . Login, R. B.; Merianos, J. J.; Biss, R. B.; Garelick, P. "Urea-hydrogen Peroxide-Polyvinylpyrrolidone" U.S. Patent 5183901, **1992.**

19. Qu, H.; Caruntu, D.; Liu, H.; O'Connor, C. J. *Langmuir* **2011**, *27*, 2271– 2278.

20. Sun, S.; Zeng, H. *J. Am. Chem. Soc.* **2002**, *124*, 8204-8205.

21. Hostetler, M. J.; Templeton, A. C.; Murray, R. W. *Langmuir* **1999**, *15*, 3782-3789.

CHAPTER 4

MULTICHANNEL SENSOR FOR RAPID IDENTIFICATION OF BIOFILMS FORMED BY BOTH LABORATORY AND PATHOGENIC BACTERIA

4.1 Introduction

Biofilms on wounds, implants, and indwelling devices generate chronic and often life-threatening infections and inflammation.[1] These persistent infections can result in tissue damage, device dysfunction, implant failure, and even death.[2, 3] Biofilm infections are notoriously difficult to treat, as the biofilm matrix provides physical protection from antibiotic treatment, which is often enhanced by the presence of antibiotic resistant bacteria. Rapid detection and identification of biofilms can provide crucial information for early diagnosis and effective treatment,[4] however, the identification of bacterial species in biofilms is challenging due to their physiological heterogeneity.[5] Conventional biofilm detection methods rely on culturing, which requires several days for diagnosis and has low sensitivity.[6, 7] More recent, molecular detection methods, such as PCR[8] and fluorescence *in situ* hybridization (FISH)[9], have been developed based on genotyping and genomic profiling. While these approaches are rapid and have the potential for increased sensitivity, it remains challenging to efficiently detect and identify biofilms.[10]

The biofilm matrix accounts for over 90% of biofilm dry mass, providing a three-dimensional microenvironment that protects the bacteria.[11] This architecture is a unique feature that defines biofilms, intimately regulating the physical and functional properties of the biofilm.[12] Both the physical structure of the biofilm and the composition of the extracellular polymeric substances (EPS) in the matrix, such as polysaccharides, proteins, nucleic acids, and lipids, vary among bacteria species.[13] For example, polysaccharides are neutral in *Streptococcus*,[14] polyanionic in *Pseudomonas*,[15] and polycationic in *Staphylococcus*.[16] Within a species, the EPS are even diverse; polysaccharides from various strains of *Streptococcus thermophilus* feature different monomer compositions and ratios and possess different molecular masses.[17]

Based on the structural and chemical differences between biofilms, we hypothesized that an array-based "chemical nose" approach could be used to detect and differentiate between species and even strains in a biofilm,[18, 19, 20] potentially minimizing the interference caused by biofilm heterogeneity[11] and phenotypic diversity of bacteria.[21, 22] Array-based sensing has been used to identify species and strains of planktonic bacteria.[23, 24] Optical sensing of biofilms is however a much more challenging prospect due to the physical heterogeneity of the films, which introduces significant variability to the sensing process.

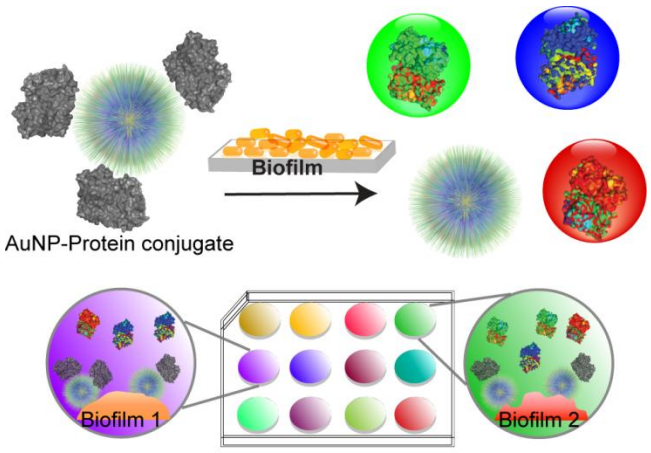

Figure 4.1. Schematic illustration of the multichannel sensing. The sensor is composed with AuNP-fluorescent protein conjugates which will be disrupted in the presence of biofilms. The disruption turns on fluorescence and gives different colored fluorescence patterns for biofilm identification.

In this chapter, I describe a gold nanoparticle (AuNP)-based multichannel fluorescence sensor to detect and identify the species composition of biofilms based on the overall biofilm physicochemical properties. This sensor features AuNP-fluorescent protein conjugates that can be disrupted to give fluorescent readouts in the presence of bioflms (Figure 4.1), generating an essentially instantaneous readout. The key feature of this sensor platform is that it uses a three-color RGB output that generates a ratiometric response, which is less sensitive to sample variability,[25, 26] enabling us to completely differentiate bacterial species and strains of six biofilms, including two pathogenic clinical isolates, within minutes. The versatility of this sensor is further

demonstrated by discrimination between two bacterial species in a co-cultured biofilm-fibroblast cell wound model.[27] These results have been written in a manuscript ready for submission.

4.2 Results and discussion

We first fabricated two AuNPs (~2 nm core), one featuring a cationic hydrophobic (NP1) and the other a hydrophilic (NP2) functional group (Figure 4.2 a). Multi-channel output is provided through reversible adsorption followed by partial displacement of three fluorescent proteins with well-separated excitation and emission spectra (Figure 4.2 b): red (tdTomato),[28] blue (EBFP2),[29] and green (EGFP).[30] These proteins feature negative surface charge, allowing electrostatic interactions with cationic NP1 and NP2. In the presence of biofilms, the fluorescently quenched[31] AuNP-fluorescent protein conjugates are disrupted by the competitive interactions between the negatively charged EPS produced by the bacterial species and the cationic AuNPs, restoring the fluorescence, and hence generate discerning patterns for species recognition in the biofilm (Figure 4.1).

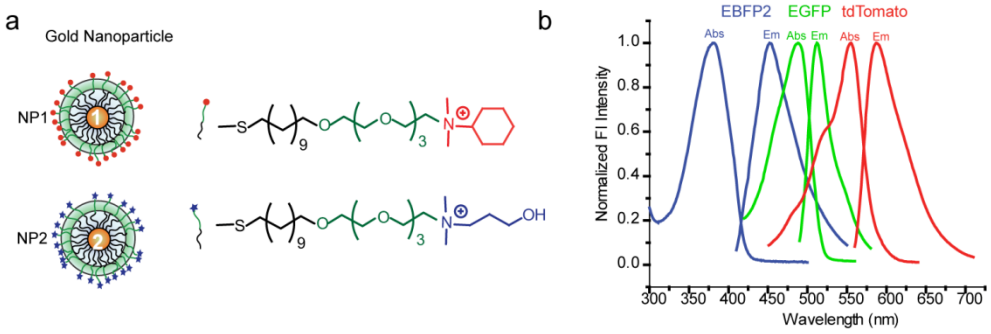

Figure 4.2. a. Molecular structure of NP surface ligand. **b.** The absorption and emission spectra of the three fluorescent proteins.

In the sensor design, NP1 and NP2 were chosen to afford selective hydrophobic and hydrophilic interactions with target biofilms. The presence of both NPs could offers competitive hydrophobic/hydrophilic interactions with biofilm EPS, maximizing biofilm species composition differences. We first studied the binding affinities of the fluorescent proteins towards the two AuNPs by fluorescence titration. In these studies, an equimolar mixture of the three fluorescent

proteins was titrated with NP1, NP2, and an equimolar mixture of NP1 and NP2 (Figure 4.3). In all cases, with increasing NP concentrations, fluorescence from the three proteins was efficiently quenched.

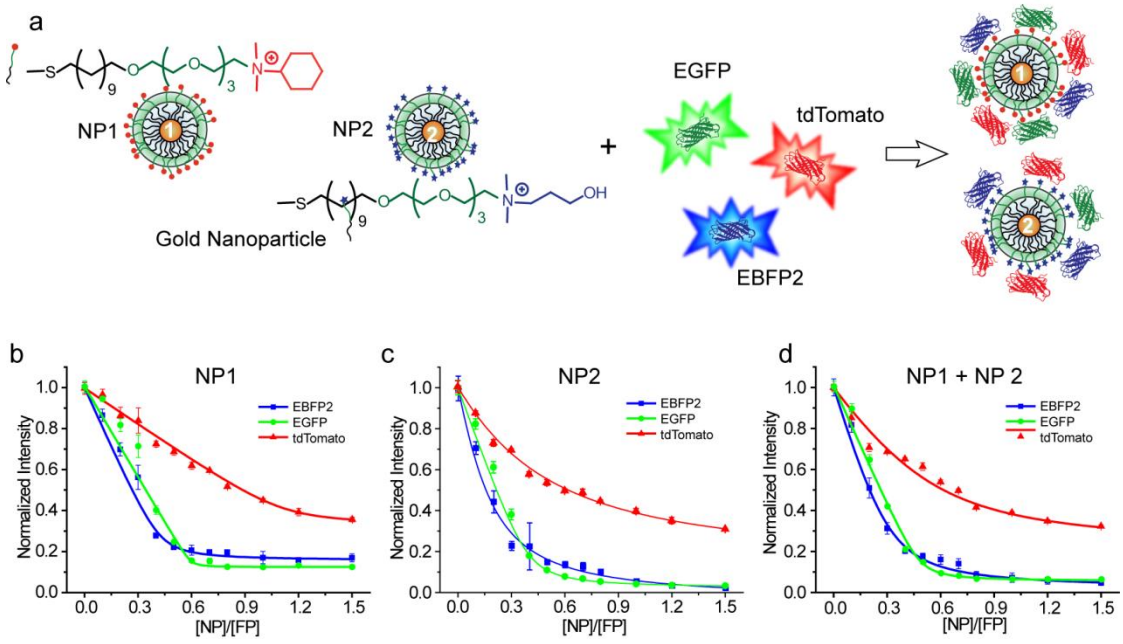

Figure 4.3. a. The sensor elements and molecular structures of the functional ligands of NP1 and NP2. Fluorescence titration with **b.** NP1, **c.** NP2, **d.** an equal molar mixture of NP1 and NP2. Each value is an average of three replicates and the error bars are standard deviations.

Nonlinear curve fitting was used to calculate the NP-protein complex stability constant (K_s) and association stoichiometry (n) (Table 4.1). The binding constant of tdTomato was significantly lower than EBFP2 and EGFP, indicating that the binding interaction of tdTomato to AuNPs was much weaker. A plausible explanation was that tdTomato is a tandom dimer and much larger than EBFP2 and EGFP in size, leading to its weaker binding interaction to AuNPs. These variations in FP-AuNP conjugate stabilities and the association stoichiometry promised the triple-channel sensing. To provide an effective dynamic range, we chose the point where the NP: fluorescent protein ratio was 0.8 (160 nM of total AuNPs and 200 nM of each fluorescent protein), generating efficient quenching of all three proteins.

Table 4.1. The binding parameters derived from the fitting of the fluorescence titration data.

AuNP	Protein	Binding constant (K_s), M^{-1}	Association stoichiometry (n)	R^2
NP1	EBFP2	$(4.18 \pm 3.15) \times 10^8$	2.34 ± 0.22	0.9822
	EGFP	$(8.03 \pm 2.09) \times 10^9$	1.68 ± 0.08	0.9837
	tdTomato	$(5.52 \pm 5.24) \times 10^8$	0.89 ± 0.03	0.9830
NP2	EBFP2	$(1.54 \pm 1.10) \times 10^7$	6.86 ± 3.34	0.9727
	EGFP	$(2.86 \pm 0.50) \times 10^8$	2.52 ± 0.08	0.9938
	tdTomato	$(6.44 \pm 6.66) \times 10^6$	4.20 ± 2.82	0.9948
NP1+NP2	EBFP2	$(7.77 \pm 3.73) \times 10^7$	3.18 ± 0.49	0.9856
	EGFP	$(7.86 \pm 2.43) \times 10^8$	2.08 ± 0.06	0.9897
	tdTomato	$(3.31 \pm 2.62) \times 10^7$	1.88 ± 0.41	0.9766

After optimization of particle/protein concentrations, we tested the discriminatory power of our sensor against six bacterial strains representing 5 species (*Amycolatopsis azurea, Bacillus licheniformic, Bacillus megaterium, Escherichia coli, Pseudomonas aeruginosa*), including one clinical isolate of uropathogenic *E. coli*. and *P. aeruginosa*. The bacteria were cultured for three days in a 96-well microplate in modified LB media (see Materials and Method) at room temperature.[32] Biofilms were observed in each of the culture wells. The particle/protein sensor solution was then added to each well and incubated for 45 minutes before reading. As shown in Figure 4.4, the six bacteria biofilms displayed distinct response patterns. The two pathogenic bacteria, *E. coli* CD-3 and *P. aeruginosa* CD-1006 showed the lowest and the highest responses, respectively, in all three channels, and thus is clearly distinguished from biofilms formed by the remaining the laboratory strains. Interestingly, the biofilms of *B. licheniformis* and *P. aeruginosa*, species known to form strong biofilms,[33, 34, 35] exhibited higher sensor responses than biofilms of the other three species, indicating stronger interactions between the AuNPs and biofilms.

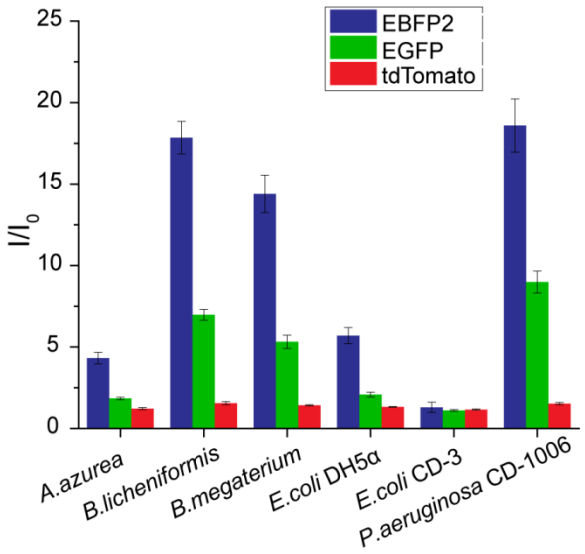

Figure 4.4. Detection and identification of biofilms formed by four laboratory strains and two uropathogenic strains. Triple-channel fluorescence response patterns in the presence of biofilms. I_0 is the fluorescence intensity in the absence of biofilms. Each value is an average of six replicates and the error bars are standard deviations.

Quantitative discrimination between the bacterial strains was obtained using linear discriminant analysis (LDA).[36] According to the jackknifed classification matrix in the LDA,[37] the six data groups each containing six points from each biofilm were classified and showed 100% separation. The canonical scores of the first two factors were plotted with 95% confidence ellipses in Figure 4.5, showing 100% discrimination between the biofilms of the six bacterial strains. Comparison between individual channels and the three channel system (Table 4.2) indicates that individual channels were incapable of complete classification, demonstrating the importance of multi-channel sensing in detecting complex analytes such as biofilms. The biofilm-based clusters did not display Gram-stain related separation. This is presumably because the structural differences between Gram-positive and Gram-negative bacteria are located primarily in their cell walls, which may be masked by the biofilm EPS in which the bacteria are embedded.

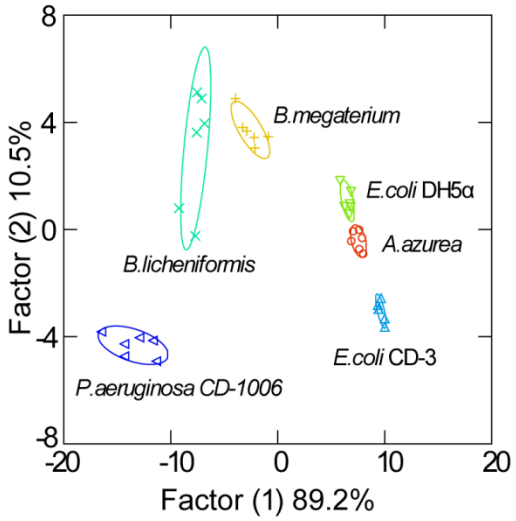

Figure 4.5. Canonical score plot of the fluorescence response patterns as obtained by LDA against the six bacterial biofilms.

Table 4.2. The jackknifed classification accuracy based on the parts of the triple-channel fluorescence (R: tdTomato, G: EGFP, and B: EBFP2).

Channel	Accuracy	Channel	Accuracy
R	61%	R+B	78%
G	90%	R+G	90%
B	66%	G+**B**	93%
R+G+**B**	100%		

In addition to clustering, LDA is capable of identifying unknown samples once the system has been "trained" using a training set of analytes.[38] In practice, four cultures of each of the six bacterial strains were prepared and labeled randomly to generate a pool of 24 unknown biofilm samples. The sensor identified 23 out of 24 samples (96%) correctly (Table 4.3), simultaneously demonstrating the diagnostic possibilities of the sensor and the robustness of the clustering.

Table 4.3. Identification of 24 unknown biofilm samples.

#	I/I_0			Identification	Verification
	Blue	Green	Red		
1	4.151	1.734	1.119	A.azu	A.azu
2	12.435	4.817	1.370	B.mega	B.mega
3	1.485	1.088	1.134	CD-3	CD-3
4	5.091	1.924	1.318	DH5α	DH5α
5	18.641	6.802	1.523	B.liche	B.liche
6	20.647	8.973	1.507	P.aeru	P.aeru
7	17.847	8.422	1.487	P.aeru	P.aeru
8	1.576	1.120	1.165	CD-3	CD-3
9	14.836	5.475	1.466	B.mega	B.mega
10	4.605	1.878	1.279	A.azu	A.azu
11	5.406	1.978	1.338	DH5α	DH5α
12	18.279	6.946	1.589	B.liche	B.liche
13	4.381	1.895	1.250	A.azu	A.azu
14	1.880	1.194	1.142	CD-3	CD-3
15	6.066	2.262	1.324	DH5α	DH5α
16	20.273	7.530	1.568	B.liche	B.liche
17	19.794	9.111	1.370	P.aeru	P.aeru
18	16.566	6.466	1.465	B.liche	B.mega
19	7.353	2.720	1.431	DH5α	DH5α
20	17.404	7.041	1.663	B.liche	B.liche
21	14.372	5.405	1.422	B.mega	B.mega
22	4.690	1.699	1.187	A.azu	A.azu
23	2.055	1.129	1.171	CD-3	CD-3
24	25.131	11.287	1.560	P.aeru	P.aeru

Identifying bacterial biofilms on surfaces such as indwelling devices and implants is a critical capability. Determination of pathogens in biofilms occurring on human tissues and organs provides an equally important and even more challenging goal. In most cases, the bacterial pathogens of interest will be embedded in human tissues within biofilms comprised of, EPS, mammalian cells and an extracellular matrix. To test the diagnostic capability of our multi-channel sensor for wound biofilms, we employed a biofilm-fibroblast cell co-culture[39,40] as a

model. Two bacteria, *B. licheniformis* and *E. coli* DH5α were chosen as representative Gram-positive and Gram-negative species. The bacteria were seeded with a confluent NIH 3T3 (mouse fibroblast) cell monolayer[41] overnight for biofilm formation. The co-cultures were washed before sensing to remove planktonic bacteria and non-adherent 3T3 cells. The sensor response patterns for *B. licheniformis* biofilm-3T3 cell, *E. coli* DH5α-biofilm-3T3 cell, and non-infected 3T3 cell were different (Figure 4.6 a), with LDA demonstrating 100% discrimination of the two co-cultures and 3T3 cells (Figure 4.6 b).

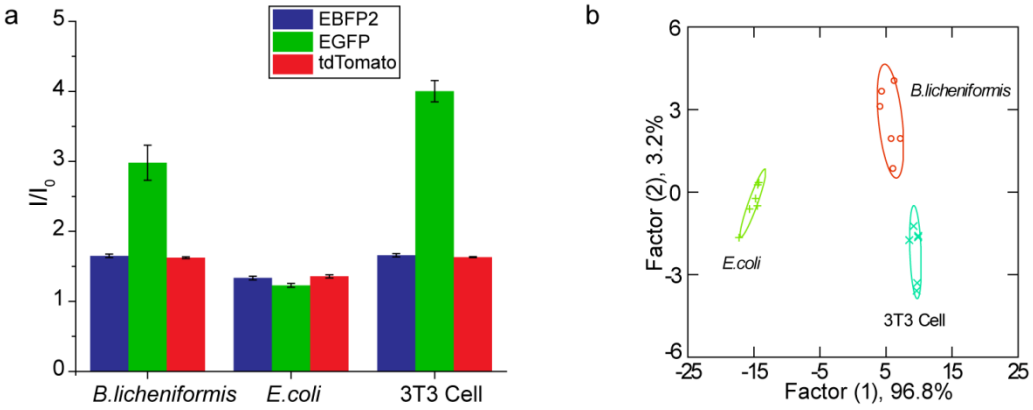

Figure 4.6. Detection and identification of biofilms grown on 3T3 fibroblast cells. **a.** Triple-channel fluorescence response patterns in the presence of biofilms grown on fibroblast cells and 3T3 fibroblast cells alone. I_0 is the fluorescence intensity in the absence of biofilms or 3T3 cells. Each value is an average of six replicates and the error bars are standard deviations. **b.** LDA canonical score plot of the fluorescence response patterns.

In the two bacteria/biofilm infected co-cultures, cells were observed to detach and float, which were washed away before sensing. Therefore the non-infected 3T3 cells had the highest number of mammalian cells. This could be the reason why 3T3 cell culture displayed the highest sensor response. As in Figure 4.2, *B. licheniformis* maintained the higher response than *E. coli*. Besides, the *E. coli* biofilm co-culture had a greater impact on mammalian cell viability than the *B. licheniformis* biofilm, resulting a lower background response from mammalian cells. As above, we tested the ability of this training set to diagnose unknown samples, recognizing 10 out of 12 samples correctly (Table 4.4). These studies indicate the potential of our system for detection and identification of biofilms in infected wounds.

Table 4.4. Identification of 12 unknown co-culture samples.

#	I/I_0			Identification	Verification
	Blue	Green	Red		
1	1.77	3.54	1.74	Cell	B.liche
2	1.47	1.47	1.51	E.coli	E.coli
3	1.69	3.63	1.71	Cell	Cell
4	1.68	3.72	1.72	Cell	Cell
5	1.53	1.44	1.51	E.coli	E.coli
6	1.63	2.99	1.62	B.liche	B.liche
7	1.75	3.74	1.76	Cell	Cell
8	1.45	1.20	1.47	E.coli	E.coli
9	1.74	3.20	1.69	B.liche	B.liche
10	1.72	3.35	1.70	B.liche	B.liche
11	1.75	3.92	1.69	Cell	Cell
12	1.62	1.87	1.57	B.liche	E.coli

4.3 Conclusions

In conclusion, I have developed a rapid (minutes) and effective multi-channel sensor for identifying bacterial species, and even strains, in biofilms. Using this AuNP multi-channel sensor, we successfully detected and differentiated biofilms formed by pathogenic and non-pathogenic bacteria. These determinations were effective with biofilms on surfaces and in a bacteria-mammalian cell co-culture wound model. The employed sensing principle demonstrated that overall biofilm physiology could be used as an alternative signature for biofilm identification, providing a brand new aspect to biofilm research. The selective instead of specific sensor construction averts the necessity of pre-knowledge of analyte biofilms, of which very little has been known. Beyond this, the described approach allows direct detection and analysis on samples, potentially eliminating the need of culturing and therefore false negative diagnosis resulted from the non-culturable cells inside biofilms.

The optical basis of this system is an added benefit, facilitating translation to both visual[42] and camera-based diagnostics.[43] Taken together, these capabilities demonstrate the diagnostic potential of our sensor system, providing a tool that could enable targeted treatment of biofilm infections in lieu of broad-spectrum antibiotics.[44]

4.4 Experimental methods

Fluorescent proteins EBFP2, **Error! Bookmark not defined.** EGFP, [45] and tdTomato**Error! Bookmark not defined.** were expressed in *E. coli* BL21 (DE3) and purified by means of Co2+-affinity chromatography. Cationic NP1 and NP2 were synthesized as previously reported.[46,47]

Nanoparticle synthesis 2nm diameter gold nanoparticles were synthetized by the Brust-Schiffrin two-phase methodology using pentanethiol as the stabilizer; these clusters were purified with successive extractions with ethanol and acetone. A Murray place exchange reaction was carried out in dry DCM to functionalize the nanoparticles with each ligand.[48,49] The monolayer-protected nanoparticles were redispersed in water and the excesses of ligand/pentanethiol were removed by dialysis using a 10,000 MWCO snake-skin membrane. The final concentration was measured by UV spectroscopy on a Molecular Devices SpectraMax M2 at 506nm according to the reported methodology.[50] NPs were characterized on a Malvern Nano Zetasizer to obtain hydrodynamic diameter (Figure 4.7) and zeta potential for surface charge (Figure 4.8).

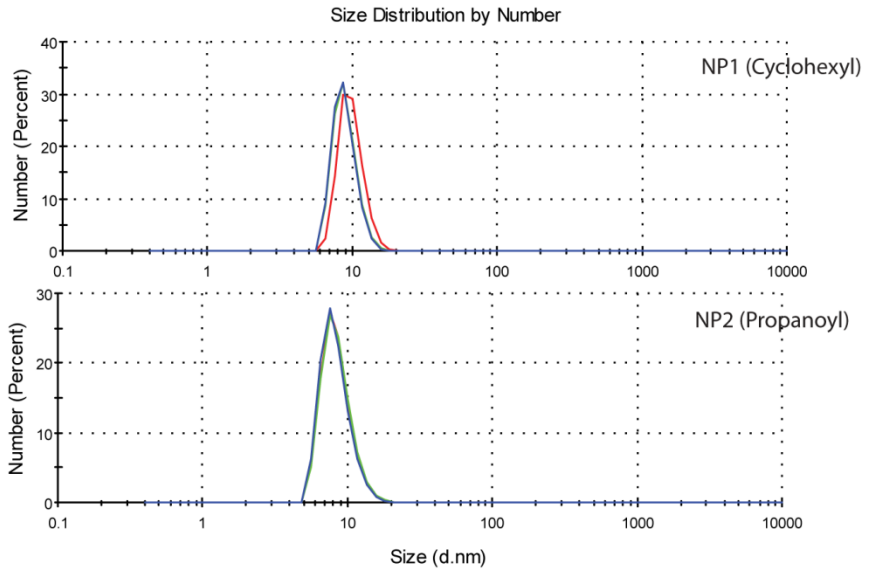

Figure 4.7. DLS size distribution of NP1 and NP2.

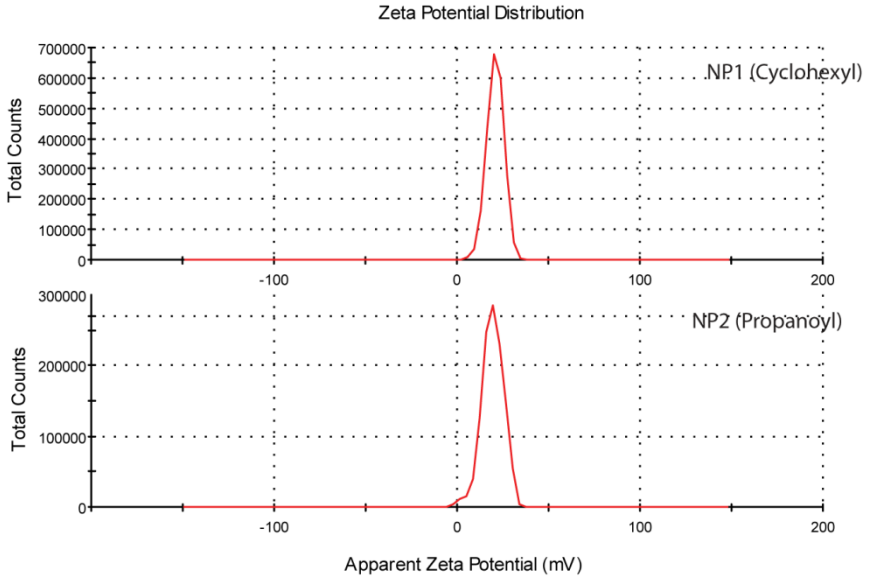

Figure 4.8. Zeta potential distribution of NP1 and NP2.

Fluorescence titration 200 nM EBFP2, 200 nM EGFP, and 200 nM tdTomato were mixed to make an equimolar solution in 5 mM phosphate buffer (PB, pH=7.4). The solution with fixed fluorescent protein concentration was then titrated with NPs at various concentrations from 0 to 150 nM. For the combination of NP1 and NP2, NPs were first mixed to make an equimolar solution, and the NP concentration was defined as the total NP concentration. After 15 minutes

incubation at room temperature, the change of fluorescence intensity from three channels was measured using a Molecular Devices SpectraMax M2 plate reader. The excitation and emission wavelengths are: 380 nm (ex) and 450 nm (em) for EBFP2; 475 nm (ex) and 510 nm (em) for EGFP; 550 nm (ex) and 585 nm (em) for tdTomato. Nonlinear least-squares curve-fitting analysis by Origin (version 8.0) was employed to estimate the binding constant (*Ks*) and association stoichiometry (*n*), using a model in which the NP is assumed to possess the n equivalent of independent binding sites. [51]

Biofilm formation in 96-well microplate Bacteria were inoculated in LB broth at 37 ℃ until stationary phase. The cultures were then harvested by centrifugation and washed with 0.85% sodium chloride solution for three times. Concentrations of re-suspended bacterial solution were determined by optical density measured at 600 nm. LB was supplemented with 0.1% glucose, 1 mM $MgSO_4$, 0.15 M ammonium sulphate, and 34 mM citrate and buffered to pH 7 to ensure bacterial adherence to the microplate. Seeding solutions were then made in this modified LB to reach OD_{600} of 0.1. 195 μL of the seeding solutions were added to each well of the microplate. Modified LB medium without bacteria was used as negative control. The plates were covered and incubated at room temperature under static conditions for three days. Fresh media was added on Day 2. Planktonic bacteria were removed before sensing by washing with PB saline three times.

Sensing of biofilms in microplate The sensor was composed of 200 nM EBFP2, 200 nM EGFP, 200 nM tdTomato, 80 nM NP1, and 80 nm NP2 in 5 mM PB. The sensor was made fresh and incubated in the dark for 15 minutes before use. It was then added (200 μL) into each well containing a biofilm and incubated for 45 minutes. The fluorescence recovery was monitored using an Optima BMG Labtech plate reader.

Biofilm-3T3 fibroblast cell co-culture 20,000 NIH 3T3 (ATCC CRL-1658) cells were cultured in Dulbecco's modified Eagle medium (DMEM; ATCC 30-2002) with 10% bovine calf serum and 1% antibiotics at 37 ℃ in a humidified atmosphere of 5% CO_2. Cells were kept for 48 hours to reach a confluent monolayer. Bacteria were inoculated and harvested as described above

and seeding solutions were made in DMEM to reach OD_{600} of 0.1. Old medium was removed from 3T3 cells followed by addition of 100 μL seeding solution. The co-cultures were then stored in a box with damp paper towels at 37 ℃ overnight. The co-cultures were washed with PB saline three times before sensing to remove planktonic bacteria and non-adherent 3T3 cells.

Sensing of biofilm-fibroblast cell co-cultures The sensor was composed as described earlier and was made fresh and incubated in the dark for 15 minutes before sensing. 150 μL of the sensing solution was added into each well containing a biofilm and then incubated for 5 minutes. The fluorescence recovery was monitored using a Molecular Devices Spectramax M2 plate reader.

LDA performance Discrimination analysis was performed using SYSTAT (version 12.0). For biofilm sensing in the microplate, the raw data contained a matrix of 6 (replicates) × 6 (biofilms) × 3 (channels). The co-culture studies generated a matrix of 6 (replicates) × 3 (biofilms plus 3T3 cells alone) × 3 (channels). All raw data were subjected to LDA to differentiate the fluorescence response of the multi-channel system against different biofilm targets. The analysis maximized the ratio of between-class variance to within-class variance in both data sets, thereby enabling maximal separation. The matrixes were transformed to canonical factors that were linear combinations of the response patterns. The canonical factors contain different percentage of the variation and the first two were plotted.

The blind test For identification of the unknown samples, we chose seeding solutions of interest and assigned them a random number. These seeding solutions were used to form biofilms and tested with the multi-channel sensor. The average response of three data points was used to represent a single unknown sample. During LDA, the Mahalanobis distance of the unknown case, which is the distance of the new case to the centroid of respective groups generated through the training set, were calculated. Then the unknown case was classified to the group with the shortest Mahalanobis distance.

4.5 References

1. Romling, U.; Balsalobre, C. *J. Intern. Med.* **2012**, *272*, 541-561.

2. Costerton, J. W.; Stewart, P. S.; Greenberg, E. P. *Science* **1999**, *284*, 1318-1322.

3. Parsek, M. R.; Singh, P. K. *Annu. Rev. Microbiol.* **2003**, *57*, 677-701.

4. Stewart, P. S.; Costerton, J. W. *Lancet* **2001**, *358*, 135-138.

5. Fux, C. A.; Stoodley, P.; Hall-Stoodley, L.; Costerton, J. W. *Expert Rev. Anti. Infect. Ther.* **2003**, *1*, 667-683.

6. Hall-Stoodley, L.; Hu, F. Z.; Gieseke, A.; Nistico, L.; Nguyen, D.; Hayes, J.; Forbes, M.; Greenberg, D. P.; Dice, B.; Burrows, A.; Wackym, P. A.; Stoodley, P.; Post, J. C.; Ehrlich, G. D.; Kerschner, J. E. *J. Am. Med. Assoc.* **2006**, *296*, 202-211.

7. Shen, Y.; Stojicic, S.; Haapasalo, M. *Journal of Endodontics* **2010**, *36*, 1820-1823.

8. Stoodley, P.; Conti, S. F.; DeMeo, P. J.; Nistico, L.; Melton-Kreft, R.; Johnson, S.; Darabi, A.; Ehrlich, G. D.; Costerton, J. W.; Kathju, S. *FEMS Immunol. Med. Microbiol.* **2011**, *62*, 66-74.

9. Hall-Stoodley, L.; Costerton, J. W.; Stoodley, P. *Nat. Rev. Microbiol.* **2004**, *2*, 95-108.

10. Hall-Stoodley, L.; Stoodley, P.; Kathju, S.; Hoiby, N.; Moser, C.; Costerton, J. W.; Moter, A.; Bjarnsholt, T. *FEMS Immunol. Med. Microbiol.* **2012**, *65*, 127-145.

11. Flemming, H. C.; Wingender, J. *Nat. Rev. Microbiol.* **2010**, *8*, 623-633.

12. Bridier, A.; Dubois-Brissonnet, F.; Boubetra, A.; Thomas, V.; Briandet, R. *J. Microbiol. Methods* **2010**, *82*, 64-70.

13. Flemming, H. C.; Neu, T. R.; Wozniak, D. J. *J. Bacteriol.* **2007**, *189*, 7945-7947.

14. Sutherland, I. W. *Microbiology-Uk* **2001**, *147*, 3-9.

15. Ryder, C.; Byrd, M.; Wozniak, D. J. *Curr. Opin. Microbiol.* **2007**, *10*, 644-648.

16. Gotz, F. *Mol. Microbiol.* **2002**, *43*, 1367-1378.

17. Vaningelgem, F.; Zamfir, M.; Mozzi, F.; Adriany, T.; Vancanneyt, M.; Swings, J.; De Vuyst, L. *Appl. Environ. Microbiol.* **2004**, *70*, 900-912.

18. Albert, K. J.; Lewis, N. S.; Schauer, C. L.; Sotzing, G. A.; Stitzel, S. E.; Vaid, T. P.; Walt, D. R. *Chem. Rev.* **2000**, *100*, 2595-2626.

19. Turner, A. P. F.; Magan, N. *Nat. Rev. Microbiol.* **2004**, *2*, 161-166.

20. Wright, A. T.; Anslyn, E. V. *Chem. Soc. Rev.* **2006**, *35*, 14-28.

21. Costerton, J. W.; Lewandowski, Z.; Caldwell, D. E.; Korber, D. R.; Lappinscott, H. M. *Annu. Rev. Microbiol.* **1995**, *49*, 711-745.

22. Donlan, R. M.; Costerton, J. W. *Clin. Microbiol. Rev.* **2002**, *15*, 167-193.

23. Phillips, R. L.; Miranda, O. R.; You, C. C.; Rotello, V. M.; Bunz, U. H. F. *Angew. Chem. Int. Ed.* **2008**, *47*, 2590-2594.

24. Duarte, A.; Chworos, A.; Flagan, S. F.; Hanrahan, G.; Bazan, G. C. *J. Am. Chem. Soc.* **2010**, *132*, 12562-12564.

25. Xue, L.; Liu, Q.; Jiang, H. *Org. Lett.* **2009**, *11*, 3454-3457.

26. Wang, Z.; Palacios, M. A.; Zyryanov, G.; Anzenhacher, P. *Chem. Eur. J.* **2008**, *14*, 8540-8546.

27. Di Giulio, M.; D'Ercole, S.; Zara, S.; Cataldi, A.; Cellini, L. *Apmis* **2012**, *120*, 139-146.

28. Nandwana, V.; Mout, R.; Yeh, Y. C.; Dickert, S.; Tuominen, M. T.; Rotello, V. M. *J. Inorg. Organomet. Polym.* **2013**, *23*, 227-232.

29. Ai, H. W.; Shaner, N. C.; Cheng, Z. H.; Tsien, R. Y.; Campbell, R. E. *Biochemistry* **2007**, *46*, 5904-5910.

30. Tsien, R. Y. *Annu. Rev. Biochem* **1998**, *67*, 509-544.

31. Bajaj, A.; Rana, S.; Miranda, O. R.; Yawe, J. C.; Jerry, D. J.; Bunz, U. H. F.; Rotello, V. M. *Chem. Sci.* **2010**, *1*, 134-138.

32. Hamon, M. A.; Lazazzera, B. A. *Mol. Microbiol.* **2001**, *42*, 1199-1209.

33. Blue, S. R.; Singh, V. R.; Saubolle, M. A. *Clin. Infect. Dis.* **1995**, *20*, 629-633.

34. Klausen, M.; Heydorn, A.; Ragas, P.; Lambertsen, L.; Aaes-Jorgensen, A.; Molin, S.; Tolker-Nielsen, T. *Mol. Microbiol.* **2003**, *48*, 1511-1524.

35. Rickard, A. H.; McBain, A. J.; Ledder, R. G.; Handley, P. S.; Gilbert, P. *FEMS Microbiol. Lett.* **2003**, *220*, 133-140.

36. Jurs, P. C.; Bakken, G. A.; McClelland, H. E. *Chem. Rev.* **2000**, *100*, 2649-2678.

37. Egan, W. J.; Morgan, S. L.; Bartick, E. G.; Merrill, R. A.; Taylor, H. J. *Anal. Bioanal. Chem.* **2003**, *376*, 1279-1285.

38. You, C. C.; Miranda, O. R.; Gider, B.; Ghosh, P. S.; Kim, I. B.; Erdogan, B.; Krovi, S. A.; Bunz, U. H. F.; Rotello, V. M. *Nat. Nanotech.* **2007**, *2*, 318-323.

39. Anderson, G. G.; Moreau-Marquis, S.; Stanton, B. A.; O'Toole, G. A. *Infect. Immun.* **2008**, *76*, 1423-1433.

40. Kim, J.; Hegde, M.; Jayaraman, A. *Lab on a Chip* **2010**, *10*, 43-50.

41. Anderson, G. G.; Kenney, T. F.; MacLeod, D. L.; Henig, N. R.; O'Toole, G. A. *Pathog. Dis.* **2013**, *67*, 39-45.

42. Geladi, P.; Esbensen, K. *J. Chemom.* **1991**, *5*, 97-111.

43. Martinez, A. W.; Phillips, S. T.; Carrilho, E.; Thomas, S. W.; Sindi, H.; Whitesides, G. M. *Anal. Chem.* **2008**, *80*, 3699-3707.

44. Krishnasami, Z.; Carlton, D.; Bimbo, L.; Taylor, M. E.; Balkovetz, D. F.; Barker, J.; Allon, M. *Kidney Int.* **2002**, *61*, 1136-1142.

45. De, M.; Rana, S.; Rotello, V. M. *Macromol. Biosci.* **2009**, *9*, 174-178.

46. Brust, M.; Walker, M.; Bethell, D.; Schiffrin, D. J.; Whyman, R. *J. Chem. Soc., Chem. Commun.* **1994**, 801-802.

47. Hostetler, M. J.; Templeton, A. C.; Murray, R. W. *Langmuir* **1999**, *15*, 3782-3789.

48. Miranda, O. R.; Chen, H. T.; You, C. C.; Mortenson, D. E.; Yang, X. C.; Bunz, U. H. F.; Rotello, V. M. *J. Am. Chem. Soc.* **2010**, *132*, 5285-5289.

49. De, M.; Rana, S.; Akpinar, H.; Miranda, O. R.; Arvizo, R. R.; Bunz, U. H. F.; Rotello, V. M. *Nat. Chem.* **2009**, *1*, 461-465.

50. Liu, X. O.; Atwater, M.; Wang, J. H.; Huo, Q. *Colloid. Surface. B* **2007**, *58*, 3-7.

51. You, C. C.; De, M.; Han, G.; Rotello, V. M. *J. Am. Chem. Soc.* **2005**, *127*, 12873-12881.

CHAPTER 5

FUNCTIONAL GOLD NANOPARTICLES AS POTENT ANTIMICROBIAL AGENTS AGAINST MULTI-DRUG-RESISTANT BACTERIA

5.1 Introduction

The emergence of resistance to antibiotics in bacteria, especially to multiple antimicrobial agents, has become a great threat to public health.[1] According to a report published by the U.S. Centers for Disease Control and Prevention, antibiotic resistant bacteria cause millions of infections and deaths every year in U.S.[2] Additionally, the significant and continuous decrease in the number of approved antibiotics in the last decade has attributed to the alarming situation.[3] Without any alternative novel antibiotics, we may soon encounter the post-antibiotic era.[4]

Nanotechnology has introduced nanoparticles (NPs) as a new paradigm in therapeutic applications with their unique properties.[5,6,7] For example, NP size range is commensurate with biomolecular and bacterial cellular systems, providing additional interactions to small molecule antibiotics.[8,9] The high surface to volume ratio allows incorporation of abundant functional ligands, enabling multivalency on NP surface to enhance interactions to target bacteria. Utilizing these characteristic features, NPs have been conjugated with known antibiotics to combat multi-drug-resistant (MDR) bacteria. The antibiotic molecules can be infused with NPs via non-covalent interactions[10,11] or be incorporated on NPs via covalent bonds.[12,13] Both methods have been reported for enhanced activity against bacteria, showing decreased minimum inhibitory concentration (MIC) in comparison with use of free antibiotics.[14,15,16] The improved performance is proposed to result from polyvalent effect of concentrated antibiotics on the NP surface as well as enhanced internalization of antibiotics by NPs.[17] Yet the dependence on existing antibiotics in these approaches may not be able to delay the onset of acquired resistance.

The functional ligands on NP surface can provide direct multivalent interactions to biological molecules, allowing NPs to be exploited as a self-therapeutic agent.[18,19,20] This strategy

can circumvent the employment and the potential limitation of existing antibiotics in the nanocarrier systems. For assembly of such self-therapeutic NPs, the essentially inert and non-toxic nature of gold makes it an attractive core material.[21] To this end, we synthesized a series of self-therapeutic gold nanoparticles (AuNPs) as an antimicrobial agent. The structure-activity relationship of the functional ligands on 2 nm core AuNP revealed that AuNP antimicrobial properties can be tailored through surface hydrophobicity, providing a new aspect to design and construct antimicrobial AuNPs. According to this relationship, we further focused on the most potent AuNP candidate, C10-AuNP, and tested with clinically isolated uropathogens. The result showed inhibited growth of various strains of uropathgens, including many MDR strains and methicillin-resistant *Staphylococcus aureus* (MRSA). This AuNP did not induce bacterial resistance even after 20 passages. At the MIC against MRSA, the C10-AuNP demonstrated low hemolytic activity and cytotoxicity. These results have been written in a manuscript that is ready for submission.

5.2 Results and discussion

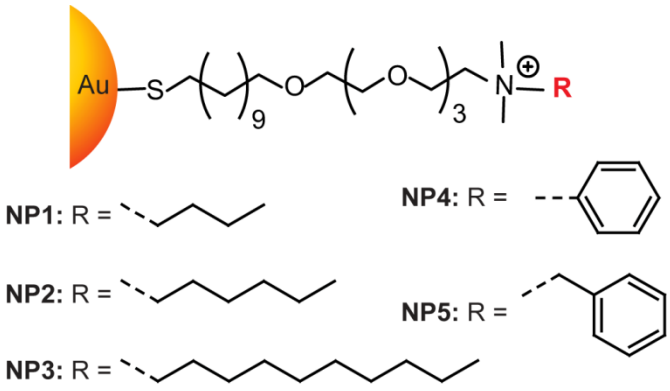

Figure 5.1. Molecular structures of functional ligands on AuNPs.

We recently reported that 2 nm core cationic monolayer-protected AuNPs can interact with cell membrane of Gram-positive and Gram-negative bacteria, resulting in formation of distinct aggregation patterns and lysis of bacterial cell.[22] Similarly, Jiang and coworkers also

demonstrated that blebbing caused by cationic AuNPs induced bacterial membrane damage.[19] Therefore we explored the antimicrobial potential of our 2 nm core functional cationic AuNPs. These AuNPs were synthesized with different cationic functionalities to systematically investigate the role of surface chemistry in NP antimicrobial property. The thiol ligands bearing ammonium end group differed in the functional **R** group, featuring different chain length, non-aromatic, and aromatic characteristics (Figure 5.1).

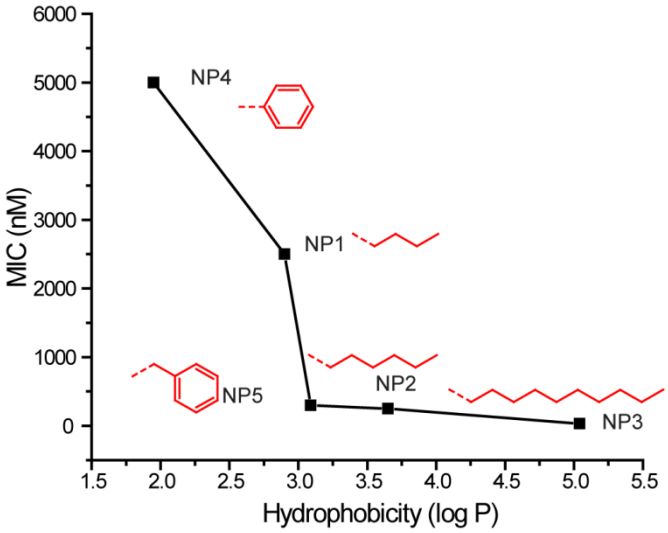

Figure 5.2. MIC values of AuNPs bearing different hydrophobic surface ligands against laboratory *E. coli*. Log *P* represents the calculated hydrophobic values of the end groups.

We first evaluated the functional AuNP antimicrobial activities on a laboratory *E. coli* strain, using the broth dilution methods to determine the minimal inhibitory concentrations (MICs).[23] AuNPs were incubated with 5×10^5 cfu/mL of *E. coli* overnight. All AuNPs were able to completely inhibit the proliferation of *E. coli* at nanomolar concentrations, the MICs of different AuNPs, however, varied by the **R** group. To correlate the antimicrobial activity with AuNP surface functionality, we plotted the MICs against the calculated AuNP end group log *P* values that quantitatively represent the relative NP surface hydrophobicity.[24] Figure 1 uncovered the activity-structure relationship, indicating more hydrophobic NPs were more effective against *E. coli* growth. This relationship revealed that the hydrophobic interaction played an important role in disruption of bacterial cell wall. Interestingly, NP4 and NP5, which differed with one

carbon in structure, exhibited great difference in antimicrobial effectiveness. This could be because that NP5 possess more flexibility with the extra space than NP4, leading to more effective interaction with bacterial cell wall and therefore stronger damaging to bacterial cell. The most hydrophobic AuNP tested, NP3 (C10-AuNP) which carried an *n*-decane end group, was capable of inhibiting *E. coli* proliferation at only 32 nM.

We next tested the antimicrobial activities of the most potent antimicrobial NP, NP3, C10-AuNP, on uropathogenic *E. coli* clinical isolates. Five isolates with different resistant levels to clinically used antibiotics (number of tested resistant drugs from 1 to 17) were used for this study. Remarkably, at a concentration of 16 nM, C10-AuNP suppressed the growth of all five uropathogenic strains of *E. coli*, including three MDR strains (Table 5.1). The comparable MIC values of MDR and laboratory strains implicated that C10-AuNP could potentially address the common mechanisms of bacterial resistance.

Table 5.1. MIC values of C10-AuNP against uropathogens.

Strain	Species	MIC (nM)	# of resistant drugs	MDR
CD-2	*E. coli*	16	1	No
CD-496	*E. coli*	16	2	Yes
CD-3	*E. coli*	16	3	Yes
CD-19	*E. coli*	16	4	Yes
CD-549	*E. coli*	16	17	Yes
CD-866	*E. cloacae complex*	16	2	Yes
CD-1412	*E. cloacae complex*	8	4	Yes
CD-1545	*E. cloacae complex*	16	7	Yes
CD-1006	*P. aeruginosa*	16	1	No
CD-23	*P. aeruginosa*	32	13	Yes
CD-1578	*S. aureus*	64	4	Yes
CD-489	*S. aureus - MRSA*	32	10	Yes

C10-AuNP was further tested with more species/strains of uropathogenic clinical isolates, including Gram-negative *Enterobacter cloacae complex* and *Pseudomonas aeruginosa* and

Gram-positive *Staphylococcus aureus* and methicillin-resistant *S. aureus* (MRSA) (Table 5.1). Among these isolates, *P. aeruginosa* has intrinsic resistance to a variety of antibiotics due to their exceptionally low outer-membrane permeability and multidrug efflux pumps.[25] MICs of C10-AuNP for the one non-MDR *P. aeruginosa* CD-1006 and MDR *P. aeruginosa* CD-23 were 16 nM and 32 nM respectively. *S. aureus* has always been a stumbling block for antimicrobial treatment, overcoming most of the therapeutic chemo-agents developed in the past five decades.[26] Particularly, MRSA has emerged as "superbug", resistant to most antibiotics commonly used for the staph infections.[27] C10-AuNP was capable of effectively inhibiting the proliferation of MDR *S. aureus* isolates, and MIC for the MRSA strain was as low as 32 nM.

In the beginning of our studies, we hypothesized that the cationic functional AuNPs could compromise the integrity of bacterial membrane, causing toxicity to bacterial cells.[22] To support this hypothesis and explore C10-AuNP mode of action, we employed the propidium iodide (PI) staining assay. PI can only penetrate bacterial cells with compromised membrane and binds with nucleic acid with enhanced red fluorescence.[28,29] *E. coli* CD-2 and *S. aureus* CD-489 were chosen as representative Gram-negative and Gram-positive strain. Bacteria (1×10^8 cfu/mL) were incubated with C10-AuNP at a final concentration of 500 nM for three hours at 37 ℃ and then stained with PI before imaging. Confocal laser scanning microscopy (CLSM) images in Figure 5.3 showed NP-induced membrane damage in both bacteria. These results indicated that the cationic gold nanoparticles use the same mode of action on both Gram-negative and Gram-positive bacteria.

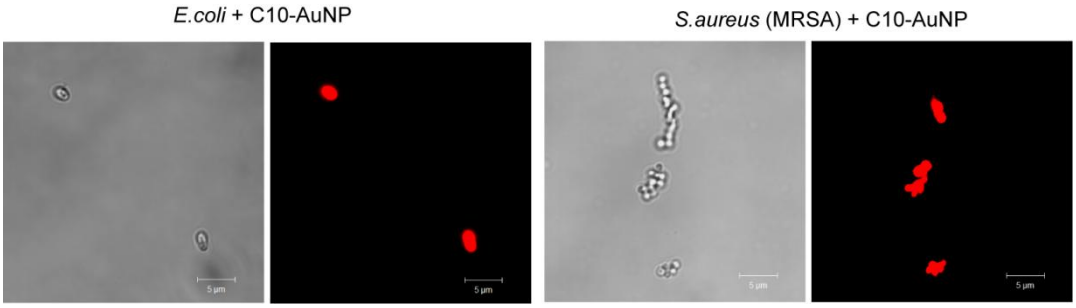

Figure 5.3. CLSM images of PI staining showing NP-induced bacterial cell membrane damage. Scale bar is 5 μm.

To study the development of bacterial resistance to C10-AuNPs, *E. coli* CD-2 was exposed to sub-MIC for sustained passages and the MIC of each passage was tested. Bacteria incubated at the sub-MIC concentrations of antibacterial agents were known to develop resistance rapidly, especially to conventional antibiotics. After 20 passages in the presence of two thirds of C10-AuNP MIC, *E. coli* remained susceptible to original MIC of 16 nM, indicating that C10-AuNP did not induce bacterial resistance as quickly as conventional antibiotics. This feature is highly valuable in design of novel antimicrobial agents, as it exhibit potential to slow the pace of bacterial resistance evolution, providing a way to control and prevent the MDR issue from the beginning.[30,31]

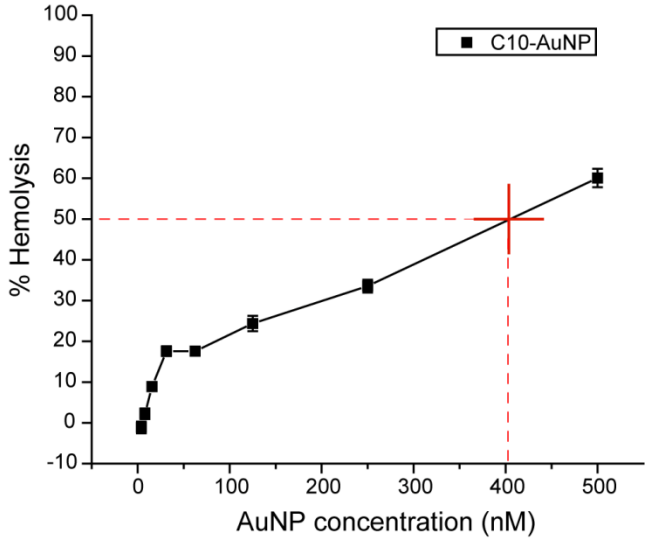

Figure 5.4. Hemolytic activity of C10-AuNPs at different concentrations. The red cross is an estimate of HC 50, the concentration to lyse 50% of human red blood cells, which turns out to be around 402 nM.

To assess the biocompatibility of our antimicrobial C10-AuNP, we performed hemolysis assay on human red blood cells as well as viability assay on mammalian cells. At all the MIC concentrations tested (in the range of 4 nM to 128 nM), C10-AuNP showed low hemolytic activity as shown in Figure 5.4. HC50, which is the concentration to lyse 50% of human red

blood cells,[32] was around 400 nM for C10-AuNP. Therefore the maximum therapeutic index of C10-AuNP, which is defined as **HC50/MIC**, was greater than 50 (402 nM/8 nM). Similarly, after treatment with C10-AuNP at all the MIC concentrations tested, NIH-3T3 mammalian cells maintained viability was moderately affected (Figure 5.5). At the MIC against the MRSA strain, this is 32 nM, the 3T3 fibroblast cell viability maintained around 80%. These studies indicated that during the time course tested, C10-NP appeared low hemolytic activity and low cytotoxicity.

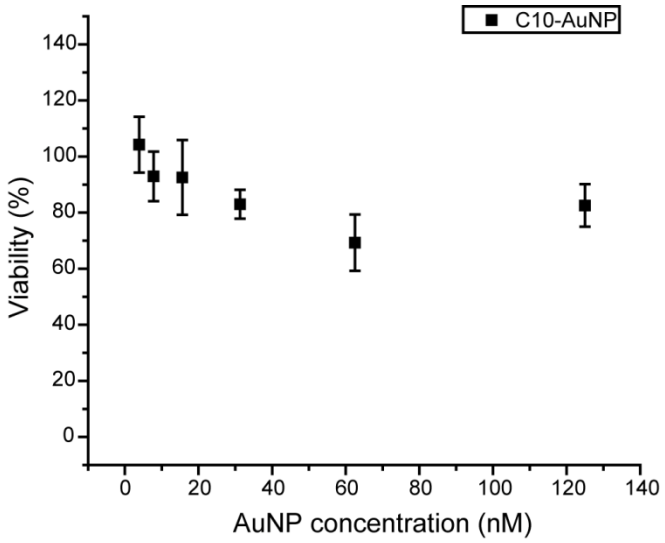

Figure 5.5. 3T3 fibroblast cell percent viability when incubated with different concentrations of C10-AuNP.

5.3 Conclusions

In this chapter, I investigate an antimicrobial strategy using self-therapeutic AuNPs to combat MDR bacteria. The cationic functionalized AuNPs effectively suppressed growth of 11 MDR clinical isolates, including both Gram-negative and Gram-positive bacteria. The NP ligand structure-activity relationship revealed that surface chemistry played an important role in AuNP antimicrobial property. Such systematic studies are promising in prediction and rational design of new antibiotic NPs. Considering the efficient antimicrobial effect on MDR bacteria, the high biocompatibility, the slow resistance developing rate, and the ease of surface modification,

functionalizing AuNPs can offer a promising alternative defense pathway to (i) combat multi-drug resistant (MDR) bacteria and (ii) lower the pace of resistance evolution by bacteria.

5.4 Experimental methods

Materials All the reagents/materials required for nanoparticle synthesis were purchased from Fisher Scientific, except for gold salt, which was obtained from Strem Chemicals Inc. The organic solvents were from Pharmco-Aaper or Fisher Scientific and used as received except for dichloromethane that was distilled in the presence of calcium hydride. NIH-3T3 cells (ATCC CRL-1658) were purchased from ATCC. Dulbecco's Modified Eagle's Medium (DMEM) (DMEM; ATCC 30-2002) and fetal bovine serum (Fisher Scientific, SH3007103) were used in cell culture.

NP synthesis 2nm diameter gold nanoparticles were synthetized by the Brust-Schiffrin two-phase methodology using pentanethiol as the stabilizer; these clusters were purified with successive extractions with ethanol and acetone. A Murray place exchange reaction was carried out in dry DCM to functionalize the nanoparticles with each ligand.[33,34] The monolayer-protected nanoparticles were redispersed in water and the excesses of ligand/pentanethiol were removed by dialysis using a 10,000 MWCO snake-skin membrane. The final concentration was measured by UV spectroscopy on a Molecular Devices SpectraMax M2 at 506nm according to the reported methodology.[35]

Determination of antimicrobial activities of cationic gold nanoparticles Bacteria were cultured in LB medium at 37 ℃ and 275 rpm till stationary phase. The cultures were then harvested by centrifugation and washed with 0.85% sodium chloride solution for three times. Concentrations of re-suspended bacterial solution were determined by optical density measured at 600 nm. M9 medium was used to make dilutions of bacterial solution to a concentration of 1×10^6 cfu/mL. 50 μL of these solutions were added into a 96-well plate and mixed with 50 μL of NP solutions in M9, giving a final bacterial concentration of 5×10^5 cfu/mL. NPs concentration

varied in half fold according to a standard protocol, ranging from 125 nM to 3.9 nM. A growth control group without NPs and a sterile control group with only growth medium were carried out at the same time. Cultures were performed in triplicates, and at least two independent experiments were repeated on different days. The MIC is defined as the lowest concentration of AuNP that inhibits visible growth as observed with the unaided eye.[23]

Propidium iodide staining assay *E. coli* CD-2 and MRSA CD-489 (1×10^8 cfu/mL) were incubated with 500 nM C10-AuNP in M9 at 37 37 ℃ and 275 rpm for three hours. The bacteria solutions were then mixed with PI (2 μM) and incubated for 30 minutes in dark. 5 μL of the samples was placed on a glass slide with a glass coverslip and observed with a confocal laser scanning microscopy, Zeiss 510 (Carl Zeiss, Jena, Germany) using a 543 nm excitation wavelength.

Resistance development *E. coli* CD-2 was inoculated in M9 medium with 10.4 nM (2/3 of 15.6 nM, MIC) at at 37 ℃ and 275 rpm for 16 hours. The culture was then harvested and tested for MIC as describe above. *E. coli* CD-2 was cultured without NP as well every time as a control for comparison of MICs.

Hemolysis assay Hemolysis assay was performed on human red blood cells as we described in previous study.[36] Briefly, citrate-stabilized human whole blood (pooled, mixed gender) was purchased from Bioreclamation LLC, NY. The red blood cells were purified and re-suspended in 10 mL phosphate buffered saline as soon as received. 0.1 mL of RBC solution was added to 0.4 mL of NP solution in PBS in 1.5 mL centrifuge tube.

The mixture was incubated at 37 ˚C, 150 rpm for 30 minutes followed by centrifugation at 4000 rpm for 5 minutes. The absorbance value of the supernatant was measured at 570 nm with absorbance at 655 nm as a reference. RBCs incubated with PBS as well as water were used as negative and positive control, respectively. All samples were prepared in triplicate. The percent hemolysis was calculated using the following formula:

% Hemolysis = ((sample absorbance-negative control absorbance)) / ((positive control absorbance-negative control absorbance)) × 100.

Mammalian cell viability assay 20,000 NIH 3T3 (ATCC CRL-1658) cells were cultured in Dulbecco's modified Eagle medium (DMEM; ATCC 30-2002) with 10% bovine calf serum and 1% antibiotics at 37 ℃ in a humidified atmosphere of 5% CO_2 for 48 hours. Old media was removed and cells were washed one time with phosphate-buffered saline (PBS) buffer before addition of NPs in the pre-warmed 10% serum containing media. Cells were incubated for 24 h at 37 ℃ under a humidified atmosphere of 5% CO2. Cell viability was determined using Alamar blue assay according to the manufacturer's protocol (Invitrogen Biosource, USA). After washing with PBS for three times, cells were treated with 220 µL of 10% alamar blue in serum containing media abd incubated at 37 ℃ under a humidified atmosphere of 5% CO2 for three hours. After incubation, 200 µL of solution from each wells was transferred in a 96-well black microplate. Red fluorescence, resulting from the reduction of Alamar blue solution, was quantified (excitation/emission: 560 nm/590 nm) on a SpectroMax M5 microplate reader (Molecular Device) to determine the cellular viability. Cells without any NPs were considered as 100% viable. Each experiment was performed in triplicates.

5.5 References

1. Neu, H. C. *Science* **1992**, *257*, 1064-1073.

2. *FY15 Detect and Protect Against Antibiotic Resistance Budget Initiative*, Centers for Disease Control and Prevention, **2003**.

3. Spellberg, B.; Powers, J. H.; Brass, E. P.; Miller, L. G.; Edwards, J. E. *Clin. Infect. Dis.* **2004**, *38*, 1279-1286.

4. Alanis, A. J. *Arch. Med. Res.* **2005,** *36*, 697-705.

5. Davis, M. E.; Chen, Z.; Shin, D. M. *Nat. Rev. Drug Discov.* **2008,** *7*, 771-782.

6. Peer, D.; Karp, J. M.; Hong, S.; FaroKhzad, O. C.; Margalit, R.; Langer, R. *Nat. Nanotech.* **2007,** *2*, 751-760.

7. De, M.; Ghosh, P. S.; Rotello, V. M. *Adv. Mater.* **2008,** *20*, 4225-4241.

8. Redl, F. X.; Black, C. T.; Papaefthymiou, G. C.; Sandstrom, R. L.; Yin, M.; Zeng, H.; Murray, C. B.; O'Brien, S. P. *J. Am. Chem. Soc.* **2004,** *126*, 14583-14599.

9. Daniel, M. C.; Astruc, D. *Chem. Rev.* **2004,** *104*, 293-346.

10. Grace, A. N.; Pandian, K.. *Colloids Surf., A* **2007,** *297*, 63-70.

11. Ahangari, A.; Salouti, M.; Heidari, Z.; Kazemizadeh, A. R.; Safari, A. A. *Drug Deliv.* **2013,** *20*, 34-39.

12. Gu, H. W.; Ho, P. L.; Tong, E.; Wang, L.; Xu, B. *Nano Lett.* **2003,** *3*, 1261-1263.

13. Rai, A.; Prabhune, A.; Perry, C. C. *J. Mater. Chem.* **2010,** *20*, 6789-6798.

14. Brown, A. N.; Smith, K.; Samuels, T. A.; Lu, J. R.; Obare, S. O.; Scott, M. E. *Appl. Environ. Microbiol.* **2012,** *78*, 2768-2774.

15. Fayaz, A. M.; Girilal, M.; Mandy, S. A.; Somsundar, S. S.; Venkatesan, R.; Kalaichelvan, P. T. *Process Biochem.* **2011,** *46*, 636-641.

16. Alekshun, M. N.; Levy, S. B. *Cell* **2007,** *128*, 1037-1050.

17. Zhao, Y. Y.; Jiang, X. Y. *Nanoscale* **2013,** *5*, 8340-8350.

18. Arvizo, R. R.; Saha, S.; Wang, E. F.; Robertson, J. D.; Bhattacharya, R.; Mukherjee, P. *Proc. Natl. Acad. Sci. U.S.A.* **2013,** *110*, 6700-6705.

19. Zhao, Y. Y.; Tian, Y.; Cui, Y.; Liu, W. W.; Ma, W. S.; Jiang, X. Y. *J. Am. Chem. Soc.* **2010,** *132*, 12349-12356.

20. Bresee, J.; Maier, K. E.; Boncella, A. E.; Melander, C.; Feldheim, D. L. *Small* **2011,** *7*, 2027-2031.

21. Connor, E. E.; Mwamuka, J.; Gole, A.; Murphy, C. J.; Wyatt, M. D. *Small* **2005**, *1*, 325-327.

22. Hayden, S. C.; Zhao, G. X.; Saha, K.; Phillips, R. L.; Li, X. N.; Miranda, O. R.; Rotello, V. M.; El-Sayed, M. A.; Schmidt-Krey, I.; Bunz, U. H. F. *J. Am. Chem. Soc.* **2012**, *134*, 6920-6923.

23. Wiegand, I.; Hilpert, K.; Hancock, R. E. W. *Nat. Protoc.* **2008**, *3*, 163-175.

24. Moyano, D. F.; Goldsmith, M.; Solfiell, D. J.; Landesman-Milo, D.; Miranda, O. R.; Peer, D.; Rotello, V. M. *J. Am. Chem. Soc.* **2012**, *134*, 3965-3967.

25. Nikaido, H. *J. Bacteriol.* **1996**, *178*, 5853-5859.

26. Hiramatsu, K.; Cui, L.; Kuroda, M.; Ito, T. *Trends. Microbiol.* **2001**, *9*, 486-493.

27. Klevens, R. M.; Morrison, M. A.; Nadle, J.; Petit, S.; Gershman, K.; Ray, S.; Harrison, L. H.; Lynfield, R.; Dumyati, G.; Townes, J. M.; Craig, A. S.; Zell, E. R.; Fosheim, G. E.; McDougal, L. K.; Carey, R. B.; Fridkin, S. K.; Investigators, A. B. M. *JAMA* **2007**, *298*, 1763-1771.

28. Boulos, L.; Prevost, M.; Barbeau, B.; Coallier, J.; Desjardins, R. *J. Microbiol. Methods* **1999**, *37*, 77-86.

29. Cox, S. D.; Mann, C. M.; Markham, J. L.; Bell, H. C.; Gustafson, J. E.; Warmington, J. R.; Wyllie, S. G. *J. Appl. Microbiol.* **2000**, *88*, 170-175.

30. Levy, S. B.; Marshall, B. *Nat. Med.* **2004**, *10*, S122-S129.

31. Davies, J.; Davies, D. *Microbiol. Mol. Biol. Rev.* **2010**, *74*, 417-433.

32. Eren, T.; Som, A.; Rennie, J. R.; Nelson, C. F.; Urgina, Y.; Nusslein, K.; Coughlin, E. B.; Tew, G. N. *Macromol. Chem. Phys.* **2008**, *209*, 516-524.

33. Miranda, O. R.; Chen, H. T.; You, C. C.; Mortenson, D. E.; Yang, X. C.; Bunz, U. H. F.; Rotello, V. M. *J. Am. Chem. Soc.* **2010**, *132*, 5285-5289.

34. De, M.; Rana, S.; Akpinar, H.; Miranda, O. R.; Arvizo, R. R.; Bunz, U. H. F.; Rotello, V. M. *Nat. Chem.* **2009**, *1*, 461-465.

35. Liu, X. O.; Atwater, M.; Wang, J. H.; Huo, Q. *Colloid. Surface. B* **2007**, *58*, 3-7.

36. Saha, K. M., D. F.; Rotello, V. M. *Mater. Horiz.* **2014**, *1*, 102-105.

CHAPTER 6

SURFACE FUNCTIONALITY CONTROLLED NP PENETRATION INTO BACTERIAL BIOFILMS

6.1 Introduction

Bacterial biofilm formation plays an important role in many persistent diseases[1] and medical device-associated infections.[2] These infections are particular challenging, as biofilm bacteria are mostly embedded in and protected by the sticky and strong framework fabricated by extracellular polymeric substances (EPS).[3] The EPS matrix possesses complex composition, architecture, and dynamic function, which is believed to result in high resistance to antibiotics.[4] For efficient treatment of biofilm-associated infections, it is crucial to understand how the complex biofilms and biofilm EPS interact with therapeutic agents, especially with novel candidate materials for alternative treatment approach.

One of the protective properties of EPS comes from its barrier characteristics, which can profoundly impede the penetration of antibiotics.[5] Moreover, EPS is capable of deactivating antibiotics in the surface layers more rapidly than they diffuse, causing limited penetration.[6] The failure of antibiotics to penetrate the full depth of biofilms is one mechanism behind the biofilm resistance.[7] Novel materials such as engineered nanoparticles (NPs) possess strong permeating ability into cells,[8] tumors,[9] and even blood-brain barrier,[10] presenting a potentially powerful vehicle to infiltrate the biofilm EPS barrier.[11] In addition, the surface functionality of NPs has been demonstrated to determine their interactions with biomolecules and cells.[12] Therefore, tailoring the surface chemistry makes NP a controllable probe for study on biofilm EPS interaction with engineered materials.

In this chapter, I report here a study of quantum dots (QDs) as a model fluorescent NP to explore the possibility of penetration into biofilms. QDs functionalized with different charges and head functional groups were used to systematically investigate the role of surface chemistry in

QD penetration and distribution inside biofilms. The results show that cationic QDs can penetrate fully into biofilms but neutral and anionic QDs cannot. In addition to the charge effect, NP surface hydrophobicity regulates the homogeneity of NP distribution within boifilms. Our studies demonstrate that control of surface functionality on NP surface provides an effective approach to predict the NP behavior in biofilms (Figure 6.1). These results have been written in a manuscript ready for submission.

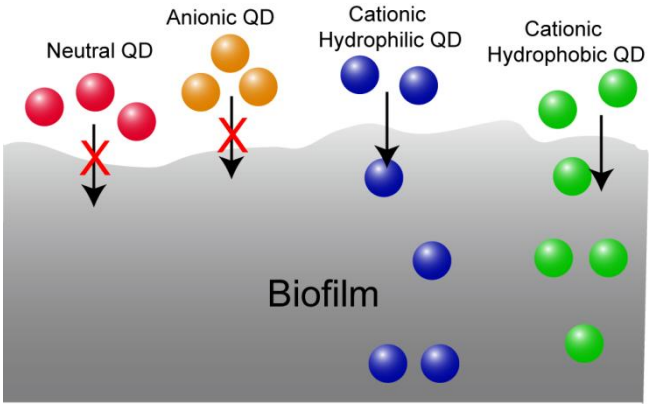

Figure 6.1. Schematic illustration of surface functionality controlled QD penetration into biofilms. Neutral and anionic QDs cannot penetrate into *E. coli* biofilms, but cationic QDs can.

6.2 Results and discussion

Green fluorescent CdSe/ZnS core-shell QDs (emission at 535 nm) were used to prepare water soluble QDs through a ligand exchange proces.[13] Dithiolate ligands[14] presenting different functional head groups were synthesized for QD surface functionalization. The design of ligands features a dihydrolipoic acid (DHLA) bidentate anchor, an oligo(ethylene glycol) (OEG) spacer and a tunable functional head group.[15] The terminal functionalities of the ligands were designed with different surface charges (i.e., neutral, anionic, and cationic). Additionally, two types of cationic ligands were synthesized to incorporate different hydrophobicity on the cationic head groups. As shown in Figure 6.2 a, the neutral QDs (PEG-QDs) were prepared by using the poly(ethelene glycol)-appended DHLA ligands, and the charged QDs were synthesized with different functionalities including carboxyl terminus (COOH-QD), trimethyl ammonium terminus

(TTMA-QD), and dimethylhexyl ammonium terminus (Hexyl-QD). The absorption peak positions of these QDs were very similar while the emission peaks showed modest differences, as is commonly observed after surface modification.[16,17] Dynamic light scattering data indicated that PEG-QD had slightly larger hydrodynamic size of 24 nm, while the other three QDs had comparable sizes, ranging from 7.5 to 11.7 nm(Figure 6.2 b).

a

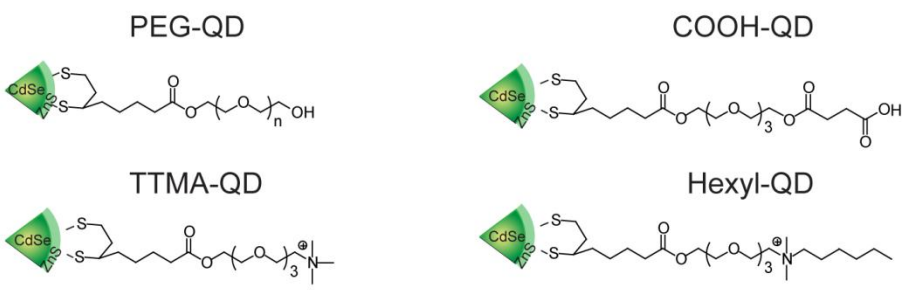

b

QDs	Absorption peak (nm)	Emission peak (nm)	Hydrodynamic diameter (nm)	Zeta potential (mV)
PEG-QD	536	550	24.4 ± 8.8	-8.0 ± 7.3
COOH-QD	540	562	11.7 ± 4.2	-29.5 ± 16.3
TTMA-QD	536	550	8.7 ± 3.0	+26.8 ± 3.2
Hexyl-QD	538	558	7.5 ± 2.0	+26.0 ± 3.8

Figure 6.2. a. Molecular structure of functionalized QD surface ligands. PEG-QD is neutral, COOH-QD is anionic, and TTMA-QD and Hexyl-QD are cationic. **b.** Physical properties of functionalized QDs.

Biofilms were produced on glass cover slips for microscopic study purpose. *E.coli* strain DH5α that expresses E2-crimson, a bright far-red fluorescent protein (emission peak at 646 nm), was chosen as a model strain for our study. The biofilms were cultured in a 1/10 strength LB broth supplemented with 100 μM IPTG (isopropyl β-D-1-thiogalactopyranoside) according to a reported protocol.[18]The penetration experiments were performed on three-day old biofilms for one hour incubation with QDs. The cover slips were mounted on glass slides using 4% anti-fade mounting solution and examined by confocal laser scanning microscopy (CLSM).

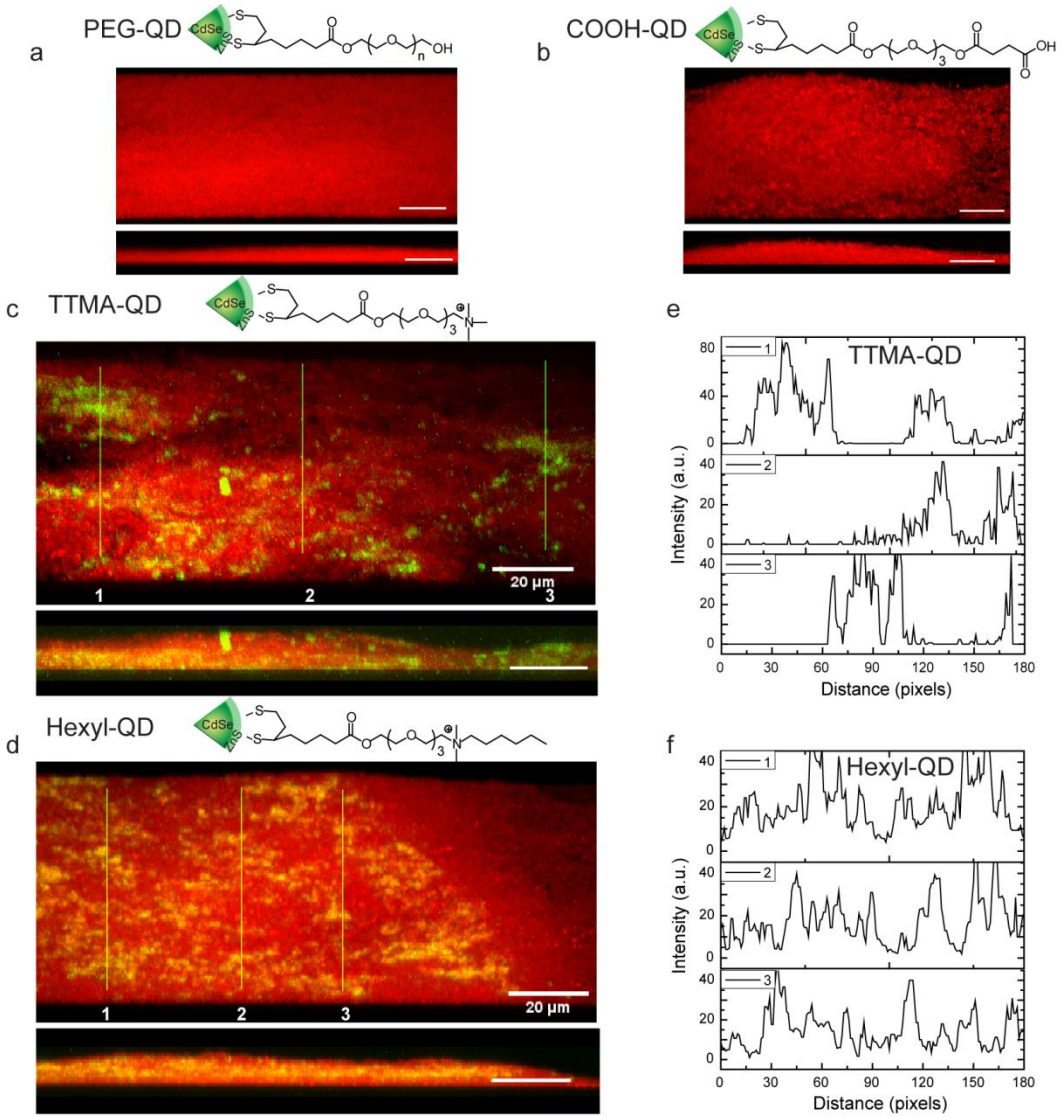

Figure 6.3. Representative 3D projection of image z-stacks showing distribution of bacterial cells (red) in *E.coli* biofilms and QDs (green): **a**, PEG-QD; **b**, COOH-QD; **c**, TTMA-QD; **d**, Hexyl-QD. Upper panels are projections at 247 °angle turning along Y axis and lower panels are at 270 ° angle turning along Y axis. Scale bar is 20 µm. **e** and **f** are plot profiles of the three linear selection (yellow lines) in **c** and **d**, illustrating horizontal distribution of **e** TTMA-QD and **f** Hexyl-QD.

The CLSM images were obtained using two different fluorescent channels to detect bacterial cells (red fluorescence) and QDs (green fluorescence) simultaneously. Figure 6.3 shows the 3D projection of images from a single z-stack to illustrate the overall contribution of QDs to the biofilms. In the case of PEG-QD and COOH-QD, there was no pronounced green fluorescence observed either on surface or inside the biofilms (Figure 6.3 a and b), indicating no

QD penetration during the one hour incubation. The absence of neutral and negative QDs on the surface of biofilms was likely due to loose absorption of QDs that was mostly disrupted during the washing step. However, Figure 6.3 c and d both display strong green fluorescence from QDs throughout the biofilms, indicating the cationic QDs, i.e., TTMA-QD and Hexyl-QD, associated with and penetrated into the biofilms. This finding is surprising, since it is reasonable to expect the cationic QDs interact with and stick to the negatively charged biofilm EPS and remain in the top layers instead of going deeper, but it is in agreement with previous reports where cationic NPs were shown to have a better penetration into negative matrix than anionic NPs.[19,20] Furthermore, the different penetration patterns of these two cationic QDs were demonstrated by the projected sample images at 270 ° angle turning along Y axis (Figure 6.3 c and d lower panel). TTMA-QD scattered from top layers to bottom layers and accumulated near the bottom of the biofilms while Hexyl-QD was more concentrated at middle layers.

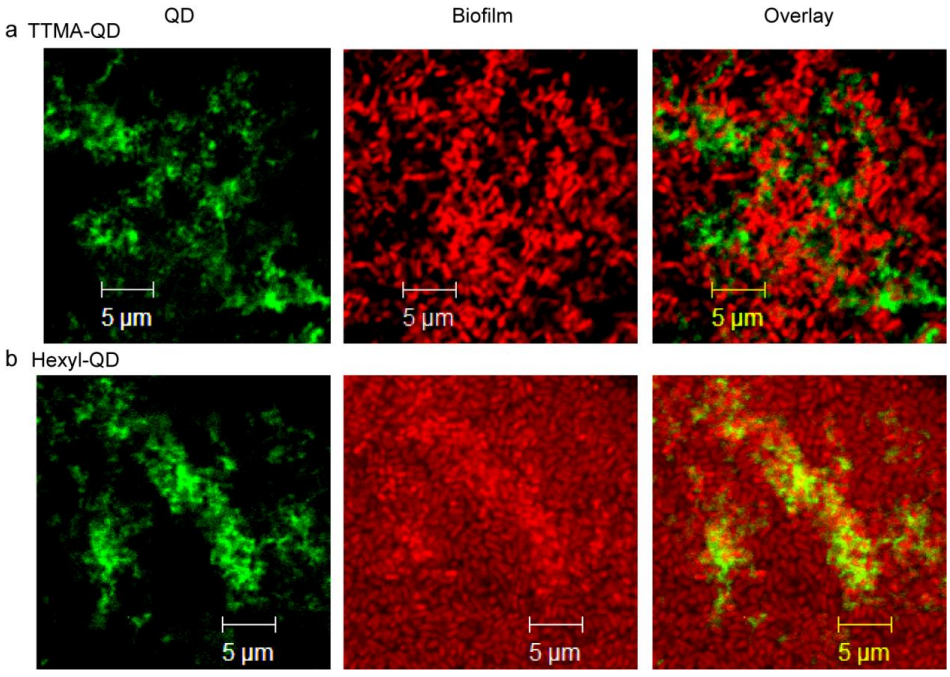

Figure 6.4. Zoomed CLSM images of biofilms after 1hr incubation with QDs, showing association sites of **a** TTMA-QD and **b** Hexyl-QD. The scale bar is 5 µm.

In addition to the penetration pattern across the biofilm depth, the localization of the TTMA-QD and Hexyl-QD was different as shown in the CLSM images. TTMA-QDs were not

colocalized with the red fluorescence from the bacteria in the biofilms (Figure 6.4 a), implying QD association with EPS. Hexyl-QDs were mostly colocalized with the red fluorescence and closely associated to bacterial cells (Figure 6.4 b). Two possible causes for the different association sites of the two QDs can be suggested: first, it could be a result from varying binding affinities of the QD head groups to different biofilm components, marking different hydrophilic/hydrophobic domains of biofilms; second, the NP surface functionality could lead to different extracellular diffusion and uptake rates,[9] and in this case, TTMA-QDs diffused faster than being uptaken by bacterial cells, resulting in heterogeneous distribution in blocks of EPS (Figure 6.3 c and e, whereas Hexyl-QDs were uptaken faster than diffusion, giving a homogeneous dispersion horizontally (Figure 6.3 d and f and concentrated localization in the middle layers of biofilms. This observation suggests that rational design of NP surface can facilitate selective targeting of biofilm components, for example, EPS matrix, for delivery of enzymes to disassociate EPS and induce dispersion of biofilms; or biofilm bacterial cell for delivery of antibiotics to kill biofilm bacteria.

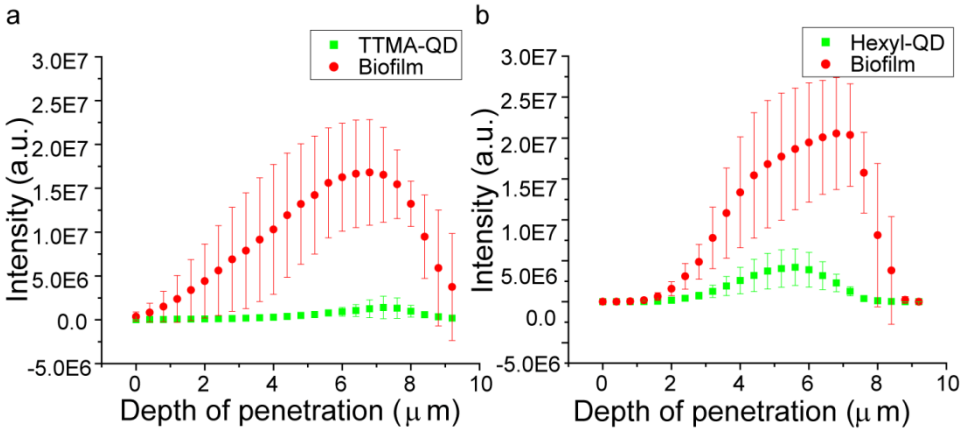

Figure 6.5. Integrated intensity of **a** TTMA-QD and biofilm and **b** Hexyl-QD and biofilm after 1hr incubation. The y-axis, normalized intensity, is the integrated QD intensity normalized by the integrated biofilm intensity. The x-axis is the depth of penetration of biofilms, where 0 μm represents the top and 10 μm represents the bottom. The data are average of three image stacks. Error bars are standard deviation.

To investigate the penetration profiles of the two cationic QDs, three stacks of CLSM images taken at random locations were analyzed using ImageJ. For every slice in one image stack,

the green and red channels were separated and then analyzed for integrated intensity within a fixed 512×512 frame. The integrated intensity from the green and red channel hence represented the intensity of QDs and bacteria in the biofilms, respectively. The integrated intensity from both channels was plotted versus the biofilm depth to illustrate the distribution of biofilms and QDs. Both TTMA-QD and Hexyl-QD were present at 7.2 μm biofilm depth, which displayed the average highest area coverage, representing the very bottom layer of biofilms (Figure 6.5 a and b). This result reveals that both QDs penetrated the full biofilm depth.

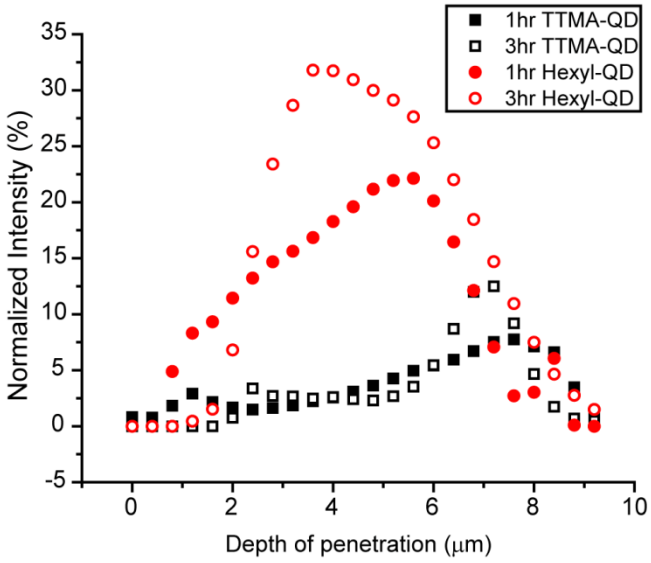

Figure 6.6. The penetration profile of TTMA-QD 1hr (square, solid), Hexyl-QD 1hr (circle, solid), TTMA-QD 3hr (square, empty), and Hexyl-QD 3hr (circle, empty). The y-axis, normalized intensity, is the integrated QD intensity normalized by the integrated biofilm intensity. The x-axis is the depth of penetration of biofilms, where 0 μm represents the top and 10 μm represents the bottom. The data are average of three image stacks.

The biofilm 3D architecture is inherently heterogeneous, causing the biofilm mass distribution vary among the three image stacks. Thus the integrated QD intensity was normalized by the biofilm intensity at the same step was plotted versus the biofilm depth. In Figure 6.6, TTMA-QD presented a relatively even dispersion along the vertical direction of biofilms and the highest density at 7.2 μm. Hexyl-QD, however, exhibited a different pattern in which the density increased till a peak value around 4.4 μm and then decreased. Moreover, Figure 6.6 indicates that

Hexyl-QD had an overall higher density than TTMA-QD. The QD penetration profiles were further investigated after a longer incubation time. No significant change of distribution was observed for both QDs after different incubation periods (Figure 6.6). This result indicates that the penetration of these two QDs occurred rapidly and reached a stabilized state within one hour.

6.3 Conclusions

In summary, we employed functionalized QDs to demonstrate that by engineering surface properties NPs can be tailored to penetrate biofilms. The engineered NPs provide a promising scaffold to effectively protect and carry antibiotics through the EPS barrier. Furthermore, NPs may be engineered to possess antimicrobial characteristics, attributing as antimicrobial agents themselves upon penetration.

Nanotechnology has attracted much attention and number of studies on how to utilize nanomaterials as novel antimicrobial agents has intensively increased. However, the interaction between nanomaterials and microorganisms is a fundamental question that is needed to be answered for application purpose. As an extension of bacterial life, biofilms have been taken into consideration when testing nanoparticle antimicrobial properties. This study not only provides a methodology for easy visualization of such material interaction with biofilms, but also reveals the important factors in regulation of such interactions.

Taken together, by accommodating surface functionality to infiltrate biofilms, it provides a new exciting strategy for designing NPs to penetrate biofilms and to combat biofilm resistance, offering a potential approach for a low-stress, surgery-free, and efficient treatment of biofilm-associated infections.

6.4 Experimental methods

Materials All chemicals were purchased from Sigma-Aldrich unless otherwise stated. The organic solvents were bought from Fisher and used as received while dichloromethane

(DCM) was distilled in the presence of calcium hydride. Flash column chromatography was performed for purification using silica gel (SiO_2, particle size 40-63 μm). Milli-Q water from a Millipore Simplicity 185 system (Millipore Corp., Billerica, MA) was also used to prepare samples.

Synthesis of water soluble ligands The syntheses of **DHLA-PEG-OH** and **DHLA-TEG-N$(CH_3)_2$-R_n** ligands have been reported in the published literature.[21] **DHLA-TEG-COOH** ligands were synthesized in a stepwise procedure (Figure 6.7 b). Briefly, Compound **1** (2 g, 5.2 mmol) was dissolved in 30 ml dry THF (30 ml). DMAP (0.64 g, 5.2 mmol) and DIPEA (0.67 g, 5.2 mmol) were added to the solution and stirred for 5 mins. Succinic anhydride (1.57 g, 15.6 mmol) was added to the solution and stirred for 24 h at room temperature. The reaction mixture was evaporated under reduced pressure to remove the solvent, and further diluted with water and extracted with DCM. Compound **2** was obtained by using column chromatography with 100 % EtOAc as eluent. $NaBH_4$ was used to reduce the disulfide bond to obtain the final product **DHLA-TEG-COOH**.

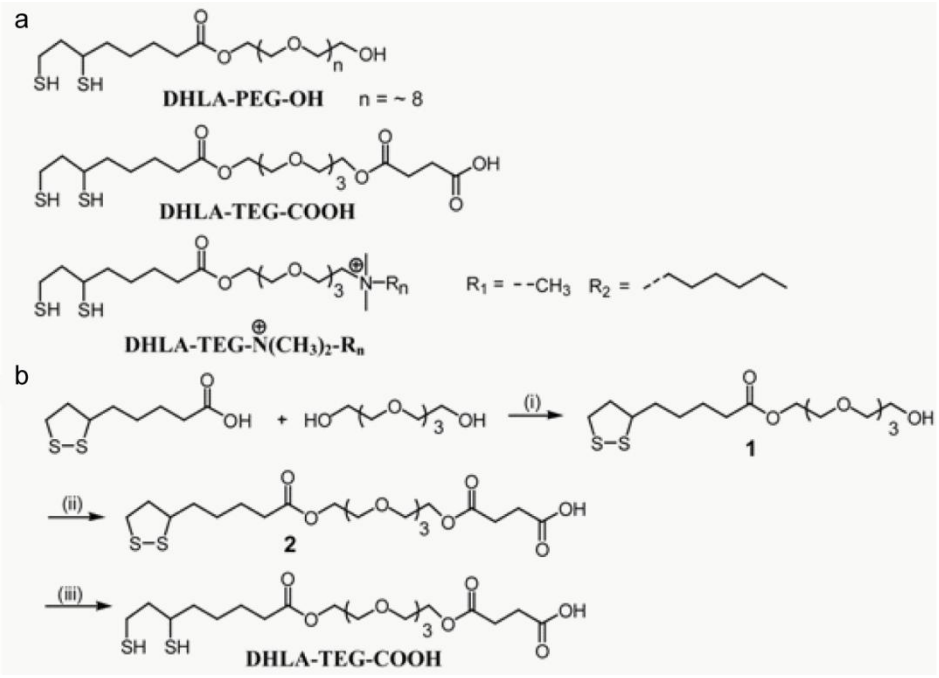

Figure 6.7. a. Structures of the ligands used in the studies. **b.** Synthetic route of **DHLA-TEG-COOH** ligand. Reagents and conditions: (i) EDC, HOBt, DIPEA, DCM, r.t., 24 h; (ii) DMAP, DIPEA, succinic anhydride, THF, r.t., 24 h; (iii) $NaBH_4$, EtOH/ H_2O, r.t., 1 h

^{1}H NMR (400 MHz, $CDCl_3$) of **DHLA-TEG-COOH**: δ 4.24 (t, 4H, COO-C$\underline{H}_2$-CH_2 and CH_2-C$\underline{H}_2$-OOC-) 3.74-3.62 (m, 12H, -CH_2-*TEG*-), 2.59-2.51 (brm, 2H, COO-CH_2-C$\underline{H}_2$-COOH), 2.47-2.40 (brm, 2H, COO-C$\underline{H}_2$-CH_2-COOH), 2.36 (t, 2H, CH_2-C$\underline{H}_2$-COO), 1.75-1.62 (m, 4H), 1.58-1.39 (m, 2H).

Preparation of water soluble QDs CdSe/ZnS core-shell QDs were synthesized according to the reported procedure. The preparations of PEG-QDs and COOH-QDs were through a ligand exchange process.[21] DHLA-PEG-OH or DHLA-TEG-COOH ligands have placed in DCM under ligand to hydrophobic trioctylphosphine oxide/trioctylphosphine (TOPO/TOP)-capped QDs ratio by weight (3: 1), and the solution was stirred at 35 ^oC for 24 h. After 24 h of stirring, DCM was evaporated and the resultant QDs were dispersed in Milli-Q water and purified by dialysis. The preparation of cationic QD (i.e., TTMA-QDs and Hexyl-QDs) was through a two-step ligand exchange reaction. Briefly, hydrophobic TOPO/TOP-capped QDs were mixed with amphiphilic HS-$(CH_2)_5$-TEG-OH ligands in MeOH and the reaction mixture was stirred at 35 ^oC for 24 h. Next step involved the purification of amphiphilic QDs with hexane and the addition of DHLA-TEG-N$(CH_3)_2$-R_n ligands to the amphiphilic QDs in MeOH. After 24 h of stirring, MeOH was evaporated and the dithiolate cationic QDs were dispersed in Milli-Q water and purified by dialysis.

DLS and zeta potential DLS experiments and zeta potential measurements were performed using a Malvern Zetasizer (Nano series, Malvern Instruments Inc, USA). Samples were sonicated and filtered with 0.2 μm syringe filter before measurement.

Biofilm culture Bacteria were inoculated in 3 mL LB broth and grown to stationary phase at 37 ℃. The cultures were then diluted 1:100 in a 1/10 strength LB broth supplemented with 100 μM IPTG (isopropyl β-D-1-thiogalactopyranoside). 25 mL of the dilution was

transferred into a petri dish containing six sterile glass cover slips (22 × 22 mm). The petri dish was kept at 25 ℃ and the biofilms were allowed to grow for three days. In general, the cover slips with biofilms were rinsed in deionized water for three times before placed in QD solutions. The biofilms were incubated in 300 nM QD solutions and free QDs were washed away by rinsing in deionized water for three times.

CLSM image The CLSM images were obtained using Zeiss510 META. The green fluorescent channel was collected at 488/505-550 bad pass and the red fluorescent channel was collected at 543/560 longpass.

6.5 Supplementary information

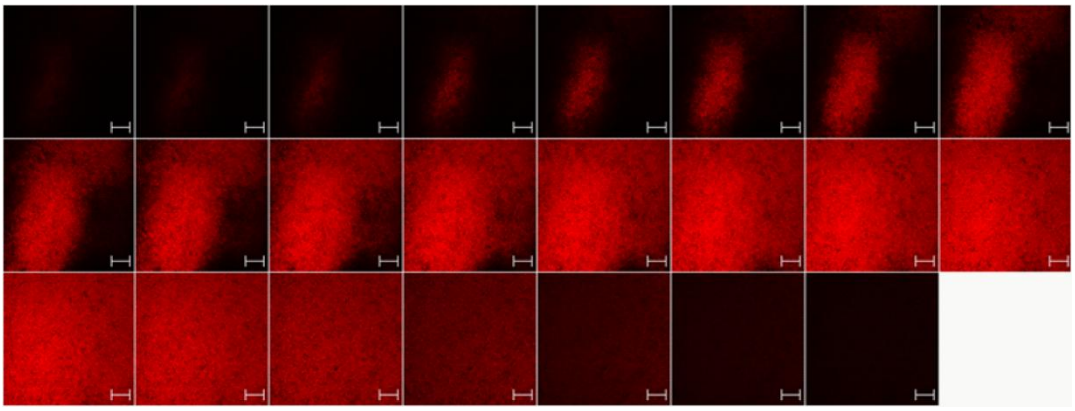

Figure 6.S1. Representative CLSM image slices of z-stack with a 0.4 μm interval showing bacterial cells (red) in *E.coli* biofilms and distribution of PEG-QD. The 3D projection of these slices is displayed in Figure 6.3 a. for a clear demonstration. The absence of green fluorescence from PEG-QD indicates no neutral QD absorbance or penetration occurred within the one hour incubation time. The scale bar is 20 μm.

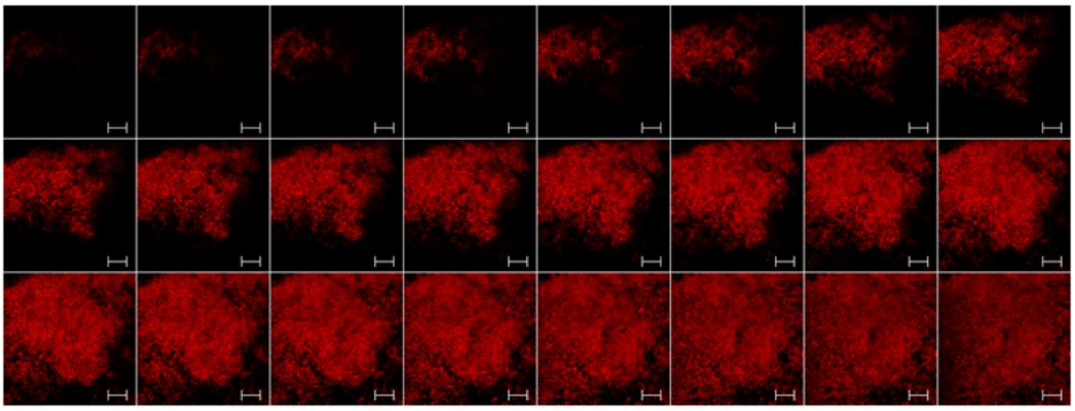

Figure 6.S2. Representative CLSM image slices of z-stack with a 0.4 μm interval showing bacterial cells (red) in E.coli biofilms and distribution of COOH-QD. The 3D projection of these slices is displayed in Figure 6.3 b. for a clearer demonstration. The absence of green fluorescence from COOH-QD indicates no anionic QD absorbance or penetration occurred within the one hour incubation time. The scale bar is 20 μm.

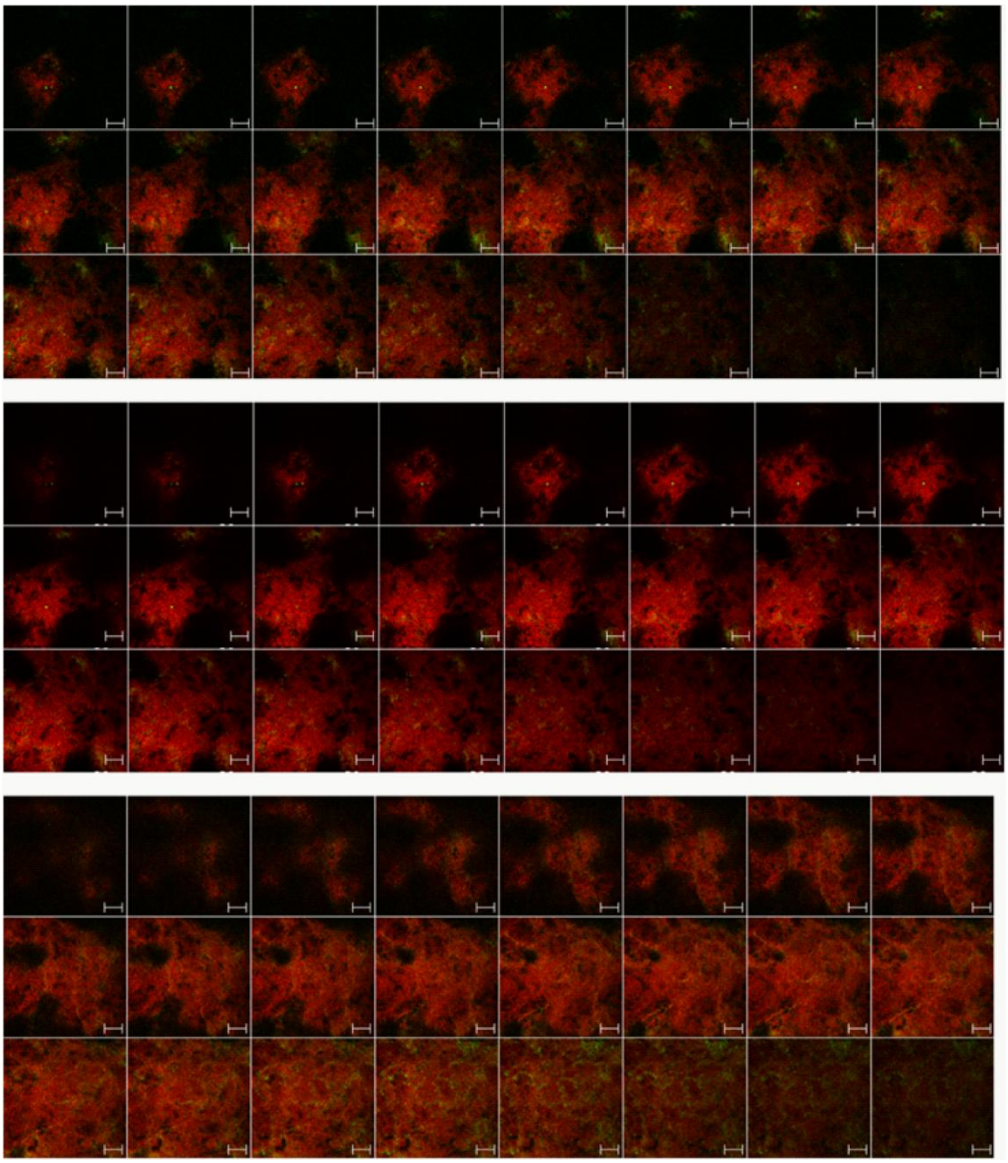

Figure 6.S3. CLSM image stacks used for analysis of TTMA-QD penetration profile after 1 hr incubation. The scale bar in these images is 20 μm.

In analysis, each image slice is split into green channel and red channel. The green channel represents QD distribution, and the integrated intensity is obtained in ImageJ. The red channel represents biofilm distribution, and the integrated intensity is also obtained in Image J. At each depth, values from these three stacks were averaged. The green channel mean integrated intensity values and the red channel mean integrated intensity values were plotted versus the

biofilm depth to make Figure 6.5 a. The green channel mean value was normalized by the mean value from red channel to make Figure 6.6.

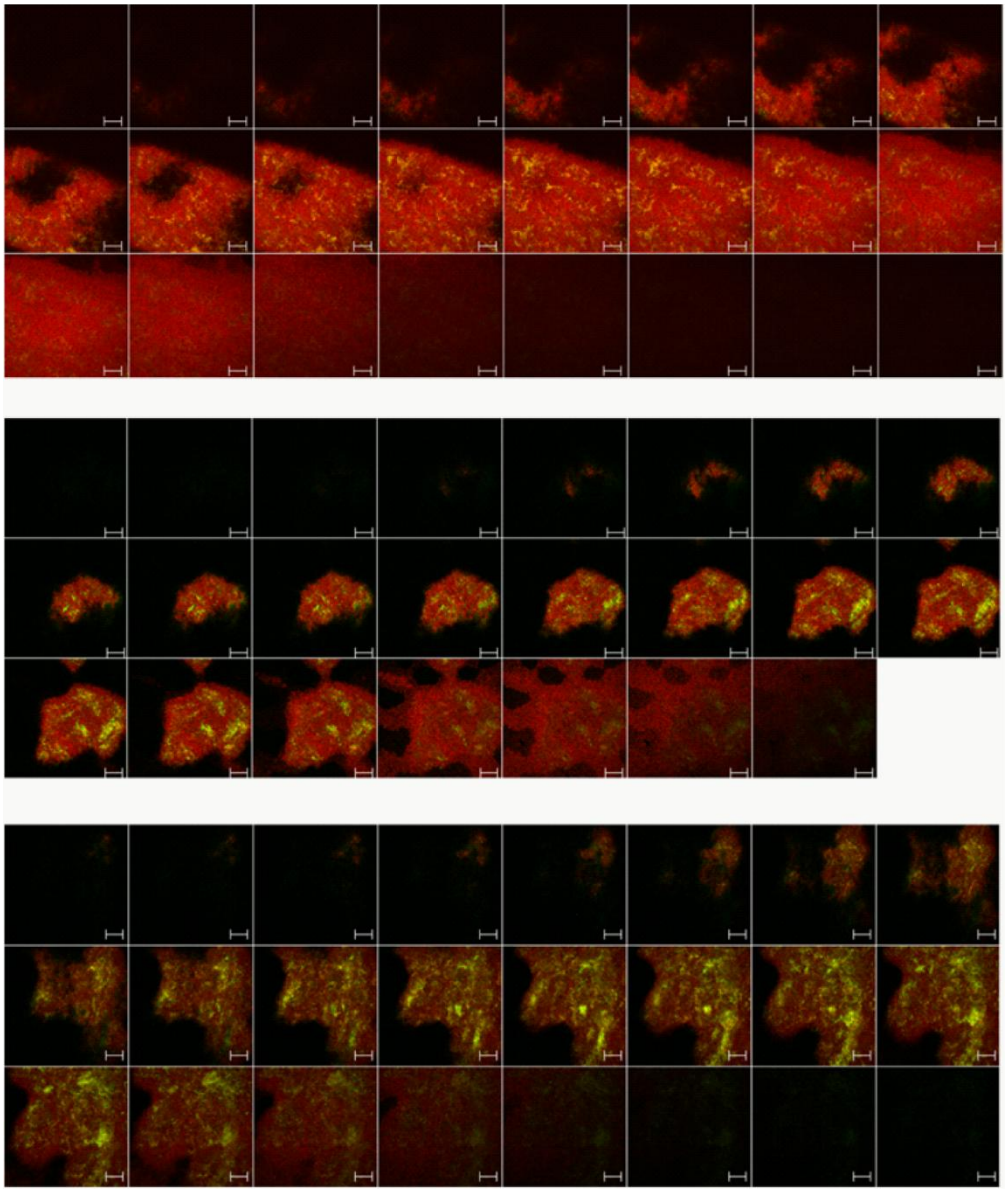

Figure 6.S4. CLSM image stacks used for analysis of Hexyl-QD penetration profile after 1 hr incubation. The scale bar in these images is 20 μm.

In analysis, each image slice is split into green channel and red channel. The green channel represents QD distribution, and the integrated intensity is obtained in ImageJ. The red channel represents biofilm distribution, and the integrated intensity is also obtained in Image J. At each depth, values from these three stacks were averaged and the mean value was plotted versus

the biofilm depth. The green channel mean integrated intensity values and the red channel mean integrated intensity values were plotted versus the biofilm depth to make Figure 6.5 b. The green channel mean value was normalized by the mean value from red channel to make Figure 6.6.

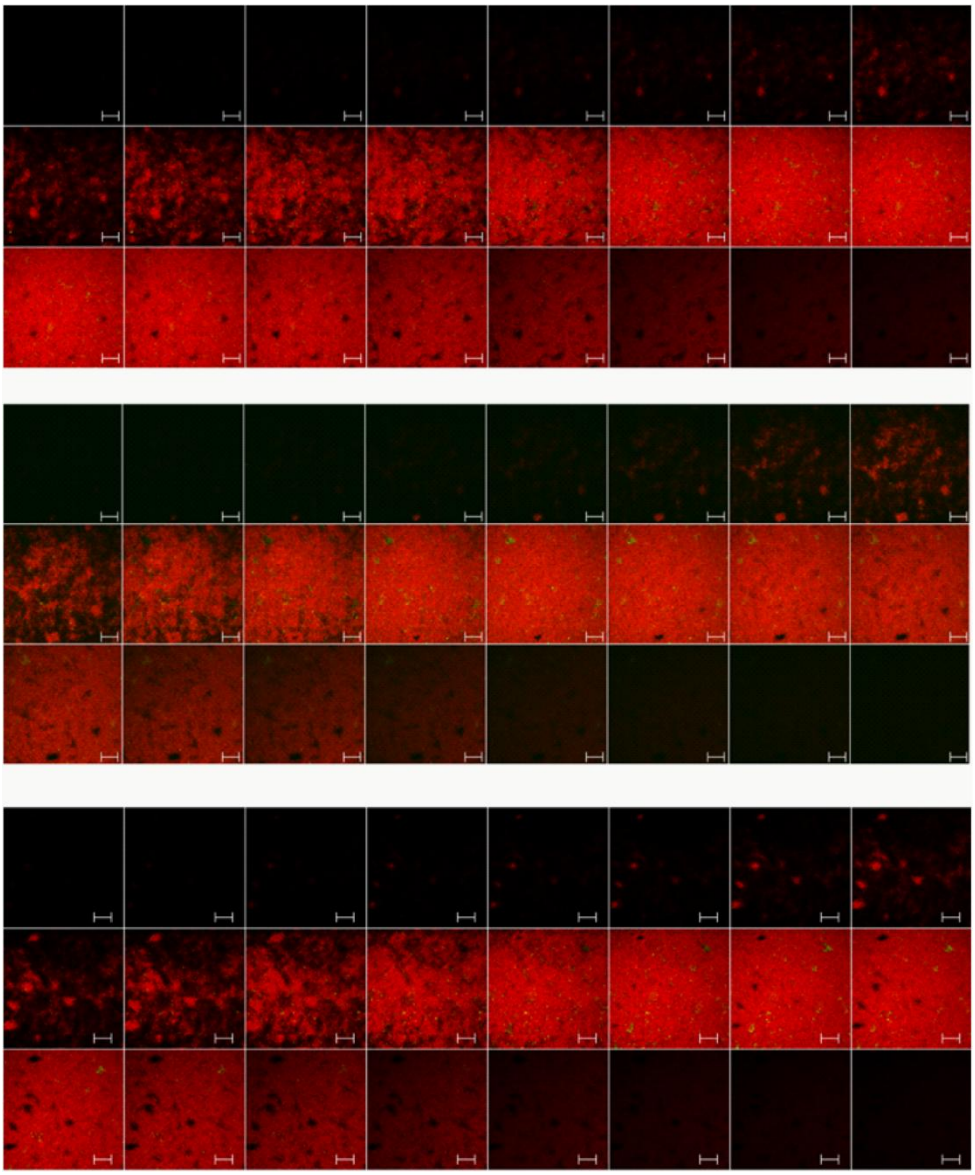

Figure 6.S5. CLSM image stacks used for analysis of TTMA-QD penetration profile after 3 hr incubation. The scale bar in these images is 20 μm.

In analysis, each image slice is split into green channel and red channel. The green channel represents QD distribution, and the integrated intensity is obtained in ImageJ. The red channel represents biofilm distribution, and the integrated intensity is also obtained in Image J. At

each depth, values from these three stacks were averaged and the mean value was plotted versus the biofilm depth. The green channel mean value was normalized by the mean value from red channel to make Figure 6.6.

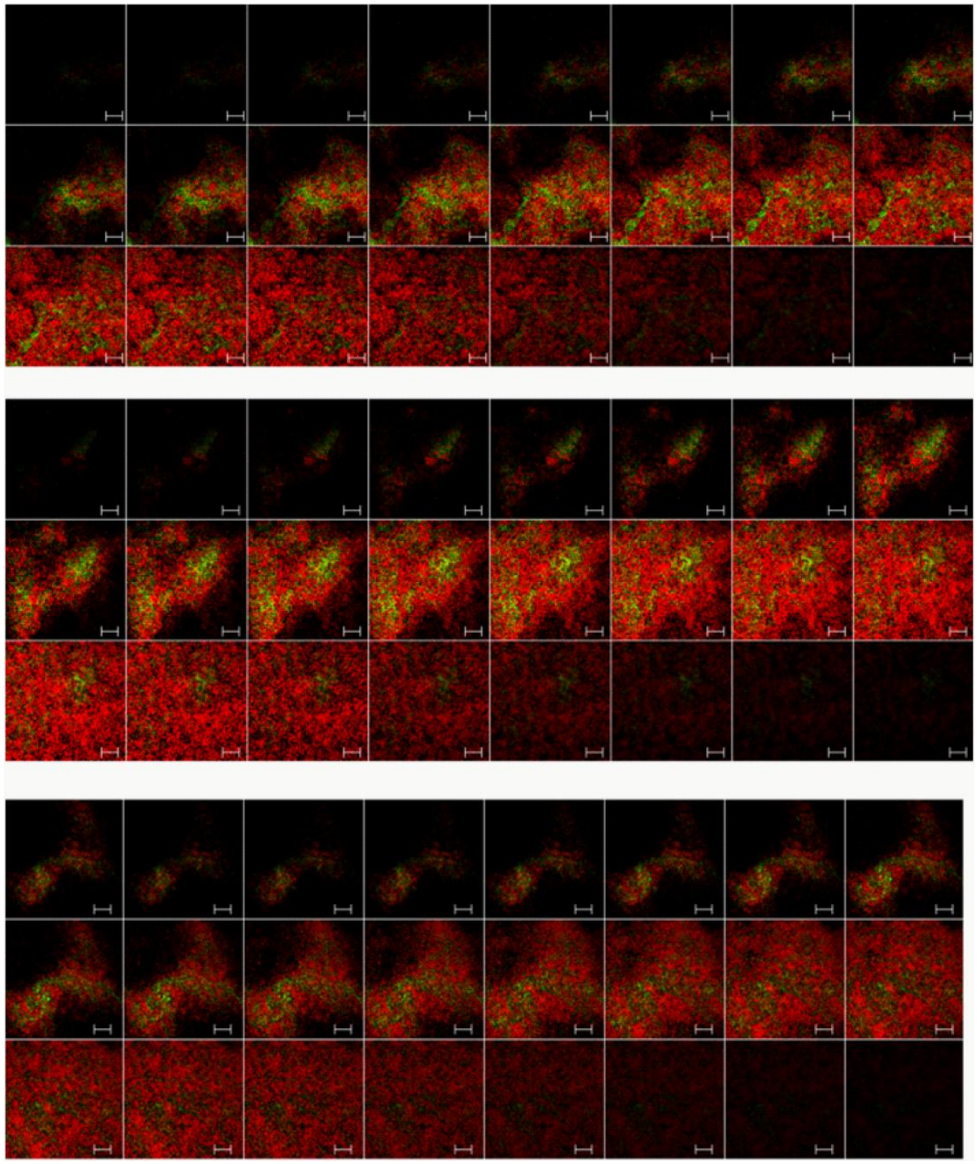

Figure 6.S6. CLSM image stacks used for analysis of Hexyl-QD penetration profile after 3 hr incubation. The scale bar in these images is 20 μm.

In analysis, each image slice is split into green channel and red channel. The green channel represents QD distribution, and the integrated intensity is obtained in ImageJ. The red

channel represents biofilm distribution, and the integrated intensity is also obtained in Image J. At each depth, values from these three stacks were averaged and the mean value was plotted versus the biofilm depth. The green channel mean value was normalized by the mean value from red channel to make Figure 6.6.

6.6 References

1. (a) Hall-Stoodley, L.; Costerton, J. W.; Stoodley, P. *Nat. Rev. Microbiol.* **2004**, *2*, 95-108. (b) Donlan, R. M. *Emerg. Infect. Dis.* **2002**, *8*, 881-890. (c) James, G. A.; Swogger, E.; Wolcott, R.; Pulcini, E. D.; Secor, P.; Sestrich, J.; Costerton, J. W.; Stewart, P. S. *Wound Repair Regen.* **2008**, *16*, 37-44.

2. (a) Costerton, J. W.; Stewart, P. S.; Greenberg, E. P. *Science* **1999**, *284*, 1318-1322. (b) . Donlan, R. M. *Emerg. Infect. Dis.* **2001**, *7*, 277-281. (c) van de Belt, H.; Neut, D.; Schenk, W.; van Horn, J. R.; van der Mei, H. C.; Busscher, H. J. *Acta Orthop. Scand.* **2001**, *72*, 557-571.

3. Flemming, H. C.; Neu, T. R.; Wozniak, D. J. *J. Bacteriol.* **2007**, *189*, 7945-7947.

4. Romling, U.; Balsalobre, C. *J. Intern. Med.* **2012**, *272*, 541-561.

5. (a) Kumon, H.; Tomochika, K.; Matunaga, T.; Ogawa, M.; Ohmori, H. *Microbiol. Immunol.* **1994**, *38*, 615-619. (b) Shigeta, M.; Tanaka, G.; Komatsuzawa, H.; Sugai, M.; Suginaka, H.; Usui, T. *Chemotherapy* **1997**, *43*, 340-345.

6. Anderl, J. N.; Franklin, M. J.; Stewart, P. S. *Antimicrob. Agents Chemother.* **2000**, *44*, 1818-1824.

7. Stewart, P. S.; Costerton, J. W. *Lancet* **2001**, *358*, 135-138.

8. Slowing, II; Vivero-Escoto, J. L.; Wu, C. W.; Lin, V. S. Y. *Adv. Drug Delivery Rev.* **2008**, *60*, 1278-1288.

9. Kim, B.; Han, G.; Toley, B. J.; Kim, C. K.; Rotello, V. M.; Forbes, N. S. *Nat. Nanotech.* **2010**, *5*, 465-472.

10. Lockman, P. R.; Mumper, R. J.; Khan, M. A.; Allen, D. D. *Drug Dev. Ind. Pharm.* **2002**, *28*, 1-13.

11. Morrow, J. B.; Arango, C.; Holbrook, R. D. *J. Environ. Qual.* **2010**, *39*, 1934-1941.

12. (a) Verma, A.; Uzun, O.; Hu, Y. H.; Hu, Y.; Han, H. S.; Watson, N.; Chen, S. L.; Irvine, D. J.; Stellacci, F. *Nat. Mater.* **2008**, *7*, 588-595. (b) Saha, K.; Bajaj, A.; Duncan, B.; Rotello, V. M. *Small* **2011**, *7*, 1903-1918.

13. Yeh, Y. C.; Patra, D.; Yan, B.; Saha, K.; Miranda, O. R.; Kim, C. K.; Rotello, V. M. *Chem. Commun.* **2011**, *47*, 3069-3071.

14. Susumu, K.; Uyeda, H. T.; Medintz, I. L.; Pons, T.; Delehanty, J. B.; Mattoussi, H. *J. Am. Chem. Soc.* **2007**, *129*, 13987-13996.

15. Moyano, D. F.; Rotello, V. M. *Langmuir* **2011**, *27*, 10376-10385.

16. Leatherdale, C. A.; Bawendi, M. G. *Phys. Rev. B* **2001**, *63*.

17. Jin, T.; Fujii, F.; Yamada, E.; Nodasaka, Y.; Kinjo, M. *J. Am. Chem. Soc.* **2006**, *128*, 9288-9289.

18. Merritt, J. H.; Kadouri, D. E.; O'Toole, G. A. *Curr. Protoc. Microbiol.* **2005**, *1B*, 1.1.

19. Lin, J. Q.; Zhang, H. W.; Chen, Z.; Zheng, Y. G. *Acs Nano* **2010**, *4*, 5421-5429.

20. Ryman-Rasmussen, J. P.; Riviere, J. E.; Monteiro-Riviere, N. A. *Toxicol. Sci.* **2006**, *91*, 159-165.

21 Uyeda, H. T.; Medintz, I. L.; Jaiswal, J. K.; Simon, S. M.; Mattoussi, H. *J. Am. Chem. Soc.* **2005**, *127*, 3870-3878.

CHAPTER 7

ANTIMICROBIAL GOLD NANOPARTICLES FOR INHIBITION AND REMOVAL OF BACTERIAL BIOFILMS

7.1 Introduction

Clinical practice that deals with device-related and other chronic bacterial infection increasingly faces a new type of infectious disease, which is quite distinguished from acute bacterial infection. Compared to acute infections, these diseases are much less aggressive, and they often progress through periods of latency alternating with periods of acute exacerbation, persisting for months or years. These chronic infections are found to be associated with bacterial biofilm.[1, 2] For example, infectious diseases such as native valve endocarditis, otitis media, periodontitis, and chronic wounds appear to be caused by biofilm-associated microorganisms.[3] Biofilms are also responsible for infections on implants and indwelling medical devices, including replacement joints, prosthetic heart valves, and urinary catheters.[4] Biofilm infections are chronic with a low-grade immune response and thus are rarely resolved by the host defense mechanism.[5] Despite the relief during the exacerbation periods provided by traditional antibiotic therapy via killing bacteria released from biofilms, most antibacterials are rarely effective against biofilms.

A bacterial biofilm is a complex community assembled by bacterial cells within an extracellular polymeric substance (EPS) matrix. The formation of biofilms is a protecting strategy that allows bacteria to survive in hostile environment. Within the three dimensional structures of biofilms, there are channels formed for nutrition circulation[6] and different regions in which bacterial cells exhibit various patterns of gene expression.[7] This structural and metabolic complexity of biofilms has lead to the analogy of biofilms to tissues of higher organisms. Non-sessile individuals, planktonic bacteria that are capable of rapid dispersion and proliferation, can be released from these sessile biofilm communities. The release of such planktonic bacteria is for

biofilm expansion as well as protection, as these non-sessile bacteria are exposed to deleterious agents in their environment, be they phage or amoeba in nature or potent antimicrobial agents in a clinical setting. Thus it is only reasonable that a great number of bacterial infections involves with biofilms, which are challenging to eradicate with conventional antibiotic treatment.

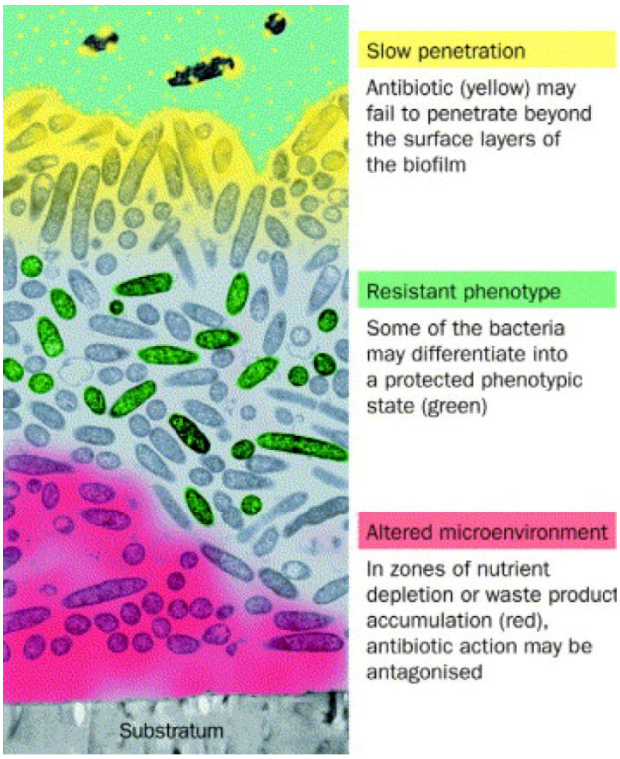

Figure 7.1. Three hypotheses for mechanisms of antibiotic resistance in biofilms. The attachment surface is shown at the bottom and the aqueous phase containing the antibiotic at the top. Adapted from reference 10.

There are three main hypotheses behind the mechanism of reistance to antibiotics in bacterial biofilms (Figure 7.1).[8] One mechanism of biofilm resistance to antibiotics is the failure of antibiotics to penetrate the full depth of biofilms. The penetration of antibiotics can be profoundly retarded due to the barrier properties of the sticky and strong extracellular polymeric substance (EPS).[9,10] Moreover, EPS is capable of deactivating antibiotics in the surface layers more rapidly than they diffuse, causing limited penetration.[11,12] For example, ampicillin cannot penetrate a biofilm formed by the β-lactamase-positive wild-type strain of *K. pneumonia*.[13] The second hypothesis relies on a chemical microenvironment that is altered inside biofilms. Nutrition

and oxygen are likely to be consumed in the surface layers of a biofilm, leading to nutrition depletion and anaerobic niches in the deep layers of the biofilms.[14] These conditions might push some bacteria to enter a non-growing state, protecting them from being killed by antibiotics such as penicillin antibiotics, which target cell-wall synthesis, kill only growing bacteria.[15] Besides, local accumulation of acidic metabolic waste products can result in pH differences greater than between the bulk fluid and the biofilm interior,[16] which could directly antagonize the action of an antibiotic. Additionally, an osmotic stress response might be induced by altered osmotic microenvironment within a biofilm, and such a response could change the relative proportions of porins to reduce cell envelope permeability to antibiotics, contributing to antibiotic resistance within a biofilm.[17] A third yet still speculative mechanism is a subpopulation of bacteria that is in a unique and highly protected phenotypic state.

Nanoparticles (NPs) possess strong permeating ability into cells,[18] tumors,[19] and even blood-brain barrier,[20] presenting a potentially powerful vehicle to infiltrate the biofilm EPS barrier. In addition, the surface functionality of NPs has been demonstrated to determine their interactions with biomolecules and cells.[21,22] Therefore, tailoring the surface chemistry makes NP a controllable platform for overcoming biofilm EPS barrier. Moreover, we have demonstrated that functionalized cationic gold nanoparticles can be used as potent antimicrobials against bacteria and even multi-drug-resistant bacteria.

Since biofilms are extremely difficult to treat once they are formed, a great portion of research and clinical efforts is focused on how to prevent formation of biofilms. In this chapter, I first examine if functional cationic gold nanoparticles (AuNPs) can be used to inhibit formation of biofilms and the relationship of effective AuNP concentrations against biofilms with MIC against planktonic bacteria. Next I probe the possibility of treatment of formed biofilms with AuNPs and discuss possible future plans based these results.

7.2 Results and discussion

I have demonstrated in Chapter 5 that our functionalized cationic C10-AuNP can inhibit both gram-positive and gram-negative pathogens, even multi-drug-resistant pathogens. Therefore, in this study, we employed C10-AuNP for pioneer studies. As shown in Figure 7.2, C10-AuNP features positive charge and a long hydrophobic 10 carbon chain at the head group. The proposed mode of action is that C10-AuNP can disrupt bacterial cell membrane and cause bacterial death. The long alkyl chain is hydrophobic, which is believed to be additional interaction to cationic charge when in contact with bacterial cell surface.

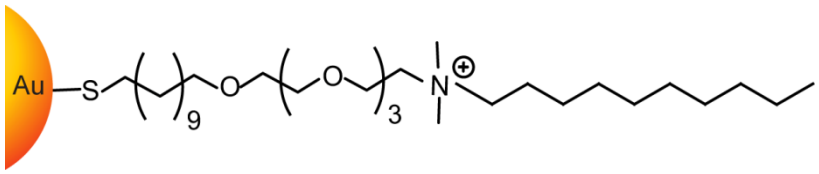

Figure 7.2. Molecular structure of functionalized cationic C10-AuNP.

C10-AuNP and one antibiotic drug, kanamycin, were tested for their MIC against bacteria *E. coli* and *P. aeruginosa* respectively. The choice of these two model bacteria is due to their relevance to the clinical formed biofilms. The MICs of C10-AuNP against *E. coli* and *P. aeruginosa* were both 16 nM, and the MICs of kanamycin against *E. coli* and *P. aeruginosa* were 4 μg/mL and 16 μg/mL respectively. AuNPs were mixed in culture medium, M9, at different folds of MIC and incubated with both *E. coli* and *P. aeruginosa*. Kanamycin was used at the same folds of MIC as AuNPs for comparison purpose. Biofilms were cultured for one day to test the inhibition effect in a short-time period, and biofilms were also cultured for two days to test AuNP and kanamycin's ability to prevent biofilm formation in a longer time period. Biofilms in medium without AuNPs nor kanamycin were used as control and counted as 0% inhibition.

As shown in Figure 7.3 a, within one-day period, kanamycin failed to inhibit *E. coli* biofilm formation at sub-MIC concentrations, and its inhibitory effect started to show only at 5 folds of MIC against planktonic *E. coli*. At lower concentrations, kanamycin even promoted

biofilm formation (% inhibition value lower than 0). On contrast, C10-AuNP was able to inhibit *E. coli* biofilm formation up to 75% at 0.75 fold of MIC against planktonic bacteria. And at 5 folds MIC concentration, there was almost no *E. coli* biofilm formation. Compared with *E. coli*, kanamycin worked more effectively on *P. aeruginosa* biofilm (Figure 7.3 b). Both kanamycin and AuNP displayed inhibitory effect at sub-MIC concentrations and both were capable of preventing *P. aeruginosa* biofilm formation up to around 75% at only half fold of MIC against planktonic bacteria. However, AuNP was able to completely inhibit *P. aeruginosa* biofilm formation at higher concentrations, whereas kanamycin could only maintain around 75% inhibitions even at higher concentrations.

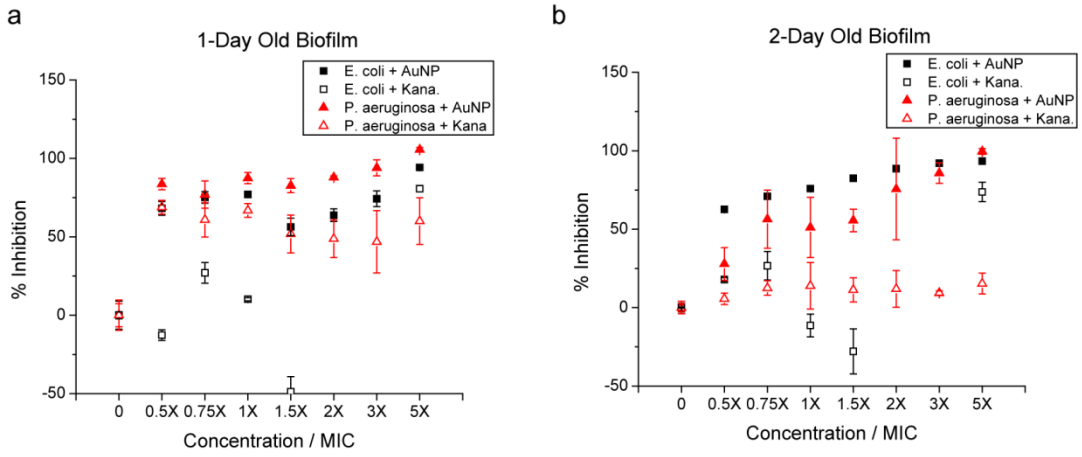

Figure 7.3. Inhibition of **a.** one-day old biofilm and **b.** two-day old biofilms of *E. coli* in the presence of C10-AuNP (black solid square) and kanamycin (black empty square) and *P. aeruginosa* in the presence of C10-AuNP (red solid triangle) and kanamycin (red empty triangle). Data are average of triplicates and error bars are standard deviation.

For a two-day incubation period (figure 7.3 b), *E. coli* biofilm formed at lower concentrations of kanamycine, and biofilm was only inhibited around 60% at 5 folds of MIC against planktonic bacteria. However, C10-AuNP reached similar inhibition effect only at half fold of MIC against planktonic *E. coli*, and the inhibition effect became stronger with the increasing AuNP concentrations. And at 5 folds of MIC against planktonic bacteria, *E. coli* biofilm formation was almost completely prevented. *P. aeruginosa* biofilms, however, were more

difficult for kanamycin to inhibit for a two-day incubation time. In fact, kanamycin failed to inhibit *P. aeruginosa* biofilm at all tested concentrations. AuNP, instead, maintained inhibitory effect against *P. aeruginosa* biofilm formation. At lower sub-MIC, AuNP still exhibited antibiofilm property and suppressed *P. aeruginosa* biofim formation to 20% and the suppressing effect increased with increasing AuNP concentration. When cultured with 5 folds of AuNP MIC against planktonic bacteria, there was almost *P. aeruginosa* biofilm formed.

This study supported that biofilm formation became more challenging with longer incubation/infection time. Results also revealed that the efficiency of traditional antibiotic therapy dropped dramatically with increasing incubation time course. However, the efficiency of AuNPs did not drop as much as kanamycin. On the contrary, at 5 folds of MIC against plaktonic bacteria, AuNPs were able to completely inhibit both *E. coli* and *P. aeruginosa* biofilm formation for up to two days. Longer incubation periods will be tested in the future work to explore the lasting efficiency of C10-AuNP against *E. coli* and *P. aeruginosa* biofilm formation.

After success in inhibiting biofilm formation, I am interested to probe the possibility of eradication of formed biofilms by C10-AuNP. For this purpose, I chose *P. aeruginosa* biofilm which is closely related to clinical chronic infections. Especially, chronic clinical bacterial infections with *P. aeruginosa* have an important role in pulmonary infection in cystic fibrosis (CF). The majority of patients with CF acquired *P. aeruginosa* that grows within microcolonies in the airways, causing chronic lung infection and repeated exacerbations and progressive deterioration in lung function, which remained major causes of morbidity and mortality.

P. aeruginosa biofilms were cultured in M9 for one day, and old medium was replaced with fresh M9 containing different concentrations of C10-AuNPs. After one day treatment, biofilms metabolic activity was examined to measure viability of remaining biofilms. When treated with sub-MIC concentrations and concentrations slightly higher than MIC, *P. aeruginosa* biofilms were not effectively eradicated. Higher AuNP concentrations increased the killing efficiency and at 50 folds of MIC against planktonic bacteria, the original one day old *P.*

aeruginosa biofilm was killed for around 80%. No higher killing efficacy was obtained at tested AuNP concentrations. Noticeably, though *P. aeruginosa* biofilms were only one-day old before treatment, however, when incubated with AuNPs, biofilms were still in medium. Therefore, there could be the possibility of re-growth from remaining biofilms after being partially killed by AuNPs at lower concentrations. This result again demonstrated the drastically increased resistance in biofilms to planktonic bacteria. Results showed promising potential for treatment of biofilms using our functionalized cationic AuNPs.

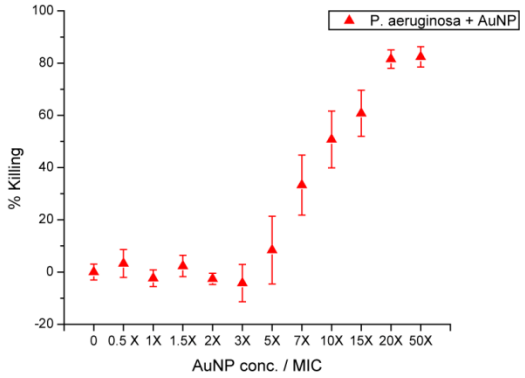

Figure. 7.4. The killing effect of C10-AuNP against one-day old *P. aeruginosa* biofilm. The biofilms were treated with AuNP for one day, and %killing is calculated by 100% minus the %viability of remaining biofilms after treatment. Data are average of triplicates and error bars are standard deviation.

7.3. Conclusions

In this chapter, I demonstrate that functional antibacterial AuNPs possess antibiofilm property as well. AuNPs successfully inhibited biofilm formation for up to two days at five folds of MIC against planktonic bacteria. Furthermore, this C10-AuNP eradicated 80% of *P. aeruginosa* biofilms. The proposed the working mechanism is the strong penetration ability plus the bacterial cell membrane disrupting ability of AuNPs. Though the effective AuNP concentrations are not high to inhibit biofilm formation, higher concentrations are required for eradication of biofilms. For treatment of more mature biofilms, therefore, one can rationally assume that even higher concentrations are necessary. Considering the penetration and membrane disrupting ability, AuNPs may be combined with other antimicrobial agents to facility these

antimicrobial agents penetration into biofilms as well as entry and uptake into bacterial cells, and thus increase antibiofilm efficiency while circumventing potential toxicity of high dosage of AuNPs. Following this strategy, research focused on combination therapy of AuNPs and conventional antibiotics is currently conducted by my junior research colleague.

7.4 Experimental methods

Materials All the reagents/materials required for nanoparticle synthesis were purchased from Fisher Scientific, except for gold salt, which was obtained from Strem Chemicals Inc. The organic solvents were from Pharmco-Aaper or Fisher Scientific and used as received except for dichloromethane that was distilled in the presence of calcium hydride. NIH-3T3 cells (ATCC CRL-1658) were purchased from ATCC. Dulbecco's Modified Eagle's Medium (DMEM) (DMEM; ATCC 30-2002) and fetal bovine serum (Fisher Scientific, SH3007103) were used in cell culture.

NP synthesis 2nm diameter gold nanoparticles were synthetized by the Brust-Schiffrin two-phase methodology using pentanethiol as the stabilizer; these clusters were purified with successive extractions with ethanol and acetone. A Murray place exchange reaction was carried out in dry DCM to functionalize the nanoparticles with each ligand. The monolayer-protected nanoparticles were redispersed in water and the excesses of ligand/pentanethiol were removed by dialysis using a 10,000 MWCO snake-skin membrane. The final concentration was measured by UV spectroscopy on a Molecular Devices SpectraMax M2 at 506nm according to the reported methodology.

Determination of antimicrobial activities of cationic gold nanoparticles Bacteria were cultured in LB medium at 37 ℃ and 275 rpm till stationary phase. The cultures were then harvested by centrifugation and washed with 0.85% sodium chloride solution for three times. Concentrations of re-suspended bacterial solution were determined by optical density measured at 600 nm. M9 medium was used to make dilutions of bacterial solution to a concentration of 1 ×

10^6 cfu/mL. 50 μL of these solutions were added into a 96-well plate and mixed with 50 μL of NP solutions in M9, giving a final bacterial concentration of 5×10^5 cfu/mL. NPs concentration varied in half fold according to a standard protocol, ranging from 125 nM to 3.9 nM. A growth control group without NPs and a sterile control group with only growth medium were carried out at the same time. Cultures were performed in triplicates, and at least two independent experiments were repeated on different days. The MIC is defined as the lowest concentration of AuNP that inhibits visible growth as observed with the unaided eye.

Biofilm culture Bacteria were inoculated in LB broth at 37 ℃ until stationary phase. The cultures were then harvested by centrifugation and washed with 0.85% sodium chloride solution for three times. Concentrations of re-suspended bacterial solution were determined by optical density measured at 600 nm. Seeding solutions were then made in M9 to reach OD_{600} of 0.1. 100 μL of the seeding solutions were added to each well of the microplate. M9 medium without bacteria was used as negative control. The plates were covered and incubated at room temperature under static conditions for desired period. Planktonic bacteria were removed before sensing by washing with PB saline three times.

Determination of biofilm inhibition activities of cationic gold nanoparticles and kanamycin Kanamycin and AuNP solutions were prepared at different concentrations in M9 respectively. These solutions were then seed with bacteria. After incubation, the biofilms were washed with PB saline for three times and stained with 0.1 % crystal violet staining solution for 15 minutes. This was followed by washing with PBS till no purple color observed in washing buffer. The plate was then left to dry in air. After drying, the plates were distained with 80% ethanol/20% acetone mixture for 15 minutes. The absorbance at 590 nm was measure afterwards. The higher absorbance represented more biofilm formation.

Determination of biofilm killing activities of cationic gold nanoparticles AuNP solutions were prepared at different concentrations in M9 and these solutions were then put into the one-day old *P. aeruginosa* biofilm. Biofilms were treated for one day at room temperature

and then washed with PBS for three times. After washing, alamar blue solution in PBS was added and the plate was incubated at 37 ℃ for two hours. After incubation the plates were measured in a plate reader at 545 nm/590 nm (ex/em).

7.5 References

1. Hall-Stoodley, L.; Costerton, J. W.; Stoodley, P. *Nat. Rev. Microbiol.* **2004**, *2*, 95-108.

2. Costerton, J. W.; Stewart, P. S.; Greenberg, E. P. *Science* **1999**, *284*, 1318-1322.

3. Donlan, R. M.; Costerton, J. W. *Clin. Microbiol. Rev.* **2002**, *15*, 167-193.

4. Lindsay, D.; von Holy, A. *J. Hosp. Infect.* **2006**, *64*, 313-325.

5. Romling, U.; Balsalobre, C. *J. Intern. Med.* **2012**, *272*, 541-561.

6. Debeer, D.; Stoodley, P.; Lewandowski, Z. *Biotechnol. Bioeng.* **1994**, *44*, 636-641.

7. Davies, D. G.; Chakrabarty, A. M.; Geesey, G. G. *Appl. Environ. Microbiol.* **1993**, *59*, 1181-1186.

8. Stewart, P. S.; Costerton, J. W. *Lancet* **2001**, *358*, 135-138.

9. Kumon, H.; Tomochika, K.; Matunaga, T.; Ogawa, M.; Ohmori, H. *Microbiol. Immunol.* **1994**, *38*, 615-619.

10. Shigeta, M.; Tanaka, G.; Komatsuzawa, H.; Sugai, M.; Suginaka, H.; Usui, T. *Chemotherapy* **1997**, *43*, 340-345.

11. Gordon, C. A.; Hodges, N. A.; Marriott, C. *J. Antimicrob. Chemother.* **1988**, *22*, 667-674.

12. Nichols, W. W.; Dorrington, S. M.; Slack, M. P. E.; Walmsley, H. L. *Antimicrob. Agents Chemother.* **1988**, *32*, 518-523.

13. Anderl, J. N.; Franklin, M. J.; Stewart, P. S. *Antimicrob. Agents Chemother.* **2000**, *44*, 1818-1824.

14. Tack, K. J.; Sabath, L. D. *Chemotherapy* **1985**, *31*, 204-210.

15. Tuomanen, E.; Cozens, R.; Tosch, W.; Zak, O.; Tomasz, A. *J. Gen. Microbiol.* **1986**, *132*, 1297-1304.

16. Zhang, T. C.; Bishop, P. L. *Water Environ. Res* **1996**, *68*, 1107-1115.

17. Prigent-Combaret, C.; Vidal, O.; Dorel, C.; Lejeune, P. *J. Bacteriol.* **1999**, *181*, 5993-6002.

18. Slowing, II; Vivero-Escoto, J. L.; Wu, C. W.; Lin, V. S. Y. *Adv. Drug Delivery Rev.* **2008**, *60*, 1278-1288.

19. Kim, J. S.; Kuk, E.; Yu, K. N.; Kim, J. H.; Park, S. J.; Lee, H. J.; Kim, S. H.; Park, Y. K.; Park, Y. H.; Hwang, C. Y.; Kim, Y. K.; Lee, Y. S.; Jeong, D. H.; Cho, M. H. *Nanomed-Nanotechnol.* **2007**, *3*, 95-101.

20. Lockman, P. R.; Mumper, R. J.; Khan, M. A.; Allen, D. D. *Drug Dev. Ind. Pharm.* **2002**, *28*, 1-13.

21. Verma, A.; Uzun, O.; Hu, Y. H.; Hu, Y.; Han, H. S.; Watson, N.; Chen, S. L.; Irvine, D. J.; Stellacci, F. *Nat. Mater.* **2008**, *7*, 588-595.

22. Saha, K.; Bajaj, A.; Duncan, B.; Rotello, V. M. *Small* **2011**, *7*, 1903-1918.

CHAPTER 8

NANOPARTICLE-BASED CAPSULES FOR TREATMENT OF BIOFILMS

8.1 Introduction

Bacterial biofilms are widely associated with persistent infections.[1] These biofilm infections occur frequently on implants and indwelling medical devices, including urinary catheters,[2] arthro-prostheses,[3] and dental implants.[4] Biofilms can also form on dead or living tissues, leading to endocarditis,[5] otitis media,[6] cystic fibrosis,[7] and chronic wounds.[8] These infections and diseases are notoriously difficult to treat, as biofilms develop high resistance to host immune responses as well as conventional antibiotics.[9] For these reasons biofilm-associated infections are commonly treated by excision of the infected parts combined with long-term antibiotic therapy, incurring high health care costs and immense patient stress.[10]

Plant-derived compounds, especially essential oils, have offered an alternative source to traditional antimicrobial agents to combat antibiotic resistant bacteria[11,12] The antibacterial properties of these essential oils have been demonstrated by their long history of use in medicine for prevention and treatment of infections.[13] Recent studies revealed that these natural compounds also possess anti-biofilm characteristics.[14,15] However, the poor solubility of such oils has substantially limited their widespread application. Previous reports have shown that encapsulating essential oils into colloidal delivery vehicles improves their stability and activity.[16,17,18] Pickering emulsions are a particularly attractive alternative to dynamic surfactant stabilizers for encapsulation, as the generated droplets possess functionalized particles that remain embedded at the interface.[19,20,21] Furthermore, nanoparticle stabilized emulsions can create dermal delivery vehicles with high payload to carrier ratios.[22]

Herein we describe the fabrication of an essential oil containing capsule stabilized by silica nanoparticles for the treatment of biofilms. Silica nanoparticles functionalized with surface amines stabilize the oil in water emulsions. The nanoparticles provide a cationic shell around the

oil droplets promoting interaction with the anionic biofilm matrix. Peppermint oil and peppermint oil doped with cinnamaldehyde were used as model hydrophobic cores. The cinnamaldehyde reacted with the amines of the nanoparticle to crosslink the nanoparticles at the oil/water interface generating a more effective delivery vehicle. The synergistic delivery of the peppermint oil doped with cinnamaldehyde effectively treated biofilm infections in a co-culture fibroblast system. Capsules were able to eradicate the biofilm while preserving the viability of the underlying fibroblasts. These results are being prepared in a manuscript for publication.

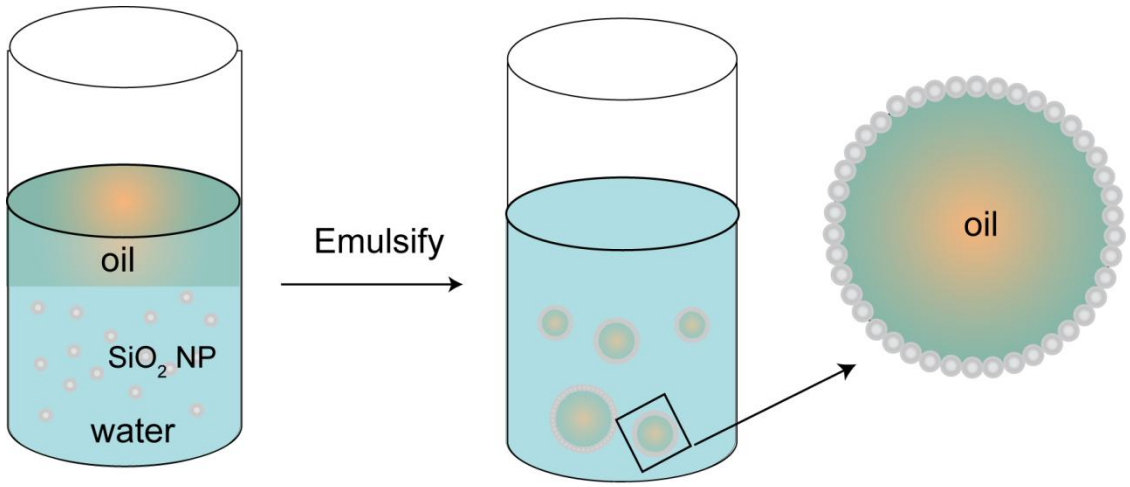

Figure 8.1. Schematic illustration of SiO_2 NP-based essential oil capsules.

8.2 Results and discussion

We first fabricated capsules consisted of only peppermint oil core (P-Cap) and capsules containing peppermint oil and cinnamaldehyde core (C-Cap). Capsules were freshly made before use and a 2% stock solution was made for all experiments. Solutions containing different capsule concentrations were made from the 2% stock solution. SiO_2 NPs alone and peppermint oil only were used as control, and these control solutions were made to contain the same amount of SiO_2 NP or peppermint oil as the capsule solutions at corresponding capsule solutions.

To test the biofilm killing capability of these capsules in a short time period, we first employed one day-old biofilm and treated them for three hours. *E. coli* and *P. aeruginosa*

biofilms were chosen as model biofilms due to their relevance to clinical biofilm-associated infections. After three hour treatment and washing, viability of the remaining biofilms were evaluated and normalized by the viability of non-treated biofilms (0%). As shown in Figure 8.2 a, the one day-old E. coli biofilms viability did not decease by SiO_2 NP, indicating SiO_2 NPs alone were not harmful for bacterial biofilms. When treated with peppermint oil alone, which acted as antimicrobial agent itself, the one day-old *E. coli* biofilm viability decreased to around 60% at 50% concentration and around 10% at 100% concentration. P-Cap containing the same amount of peppermint oil, however, did not show as high anti-biofilm effect as peppermint oil, and the one day-old *E. coli* biofilm viability only dropped to around 75% at the highest concentration tested. C-Cap possessed the highest biofilm killing capability and eradicated almost 100% one day-old *E. coli* biofilms at 50% concentration.

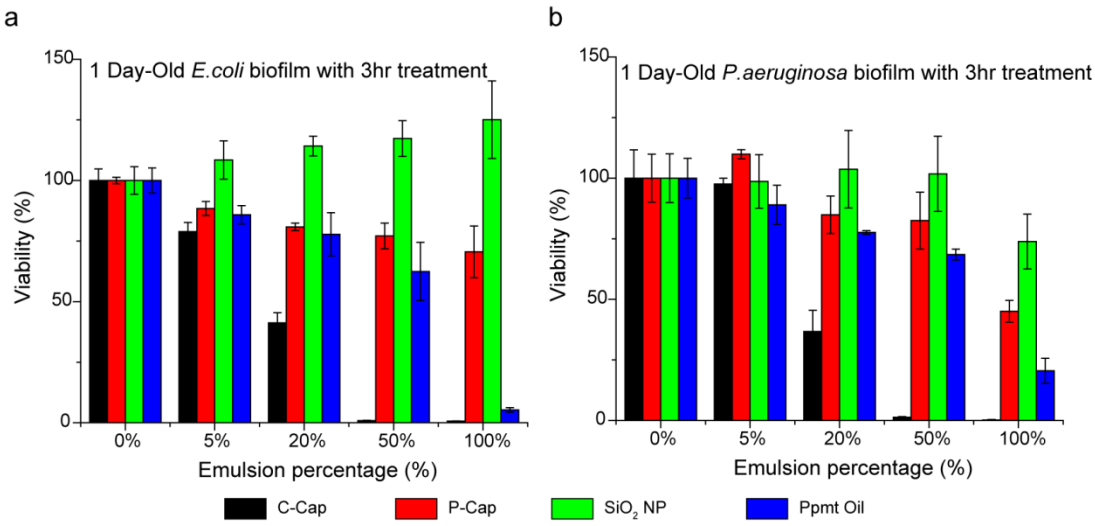

Figure 8.2. Viability of **a.** one day-old *E. coli* biofilms and **b.** one day-old *P. aeruginosa* biofilms after three hour treatment with different concentrations of capsules containing peppermint oil and cinnamaldehyde (C-Cap, black), capsules containing only peppermint oil (P-Cap, red), SiO2 NP (green), and peppermint oil (Ppmt Oil, blue). Data are average of triplicates and error bars are standard deviation.

Similarly for one day-old *P. aeruginosa* biofilms, SiO_2 NP did not significantly affect their viability except at the highest concentration; peppermint oil reduced biofilm viability; P-Cap

reduce biofilm viability as well but as much as peppermint oil alone; C-Cap showed the highest biofilm killing property and reduced biofilm viability to around 40% at 20% concentration.

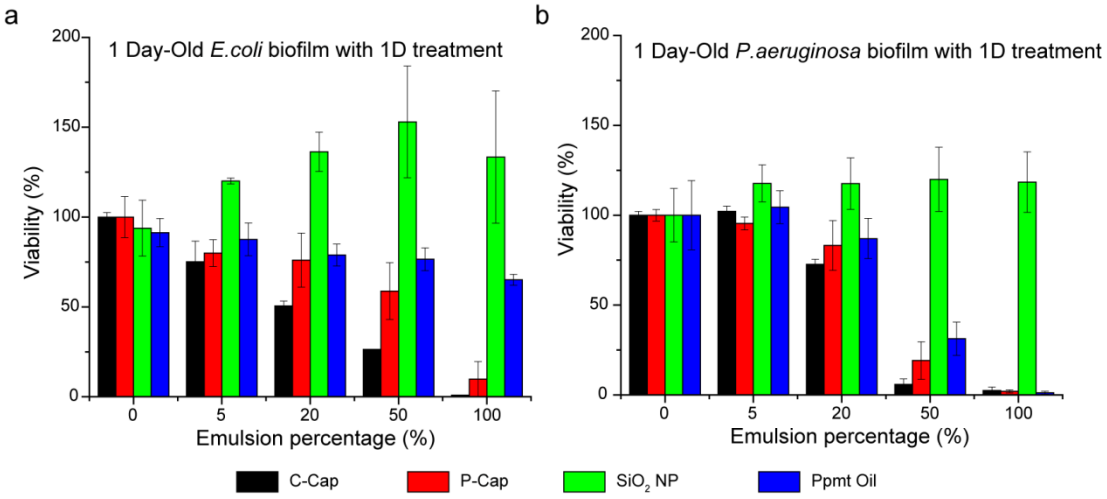

Figure 8.3. Viability of **a.** one day-old *E. coli* biofilms and **b.** one day-old *P. aeruginosa* biofilms after one day treatment with different concentrations of capsules containing peppermint oil and cinnamaldehyde (C-Cap, black), capsules containing only peppermint oil (P-Cap, red), SiO2 NP (green), and peppermint oil (Ppmt Oil, blue). Data are average of triplicates and error bars are standard deviation.

As proposed earlier in Chapter 7, when treated with antibiotilm agents for a longer time, biofilms could recover from initial shocking stage. Therefore, in next step we tested both capsules and control groups on the one day-old biofilms for longer treatment time, one day period. As displayed in Figure 8.3, SiO2 NP was still not harmful for one day-old *E. coli* biofilm after one day treatment. The killing effect of peppermint oil was not as effective as three hour treatment, and in fact at 100% concentration, peppermint oil treated one day-old *E. coli* biofilm viability was only reduce to around 75% after one day treatment, which was 60% higher than that after three hour treatment. This result indicated that though peppermint oil could suppress biofilm viability in a short time course, it could not consistently control or kill biofilms after the initial shocking stage. To the opposite, P-Cap containing the same amount of peppermint oil showed better killing and controlling property in the longer treatment period. And C-Cap remained effective on one day-old *E. coli* biofilm in the one day treatment period. Similar trends were observed in one day-old *P. aeruginosa* biofilms after one day treatment.

These initial results demonstrated the improved antibiofilm properties of NP-based essential oil capsules. Synergistic effect was observed on early biofilms in longer co-incubation time course. The impact of these capsules on mature biofilms, however, needed to be evaluated as well. For this purpose, three day-old *E. coli* and *P. aeruginosa* biofilms were cultured and treated with capsules and control groups for one day.

Figure 8.4 showed that peppermint oil completely failed to affect biofilm viability at the highest concentration tested, at which worked well on one day-old *E. coli* and *P. aeruginosa* biofilms for three hour treatment time. SiO2 NP remained unharmful for both three day-old *E. coli* and *P. aeruginosa* biofilms. Both P-Cap and C-Cap were effective after one day co-incubation time and C-Cap was capable of eradicating both three day-old *E. coli* and *P. aeruginosa* biofilms.

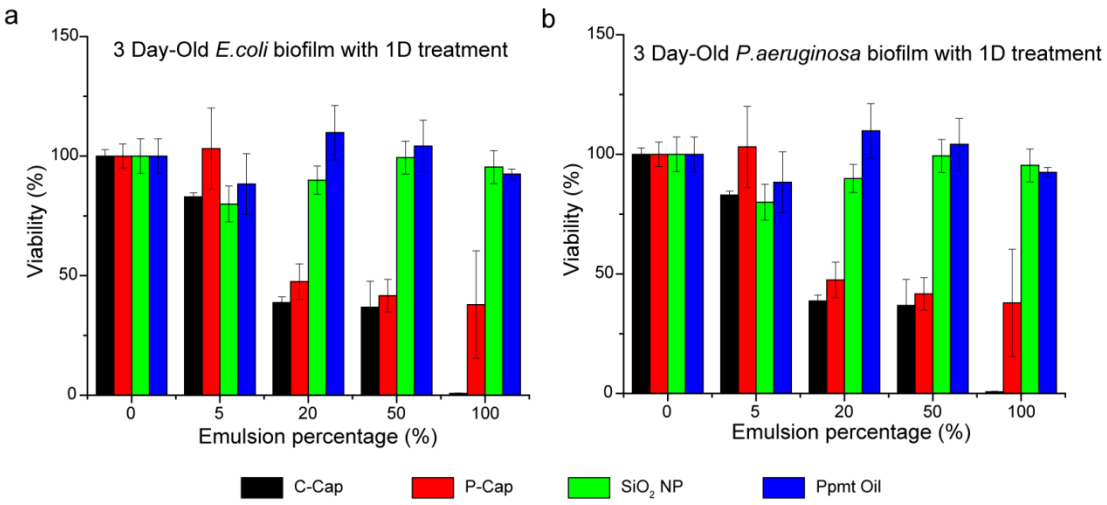

Figure 8.4. Viability of **a.** three day-old *E. coli* biofilms and **b.** three day-old *P. aeruginosa* biofilms after one day treatment with different concentrations of capsules containing peppermint oil and cinnamaldehyde (C-Cap, black), capsules containing only peppermint oil (P-Cap, red), SiO2 NP (green), and peppermint oil (Ppmt Oil, blue). Data are average of triplicates and error bars are standard deviation.

The treatment of biofilms with these capsules, especially the hybrid C-Cap capsule showed promising antibiofilm results. The low cost of all materials including SiO_2 NP and essential oils and the simple fabrication process made this system a great candidate for topical

treatment of chronic wounds. Therefore, we next employed an in *vitro* wound model, which was composed of fibroblast cells and co-cultured biofilms. This co-culture model study was conducted to probe the efficiency of these capsules to eradicate biofilms in the presence of mammalian cells as well as the toxicity of these capsules to mammalian cells.

E. coli biofilms in co-culture model was allowed to grow on a confluent monolayer of 3T3 fibroblast cells overnight. These co-cultures were then washed and treated with capsules as well as control groups for three hours. The viability of *E. coli* biofilm and 3T3 cells were evaluated respectively in each experimental group. And biofilm viability was measured by counting viable colonies after treatment. In the presence of bacteria and bacterial biofilms over night, 3T3 cells monolayer was observed to have some extension of damage. A few cells floated and died and they were washed away before treatment. Mammalian cell viability assessment was thus based on this point as starting point. And the toxicity evaluation was defined as additional damage caused to the remaining fibroblast cells by addition of capsules or control components.

As shown in Figure 8.5, the hybrid capsule, C-Cap, was able to reduce log viable colonies in *E. coli* biofilms from 7 to 2 at 100% concentration. Considering $\log_{10}$cfu of 2 is the limit of sensitivity, we can assume biofilms were completely eradicated in the co-culture. Remarkably, C-Cap did not decrease fibroblast cell viability in the co-culture at the same concentration. This result demonstrated that C-Cap was able to remove biofilms in the co-culture model without damaging mammalian cells. P-Cap also showed removal of the *E. coli* biofilms in the co-culture model with slight toxicity at 100% concentration. SiO_2 NP did not affect *E. coli* biofilms or fibroblast cells as expected. Peppermint oil was capable of reducing viable colonies in the *E. coli* biofilm by $\log_{10}$cfu of 1 at the highest concentration; however, 3T3 cell viability was also reduced to 20% by peppermint oil.

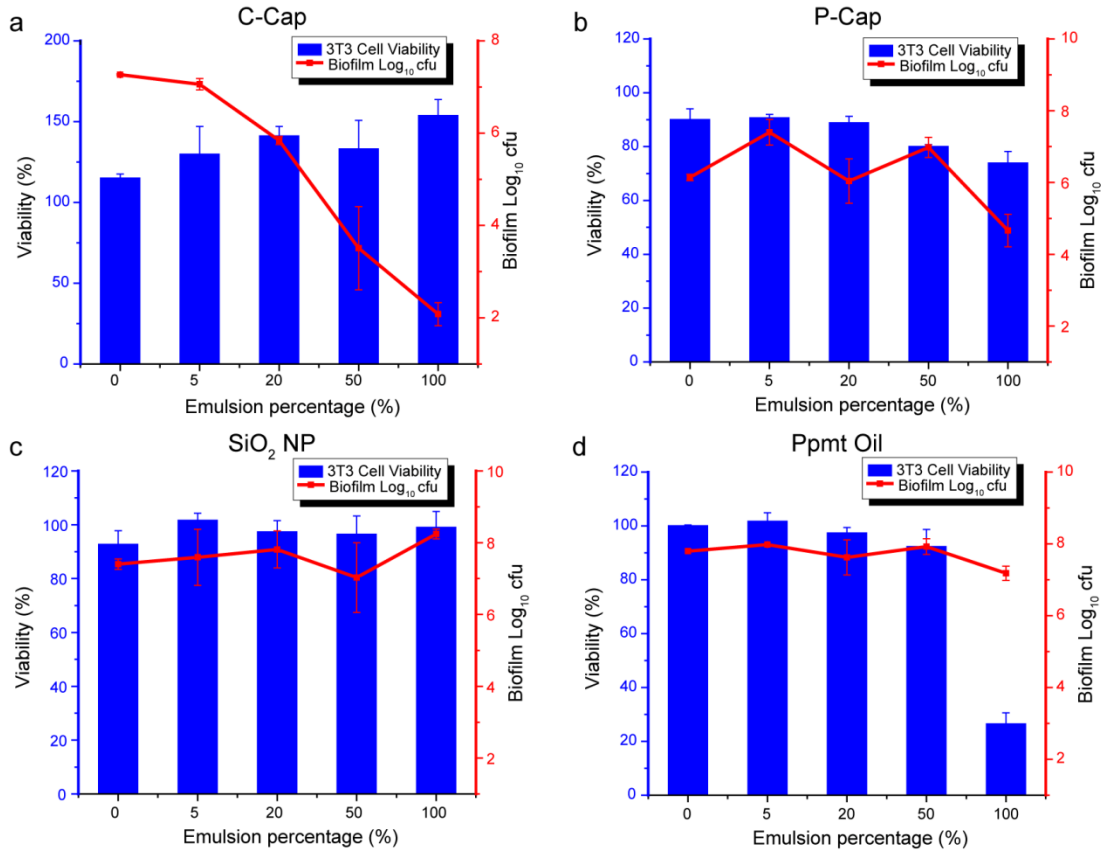

Figure 8.5. Viability of 3T3 fibroblast cell and *E. coli* biofilms in the co-culture model after three hour treatment with **a.** C-Cap, **b.** P-Cap, **c.** SiO2 NP, and **d.** Peppermint oil. The left y axis represents the viability of 3T3 cells (blue histogram) and data are average of triplicates and error bars are standard deviation. The right y axis represents the $\log_{10}$cfu of viable colonies in *E. coli* biofilms and data are average of duplicates and error bars are standard deviation.

Encapsulation of essential oils can increase their stability and solubility, extending their antimicrobial application. Results in our study suggested that in addition to increased solubility, there may be other action pathways to increase capsule antibiofilm effect, as capsules containing the same amount of essential oil possessed higher killing effect. We hypothesized that the capsule shell formed by the amine-functionalized SiO_2 NP was cationic as well, which may interact with biofilms, stick with biofilm anionic matrix, and release and facility cargo penetration into biofilms, increasing the antibiofilm property. To test this hypothesis, confocal laser scanning microscopy (CLSM) was employed to track capsule distribution into biofilms. SiO_2 NPs used for capsulation were labeled with fluorescein isothiocyanate (FITC), a green fluorescent chemical,

and *E. coli* biofilms were culture with a far-red fluorescent protein, crimson, expressing *E. coli*. The 3D projection of CLSM stack images showed that when incubated with capsules, both C-Cap and P-Cap, FITC-SiO_2 NP distributed through and all over *E. coli* biofilm and penetrate to the biofilm bottom (Figure 8.6 a, b). In the case of C-Cap, biofilm was partially eradicated and exhibited islands instead of layers. SiO_2 NP alone also penetrated into biofilm but in very limited quantity. These CLSM images demonstrated that capsules could stick on top of biofilms and facility cargo penetration into biofilms to escalate killing efficiency.

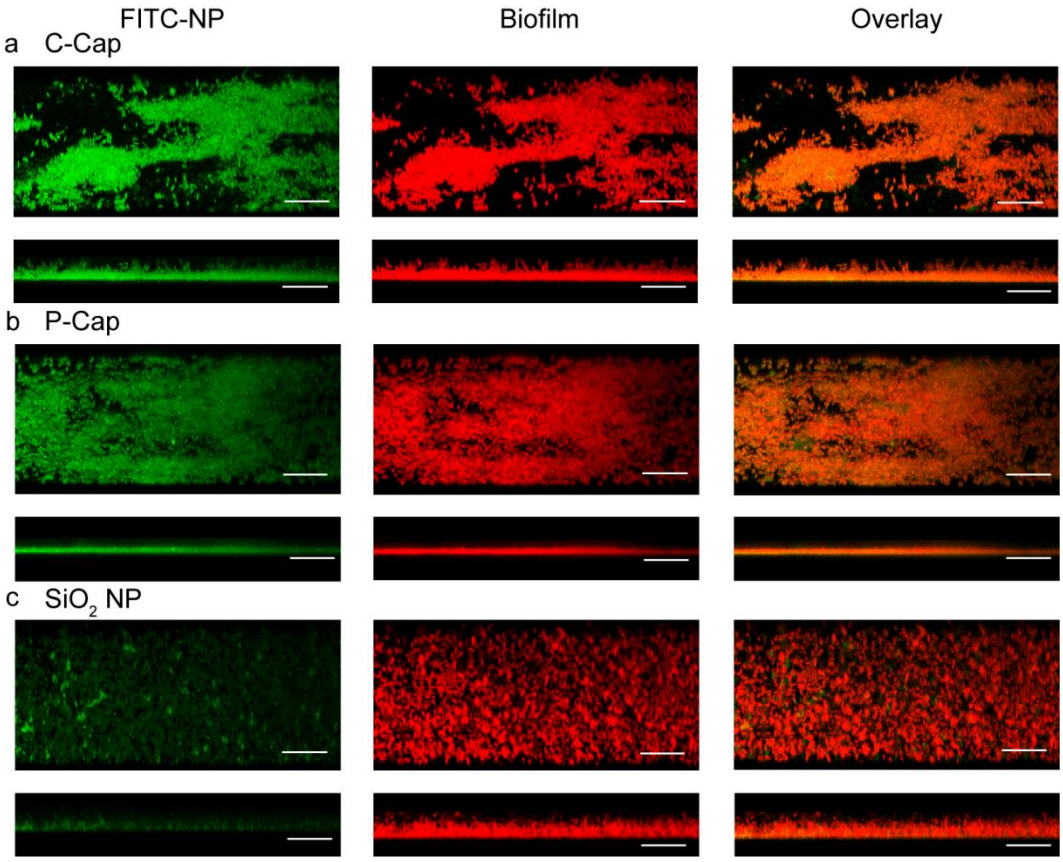

Figure 8.6. Representative three dimensional projections of confocal laser scanning microscopic z-stack images of E. coli biofilms (red) after incubation with a. C-Cap, b. P-Cap, and c. SiO2 NP alone. The left panels show the green fluorescence from FITC-labeled-SiO2 NP. The middle panels show the red fluorescence from crimson-expressing E. coli biofilm. The right panels show overlay of the corresponding left and middle panel images. The z-stack images were taken at a o.4 μm intervals. The scale bar is 20 μm.

8.3 Conclusions

In this chapter, I demonstrated the nanoparticle application for treatment of biofilms in the extension of nanoparticle-based capsules. SiO_2 NP-based essential oil capsules showed improved biofilm killing effect compared to essential oil alone. The combination of cinnamaldehyde and peppermint oil not only improved capsule stability by cross-linking amine functionalized SiO_2 NP, but also promoted antibiofilm efficiency. The hybrid capsule containing both cinnamaldehyde and peppermint oil was able to eradicate one day-old and three day-old *E. coli* and *P. aeruginosa* biofilms. Moreover, this hybrid capsule managed to eliminate *E. coli* biofilms formed on an *in vitro* wound model without causing harm to fibroblast cells underneath biofilms. The longer term studies, in which essential oil lost its antibiofilm effect completely whereas capsules preserved their killing capability, revealed the importance of using capsules instead of essential oils alone. This approach showed promising antibiofilm effect for application of treatment of biofilms as a topic emulsion agent.

8.4 Experimental methods

Biofilm formation in 96-well microplate Bacteria were inoculated in LB broth at 37 ℃ until stationary phase. The cultures were then harvested by centrifugation and washed with 0.85% sodium chloride solution for three times. Concentrations of re-suspended bacterial solution were determined by optical density measured at 600 nm. LB was supplemented with 0.1% glucose, 1 mM $MgSO_4$, 0.15 M ammonium sulphate, and 34 mM citrate and buffered to pH 7 to ensure bacterial adherence to the microplate. Seeding solutions were then made in this modified LB to reach OD_{600} of 0.1. 100 μL of the seeding solutions were added to each well of the microplate. Modified LB medium without bacteria was used as negative control. The plates were covered and incubated at room temperature under static conditions for three days. Fresh media was added on Day 2. Planktonic bacteria were removed before treatment by washing with PB saline three times.

Treatment of biofilms in 96-well plate Capsules were freshly made before use and a 2% stock solution was made in LB medium for all experiments in treatment of biofilms in 96-well plate. Solutions containing different capsule concentrations were made from the 2% stock solution. SiO_2 NPs alone and peppermint oil only were used as control, and these control solutions were made to contain the same amount of SiO_2 NP or peppermint oil as the capsule solutions at corresponding capsule solutions. One day-old or three day-old biofilms were washed with PBS for three times before treatment. 100 μL of treating solutions were then added and the plates were kept at room temperature for desired time course. After incubation, biofilms were washed again with PBS for three times, followed by addition of 100 μL of alamar blue solution. The plates containing alamar blue solutions were then kept at 37 ℃ for two hours and viability was measure by a plate reader at 545 nm/590 nm (Ex/Em).

Biofilm-3T3 fibroblast cell co-culture 20,000 NIH 3T3 (ATCC CRL-1658) cells were cultured in Dulbecco's modified Eagle medium (DMEM; ATCC 30-2002) with 10% bovine calf serum and 1% antibiotics at 37 ℃ in a humidified atmosphere of 5% CO_2. Cells were kept for 48 hours to reach a confluent monolayer. Bacteria were inoculated and harvested as described above and seeding solutions were made in HEPEs buffered DMEM with 2% glucose and 10% bovine calf serum to reach OD_{600} of 0.1. The buffered medium was used to maintain pH during incubation without CO_2. And the supplemented glucose was used to maintain bacteria and bacterial biofilm growth. No antibiotics were added. Old medium was removed from 3T3 cells followed by addition of 100 μL seeding solution. The co-cultures were then stored in a box with damp paper towels at 37 ℃ overnight. The co-cultures were washed with PB saline three times before treatment to remove planktonic bacteria and non-adherent 3T3 cells.

Treatment of biofilms in co-cultures Capsules were freshly made before use and a 2% stock solution was made in warm HEPEs buffered DMEM for all experiments in treatment of biofilms in co-cultures. Solutions containing different capsule concentrations were made from the 2% stock solution. SiO_2 NPs alone and peppermint oil only were used as control, and these

control solutions were made to contain the same amount of SiO_2 NP or peppermint oil as the capsule solutions at corresponding capsule solutions. Co-cultures were washed with PBS for three times before treatment. 100 μL of treating solutions were then added and the plates were kept at 37 ℃ for three hours.

To evaluate 3T3 fibroblast cell viability, LDH (lactose dehydrogenase) cytotoxicity assay was used. For negative controls (spontaneous LDH activity controls), medium of one set of triplicate wells was removed, and 100 μL of fresh warm DMEM and 10 μL of sterile MQ H_2O was added. For positive controls (maximum LDH activity controls), medium of another set of triplicate wells was removed, and 100 μL of fresh warm DMEM and 10 μL of Lysis Buffer (10X, from the LDH kit) was added. After incubation, 50 μL of each sample medium (e.g., experiment wells, spontaneous LDH activity controls, and maximum LDH activity controls) was transferred to a clear 96-well plate, and 50 μL of reaction mixture was added to each sample well. The plate was then incubated at dark at room temperature for 30 minutes, followed by addition of 50 μL of stopping solution to each well and mixed by gentle tapping. The absorbance was then measure by a plate reader at 490 nm and 680 nm. The LDH activity was calculated by subtracting the 680 nm absorbance value from the 490 nm absorbance value. %Cytotoxicity = (Compound-treated LDH activity – Spontaneous LDH activity)/(Maximum LDH activity – Spontaneous LDH activity) × 100. 3T3 fibroblast cell viability was then calculated by subtracting %Cytotoxicity from 100%.

To evaluate biofilm viability, co-cultures were washed with PBS once after the three hour incubation time. 200 μL of sterile PBS was then added into each well and the plate was sealed with parafilm and sonicated for 20 minutes. After sonication, plate was carefully wiped dry. Each well was then scratched with a clean sterile pipette tip and mix well. Series dilution was done and 10 μL of dilution of interest were placed on LB agar. Agar plates were kept at 37 ℃ over night and colonies were counted. Biofilm colonies were defined as Colonies/10 μL × Dilution times × 200 μL, and log reduction = Log_{10} (Untreated biofilm colonies) – Log_{10} (Treated biofilm colonies).

Biofilm culture for CLSM Bacteria were inoculated in 3 mL LB broth and grown to stationary phase at 37 ℃. The cultures were then diluted 1:100 in a 1/10 strength LB broth supplemented with 100 μM IPTG (isopropyl β-D-1-thiogalactopyranoside). 25 mL of the dilution was transferred into a petri dish containing six sterile glass cover slips (22 × 22 mm). The petri dish was kept at 25 ℃ and the biofilms were allowed to grow for three days. In general, the cover slips with biofilms were rinsed in deionized water for three times before placed in capsule solutions. The biofilms were incubated in 100% capsule solutions for one hour and free capsules were washed away by rinsing in deionized water for three times.

CLSM image The CLSM images were obtained using Zeiss510 META. The green fluorescent channel was collected at 488/505-550 bad pass and the red fluorescent channel was collected at 543/560 longpass.

8.5 References

1. Costerton, J. W.; Stewart, P. S.; Greenberg, E. P. *Science* **1999**, *284*, 1318-1322.

2. Lindsay, D.; von Holy, A. *J. Hosp. Infect.* **2006**, *64*, 313-325.

3. Costerton, J. W.; Montanaro, L.; Arciola, C. R. *Int. J. Artif. Organs* **2005**, *28*, 1062-1068.

4. Busscher, H. J.; Rinastiti, M.; Siswomihardjo, W.; van der Mei, H. C. *J. Clin. Invest.* **2010**, *89*, 657-665.

5. Costerton, W.; Veeh, R.; Shirtliff, M.; Pasmore, M.; Post, C.; Ehrlich, G. *J. Clin. Invest.* **2003**, *112*, 1466-1477.

6. Ehrlich, G. D.; Veeh, R.; Wang, X.; Costerton, J. W.; Hayes, J. D.; Hu, F. Z.; Daigle, B. J.; Ehrlich, M. D.; Post, J. C. *Jama* **2002**, *287*, 1710-1715.

7. Lyczak, J. B.; Cannon, C. L.; Pier, G. B. *Clin. Microbiol. Rev.* **2002**, *15*, 194-222.

8. James, G. A.; Swogger, E.; Wolcott, R.; Pulcini, E. D.; Secor, P.; Sestrich, J.; Costerton, J. W.; Stewart, P. S. *Wound Repair Regen.* **2008**, *16*, 37-44.

9. Stewart, P. S.; Costerton, J. W. *Lancet* **2001**, *358*, 135-138.

10. Lynch, A. S.; Robertson, G. T. *Annu. Rev. Med.* **2008**, *59*, 415-428.

11. Kalemba, D.; Kunicka, A. *Curr. Med. Chem.* **2003**, *10*, 813-829.

12. Hemaiswarya, S.; Kruthiventi, A. K.; Doble, M. *Phytomedicine* **2008**, *15*, 639-652.

13. Burt, S. *Int. J. Food Microbiol.* **2004**, *94*, 223-253.

14. Kavanaugh, N. L.; Ribbeck, K. *Appl. Environ. Microbiol.* **2012**, *78*, 4057-4061.

15. Nostro, A.; Roccaro, A. S.; Bisignano, G.; Marino, A.; Cannatelli, M. A.; Pizzimenti, F. C.; Cioni, P. L.; Procopio, F.; Blanco, A. R. *J. Med. Microbiol.* **2007**, *56*, 519-523.

16. Chang, Y. H.; McLandsborough, L.; McClements, D. J. *J. Agric. Food. Chem.* **2013**, *61*, 8906-8913.

17. Liang, R.; Xu, S. Q.; Shoemaker, C. F.; Li, Y.; Zhong, F.; Huang, Q. R. *J. Agric. Food. Chem.* **2012**, *60*, 7548-7555.

18. Gomes, C.; Moreira, R. G.; Castell-Perez, E. *J. Food Sci.* **2011**, *76*, S16-S24.

19. Binks, B. P. *Curr. Opin. Colloid Interface Sci.* **2002**, *7*, 21-41.

20. Ramsden, W. *Proceedings of the Royal Society of London* **1903**, *72*, 156-164.

21. Pickering, S. U. *J. Chem. Soc.* **1907**, *91*, 2001-2021.

22. Eskandar, N. G.; Simovic, S.; Prestidge, C. A. *J. Pharm. Sci.* **2010**, *99*, 890-904.

BIBLIOGRAPHY

Adams, M. R.; Moss, M. O. Food Microbiology; 2nd ed.; Royal Society of Chemistry: Guildford, 2000.

Ahangari, A.; Salouti, M.; Heidari, Z.; Kazemizadeh, A. R.; Safari, A. A. Drug Deliv. 2013, 20, 34-39.

Ai, H. W.; Shaner, N. C.; Cheng, Z. H.; Tsien, R. Y.; Campbell, R. E. Biochemistry 2007, 46, 5904-5910.

Aili, D.; Selegard, R.; Baltzer, L.; Enander, K.; Liedberg, B. Small 2009, 5, 2445-2452.

Alanis, A. J. Arch. Med. Res. 2005, 36, 697-705.

Albert, K. J.; Lewis, N. S.; Schauer, C. L.; Sotzing, G. A.; Stitzel, S. E.; Vaid, T. P.; Walt, D. R. Chem. Rev. 2000, 100, 2595-2626.

Alekshun, M. N.; Levy, S. B. Cell 2007, 128, 1037-1050.

Allen, M. J.; Edberg, S. C.; Reasoner, D. J. Int. J. Food Microbiol. 2004, 92, 265-274.

Anderl, J. N.; Franklin, M. J.; Stewart, P. S. Antimicrob. Agents Chemother. 2000, 44, 1818-1824.

(12) Anderson, G. G.; Kenney, T. F.; MacLeod, D. L.; Henig, N. R.; O'Toole, G. A. Pathog. Dis. 2013, 67, 39-45.

Anderson, G. G.; Moreau-Marquis, S.; Stanton, B. A.; O'Toole, G. A. Infect. Immun. 2008, 76, 1423-1433.

Arvizo, R. R.; Saha, S.; Wang, E. F.; Robertson, J. D.; Bhattacharya, R.; Mukherjee, P. Proc. Natl. Acad. Sci. U.S.A. 2013, 110, 6700-6705.

Asati, A.; Santra, S.; Kaittanis, C.; Nath, S.; Perez, J. M. Angewandte Chemie-International Edition 2009, 48, 2308-2312.

Bajaj, A.; Miranda, O. R.; Kim, I. B.; Phillips, R. L.; Jerry, D. J.; Bunz, U. H. F.; Rotello, V. M. Proc. Natl. Acad. Sci. U.S.A. 2009, 106, 10912-10916.

Bajaj, A.; Rana, S.; Miranda, O. R.; Yawe, J. C.; Jerry, D. J.; Bunz, U. H. F.; Rotello, V. M. Chem. Sci. 2010, 1, 134-138.

Barradell, L. B.; Bryson, H. M. Drugs 1994, 47, 471-505.

Berry, V.; Gole, A.; Kundu, S.; Murphy, C. J.; Saraf, R. F. J. Am. Chem. Soc. 2005, 127, 17600-17601.

Binks, B. P. Curr. Opin. Colloid Interface Sci. 2002, 7, 21-41.

Blue, S. R.; Singh, V. R.; Saubolle, M. A. Clin. Infect. Dis. 1995, 20, 629-633.

Bonifacio, L. D.; Puzzo, D. P.; Breslav, S.; Willey, B. M.; McGeer, A.; Ozin, G. A. Adv. Mater. 2010, 22, 1351-+.

Bos, M. P.; Tefsen, B.; Geurtsen, J.; Tommassen, J. Proc. Natl. Acad. Sci. U.S.A. 2004, 101, 9417-9422.

Boulos, L.; Prevost, M.; Barbeau, B.; Coallier, J.; Desjardins, R. J. Microbiol. Methods 1999, 37, 77-86.

Brenner, K. P.; Rankin, C. C.; Roybal, Y. R.; Stelma, G. N.; Scarpino, P. V.; Dufour, A. P. Appl. Environ. Microbiol. 1993, 59, 3534-3544.

Bresee, J.; Bond, C. M.; Worthington, R. J.; Smith, C. A.; Gifford, J. C.; Simpson, C. A.; Carter, C. J.; Wang, G. K.; Hartman, J.; Osbaugh, N. A.; Shoemaker, R. K.; Melander, C.; Feldheim, D. L. J. Am. Chem. Soc. 2014, 136, 5295-5300.

Bresee, J.; Maier, K. E.; Boncella, A. E.; Melander, C.; Feldheim, D. L. Small 2011, 7, 2027-2031.

Bridier, A.; Dubois-Brissonnet, F.; Boubetra, A.; Thomas, V.; Briandet, R. J. Microbiol. Methods 2010, 82, 64-70.

Brown, A. N.; Smith, K.; Samuels, T. A.; Lu, J. R.; Obare, S. O.; Scott, M. E. Appl. Environ. Microbiol. 2012, 78, 2768-2774.

Brust, M.; Walker, M.; Bethell, D.; Schiffrin, D. J.; Whyman, R. J. Chem. Soc., Chem. Commun. 1994, 801-802.

Bull, A. T.; Ward, A. C.; Goodfellow, M. Microbiol. Mol. Biol. Rev. 2000, 64, 573-606.

Bunn, H. F.; Jandl, J. H. J. Biol. Chem. 1968, 243, 465-&.

Burt, S. Int. J. Food Microbiol. 2004, 94, 223-253.

Burtscher, C.; Wuertz, S. Appl. Environ. Microbiol. 2003, 69, 4618-4627.

Busscher, H. J.; Rinastiti, M.; Siswomihardjo, W.; van der Mei, H. C. J. Clin. Invest. 2010, 89, 657-665.

CBE Biofilms: The Hypertextbook; National Science Foundation.

CDC Antibiotic resistance threats in the United States, 2013.

Chang, Y. H.; McLandsborough, L.; McClements, D. J. J. Agric. Food. Chem. 2013, 61, 8906-8913.

Charych, D. H.; Nagy, J. O.; Spevak, W.; Bednarski, M. D. Science 1993, 261, 585-588.

Chen, C. L.; Yu, J. C.; Holme, S.; Jacobs, M. R.; Yomtovian, R.; McDonald, C. P. Transfusion 2008, 48, 1550-1557.

Cole, L. A. Sci. Am. 1996, 275, 60-65.

Connor, E. E.; Mwamuka, J.; Gole, A.; Murphy, C. J.; Wyatt, M. D. Small 2005, 1, 325-327.

Costerton, J. W.; Cheng, K. J.; Geesey, G. G.; Ladd, T. I.; Nickel, J. C.; Dasgupta, M.; Marrie, T. J. Annu. Rev. Microbiol. 1987, 41, 435-464.

Costerton, J. W.; Lewandowski, Z.; Caldwell, D. E.; Korber, D. R.; Lappinscott, H. M. Annu. Rev. Microbiol. 1995, 49, 711-745.

Costerton, J. W.; Montanaro, L.; Arciola, C. R. Int. J. Artif. Organs 2005, 28, 1062-1068.

Costerton, J. W.; Stewart, P. S.; Greenberg, E. P. Science 1999, 284, 1318-1322.

Costerton, W.; Veeh, R.; Shirtliff, M.; Pasmore, M.; Post, C.; Ehrlich, G. J. Clin. Invest. 2003, 112, 1466-1477.

Courvalin, P. Clin. Infect. Dis. 2006, 42, S25-S34.

Cox, S. D.; Mann, C. M.; Markham, J. L.; Bell, H. C.; Gustafson, J. E.; Warmington, J. R.; Wyllie, S. G. J. Appl. Microbiol. 2000, 88, 170-175.

Cui, L. Z.; Iwamoto, A.; Lian, J. Q.; Neoh, H. M.; Maruyama, T.; Horikawa, Y.; Hiramatsu, K. Antimicrob. Agents Chemother. 2006, 50, 428-438.

Daniel, M. C.; Astruc, D. Chem. Rev. 2004, 104, 293-346.

Davies, D. G.; Chakrabarty, A. M.; Geesey, G. G. Appl. Environ. Microbiol. 1993, 59, 1181-1186.

Davies, J.; Davies, D. Microbiol. Mol. Biol. Rev. 2010, 74, 417-433.

Davies, J.; Wright, G. D. Trends. Microbiol. 1997, 5, 234-240.

Davis, M. E.; Chen, Z.; Shin, D. M. Nat. Rev. Drug Discov. 2008, 7, 771-782.

De, M.; Ghosh, P. S.; Rotello, V. M. Adv. Mater. 2008, 20, 4225-4241.

De, M.; Rana, S.; Akpinar, H.; Miranda, O. R.; Arvizo, R. R.; Bunz, U. H. F.; Rotello, V. M. Nat. Chem. 2009, 1, 461-465.

De, M.; Rana, S.; Rotello, V. M. Macromol. Biosci. 2009, 9, 174-178.

Debeer, D.; Stoodley, P.; Lewandowski, Z. Biotechnol. Bioeng. 1994, 44, 636-641.

Deisingh, A. K.; Thompson, M. Analyst 2002, 127, 567-581.

Deisingh, A. K.; Thompson, M. Can. J. Microbiol. 2004, 50, 69-77.

Demerec, M. J. Bacteriol. 1948, 56, 63-74.

Di Giulio, M.; D'Ercole, S.; Zara, S.; Cataldi, A.; Cellini, L. Apmis 2012, 120, 139-146.

Dmitriev, B.; Toukach, F.; Ehlers, S. Trends. Microbiol. 2005, 13, 569-574.

Donlan, R. M. Emerg. Infect. Dis. 2001, 7, 277-281.

Donlan, R. M. Emerg. Infect. Dis. 2002, 8, 881-890.

Donlan, R. M.; Costerton, J. W. Clin. Microbiol. Rev. 2002, 15, 167-193.

Duarte, A.; Chworos, A.; Flagan, S. F.; Hanrahan, G.; Bazan, G. C. J. Am. Chem. Soc. 2010, 132, 12562-12564.

Egan, W. J.; Morgan, S. L.; Bartick, E. G.; Merrill, R. A.; Taylor, H. J. Anal. Bioanal. Chem. 2003, 376, 1279-1285.

Ehrlich, G. D.; Veeh, R.; Wang, X.; Costerton, J. W.; Hayes, J. D.; Hu, F. Z.; Daigle, B. J.; Ehrlich, M. D.; Post, J. C. Jama 2002, 287, 1710-1715.

Elahifard, M. R.; Rahimnejad, S.; Haghighi, S.; Gholami, M. R. J. Am. Chem. Soc. 2007, 129, 9552-+.

Elghanian, R.; Storhoff, J. J.; Mucic, R. C.; Letsinger, R. L.; Mirkin, C. A. Science 1997, 277, 1078-1081.

Eren, T.; Som, A.; Rennie, J. R.; Nelson, C. F.; Urgina, Y.; Nusslein, K.; Coughlin, E. B.; Tew, G. N. Macromol. Chem. Phys. 2008, 209, 516-524.

Eskandar, N. G.; Simovic, S.; Prestidge, C. A. J. Pharm. Sci. 2010, 99, 890-904.

Euliss, L. E.; DuPont, J. A.; Gratton, S.; DeSimone, J. M. Chem. Soc. Rev. 2006, 35, 1095-1104.

Falagas, M. E.; Grammatikos, A. P.; Michalopoulos, A. Expert Rev. Anti. Infect. Ther. 2008, 6, 593-600.

Falagas, M. E.; Kasiakou, S. K. Clin. Infect. Dis. 2005, 40, 1333-1341.

Fayaz, A. M.; Girilal, M.; Mandy, S. A.; Somsundar, S. S.; Venkatesan, R.; Kalaichelvan, P. T. Process Biochem. 2011, 46, 636-641.

Fenselau, C.; Demirev, P. A. Mass Spectrom. Rev. 2001, 20, 157-171.

Finlay, B. B.; Falkow, S. Microbiol. Mol. Biol. Rev. 1997, 61, 136-169.

Flemming, H. C.; Neu, T. R.; Wozniak, D. J. J. Bacteriol. 2007, 189, 7945-7947.

Flemming, H. C.; Wingender, J. Nat. Rev. Microbiol. 2010, 8, 623-633.

Folmer-Andersen, J. F.; Kitamura, M.; Anslyn, E. V. J. Am. Chem. Soc. 2006, 128, 5652-5653.

Ford, E. E.; Colwell, R. R. A global decline in microbiological safety: a call for action. A report from The American Academy of Microbiology Washington, D.C., 1996.

Fowler, A. V.; Brake, A. J.; Zabin, I. J. Biol. Chem. 1978, 253, 5515-5520.

Francois, P.; Pittet, D.; Bento, M.; Pepey, B.; Vaudaux, P.; Lew, D.; Schrenzel, J. J. Clin. Microbiol. 2003, 41, 254-260.

Frischer, M. E.; Danforth, J. M.; Foy, T. F.; Juraske, R. J. Environ. Qual. 2005, 34, 1328-1336.

Fux, C. A.; Stoodley, P.; Hall-Stoodley, L.; Costerton, J. W. Expert Rev. Anti. Infect. Ther. 2003, 1, 667-683.

Gao, L. Z.; Zhuang, J.; Nie, L.; Zhang, J. B.; Zhang, Y.; Gu, N.; Wang, T. H.; Feng, J.; Yang, D. L.; Perrett, S.; Yan, X. Nat. Nanotech. 2007, 2, 577-583.

Geladi, P.; Esbensen, K. J. Chemom. 1991, 5, 97-111.

Gerba, C. P. Pathogens in the environment; Academic Press: New York, 1996.

Giuliani, A.; Rinaldi, A. C. Cell. Mol. Life Sci. 2011, 68, 2255-2266.

Gomes, C.; Moreira, R. G.; Castell-Perez, E. J. Food Sci. 2011, 76, S16-S24.

Gordon, C. A.; Hodges, N. A.; Marriott, C. J. Antimicrob. Chemother. 1988, 22, 667-674.

Gotz, F. Mol. Microbiol. 2002, 43, 1367-1378.

Grace, A. N.; Pandian, K. . Colloids Surf., A 2007, 297, 63-70.

Greene, N. T.; Shimizu, K. D. J. Am. Chem. Soc. 2005, 127, 5695-5700.

Grossman, H. L.; Myers, W. R.; Vreeland, V. J.; Bruehl, R.; Alper, M. D.; Bertozzi, C. R.; Clarke, J. Proc. Natl. Acad. Sci. U.S.A. 2004, 101, 129-134.

Grundmann, H.; Aires-De-Sousa, M.; Boyce, J.; Tiemersma, E. Lancet 2006, 368, 874-885.

Gu, H. W.; Ho, P. L.; Tong, E.; Wang, L.; Xu, B. Nano Lett. 2003, 3, 1261-1263.

Guo, Y. J.; Deng, L.; Li, J.; Guo, S. J.; Wang, E. K.; Dong, S. J. Acs Nano 2011, 5, 1282-1290.

Haa, E. A. H. Biosensors; Open University Press: Buckinghan, 1990.

Hacker, J.; Kaper, J. B. Annu. Rev. Microbiol. 2000, 54, 641-679.

Hajipour, M. J.; Fromm, K. M.; Ashkarran, A. A.; de Aberasturi, D. J.; de Larramendi, I. R.; Rojo, T.; Serpooshan, V.; Parak, W. J.; Mahmoudi, M. Trends Biotechnol. 2012, 30, 499-511.

Hall, M.; Eldridge, D. B.; Saunders, R. D.; Fairclough, D. L.; Bateman, R. C. Food Biotechnol. 1995, 9, 39-57.

Hall-Stoodley, L.; Costerton, J. W.; Stoodley, P. Nat. Rev. Microbiol. 2004, 2, 95-108.

Hall-Stoodley, L.; Hu, F. Z.; Gieseke, A.; Nistico, L.; Nguyen, D.; Hayes, J.; Forbes, M.; Greenberg, D. P.; Dice, B.; Burrows, A.; Wackym, P. A.; Stoodley, P.; Post, J. C.; Ehrlich, G. D.; Kerschner, J. E. Jama 2006, 296, 202-211.

Hall-Stoodley, L.; Stoodley, P.; Kathju, S.; Hoiby, N.; Moser, C.; Costerton, J. W.; Moter, A.; Bjarnsholt, T. FEMS Immunol. Med. Microbiol. 2012, 65, 127-145.

Hamon, M. A.; Lazazzera, B. A. Mol. Microbiol. 2001, 42, 1199-1209.

Hancock, R. E. W. Annu. Rev. Microbiol. 1984, 38, 237-264.

Hayden, S. C.; Zhao, G. X.; Saha, K.; Phillips, R. L.; Li, X. N.; Miranda, O. R.; Rotello, V. M.; El-Sayed, M. A.; Schmidt-Krey, I.; Bunz, U. H. F. J. Am. Chem. Soc. 2012, 134, 6920-6923.

Heal, J. S.; Blom, A. W.; Titcomb, D.; Taylor, A.; Bowker, K.; Hardy, J. R. W. J. Hosp. Infect. 2003, 53, 136-139.

Hemaiswarya, S.; Kruthiventi, A. K.; Doble, M. Phytomedicine 2008, 15, 639-652.

Higgins, M. K.; Bokma, E.; Koronakis, E.; Hughes, C.; Koronakis, V. Proc. Natl. Acad. Sci. U.S.A. 2004, 101, 9994-9999.

Hilpert, K.; Hancock, R. E. W. Nat. Protoc. 2007, 2, 1652-1660.

Hiramatsu, K.; Cui, L.; Kuroda, M.; Ito, T. Trends. Microbiol. 2001, 9, 486-493.

Hitching.Gh J. Infect. Dis. 1973, 128, S433-S436.

Ho, H. A.; Najari, A.; Leclerc, M. Acc. Chem. Res. 2008, 41, 168-178.

Hoffmann, O.; Keilwerth, N.; Bille, M. B.; Reuter, U.; Angstwurm, K.; Schumann, R. R.; Dirnagl, U.; Weber, J. R. J. Cerebr. Blood F. Met. 2002, 22, 988-996.

Holme, S.; McAlister, M. B.; Ortolano, G. A.; Chong, C.; Cortus, M. A.; Jacobs, M. R.; Yomtovian, R.; Freundlich, L. F.; Wenz, B. Transfusion 2005, 45, 984-993.

Hostetler, M. J.; Templeton, A. C.; Murray, R. W. Langmuir 1999, 15, 3782-3789.

Hsieh, B. Y.; Chang, Y. F.; Ng, M. Y.; Liu, W. C.; Lin, C. H.; Wu, H. T.; Chou, C. Anal. Chem. 2007, 79, 3487-3493.

Huang, C. C.; Huang, Y. F.; Cao, Z. H.; Tan, W. H.; Chang, H. T. Anal. Chem. 2005, 77, 5735-5741.

Hugo, W. B.; Russell, A. D. Pharmaceutical Microbiology; 6th ed.; Blackwell: Oxford, 1998.

Huh, A. J.; Kwon, Y. J. J. Controlled Release 2011, 156, 128-145.

Inglesby, T. V.; O'Toole, T.; Henderson, D. A.; Bartlett, J. G.; Ascher, M. S.; Eitzen, E.; Friedlander, A. M.; Gerberding, J.; Hauer, J.; Hughes, J.; McDade, J.; Osterholm, M. T.; Parker, G.; Perl, T. M.; Russell, P. K.; Tonat, K.; Biodef, W. G. C. Jama 2002, 287, 2236-2252.

Jacobson, R. H.; Zhang, X. J.; Dubose, R. F.; Matthews, B. W. Nature 1994, 369, 761-766.

Jakon, H.; Leininger, S.; Lehmann, T.; Jacobi, S.; Gutewort, S. Peroxo compounds, inorganic; 6th ed.; Wiley-VCH: Weinheim, 2003.

James, G. A.; Swogger, E.; Wolcott, R.; Pulcini, E. D.; Secor, P.; Sestrich, J.; Costerton, J. W.; Stewart, P. S. Wound Repair Regen. 2008, 16, 37-44.

Jenssen, H.; Hamill, P.; Hancock, R. E. W. Clin. Microbiol. Rev. 2006, 19, 491-+.

Ji, J.; Schanzle, A.; Tabacco, M. B. Anal. Chem. 2004, 76, 1411-1418.

Jin, T.; Fujii, F.; Yamada, E.; Nodasaka, Y.; Kinjo, M. J. Am. Chem. Soc. 2006, 128, 9288-9289.

Ju, H. X.; Zhang, X. J.; Wang, J. In Nanobiosensing: Principles, Development and Application 2011, p 39-84.

Jurs, P. C.; Bakken, G. A.; McClelland, H. E. Chem. Rev. 2000, 100, 2649-2678.

Jv, Y.; Li, B. X.; Cao, R. Chem. Commun. 2010, 46, 8017-8019.

Kalemba, D.; Kunicka, A. Curr. Med. Chem. 2003, 10, 813-829.

Kanaras, A. G.; Kamounah, F. S.; Schaumburg, K.; Kiely, C. J.; Brust, M. Chem. Commun. 2002, 2294-2295.

Kavanaugh, N. L.; Ribbeck, K. Appl. Environ. Microbiol. 2012, 78, 4057-4061.

Kay, E.; Vogel, T. M.; Bertolla, F.; Nalin, R.; Simonet, P. Appl. Environ. Microbiol. 2002, 68, 3345-3351.

Kim, B.; Han, G.; Toley, B. J.; Kim, C. K.; Rotello, V. M.; Forbes, N. S. Nat. Nanotech. 2010, 5, 465-472.

Kim, J.; Hegde, M.; Jayaraman, A. Lab on a Chip 2010, 10, 43-50.

Kim, J. S.; Kuk, E.; Yu, K. N.; Kim, J. H.; Park, S. J.; Lee, H. J.; Kim, S. H.; Park, Y. K.; Park, Y. H.; Hwang, C. Y.; Kim, Y. K.; Lee, Y. S.; Jeong, D. H.; Cho, M. H. Nanomed-Nanotechnol. 2007, 3, 95-101.

Klausen, M.; Heydorn, A.; Ragas, P.; Lambertsen, L.; Aaes-Jorgensen, A.; Molin, S.; Tolker-Nielsen, T. Mol. Microbiol. 2003, 48, 1511-1524.

Klevens, R. M.; Morrison, M. A.; Nadle, J.; Petit, S.; Gershman, K.; Ray, S.; Harrison, L. H.; Lynfield, R.; Dumyati, G.; Townes, J. M.; Craig, A. S.; Zell, E. R.; Fosheim, G. E.; McDougal, L. K.; Carey, R. B.; Fridkin, S. K.; Investigators, A. B. M. Jama 2007, 298, 1763-1771.

Koch, A. L. Clin. Microbiol. Rev. 2003, 16, 673-687.

Kresse, H.; Belsey, M. J.; Rovini, H. Nat. Rev. Drug Discovery 2007, 6, 19-20.

Krishnasami, Z.; Carlton, D.; Bimbo, L.; Taylor, M. E.; Balkovetz, D. F.; Barker, J.; Allon, M. Kidney Int. 2002, 61, 1136-1142.

Kumon, H.; Tomochika, K.; Matunaga, T.; Ogawa, M.; Ohmori, H. Microbiol. Immunol. 1994, 38, 615-619.

Leatherdale, C. A.; Bawendi, M. G. Phys. Rev. B 2001, 63.

Lee, J. S.; Han, M. S.; Mirkin, C. A. Angew. Chem. Int. Ed. 2007, 46, 4093-4096.

Levy, S. B.; Marshall, B. Nat. Med. 2004, 10, S122-S129.

Li, X. N.; Wen, F.; Creran, B.; Jeong, Y. D.; Zhang, X. R.; Rotello, V. M. Small 2012, 8, 3589-3592.

Li, X. Z.; Nikaido, H. Drugs 2004, 64, 159-204.

Liang, R.; Xu, S. Q.; Shoemaker, C. F.; Li, Y.; Zhong, F.; Huang, Q. R. J. Agric. Food. Chem. 2012, 60, 7548-7555.

Lin, J.; Qiu, S. Y.; Lewis, K.; Klibanov, A. M. Biotechnol. Progr. 2002, 18, 1082-1086.

Lin, J. Q.; Zhang, H. W.; Chen, Z.; Zheng, Y. G. Acs Nano 2010, 4, 5421-5429.

Lindsay, D.; von Holy, A. J. Hosp. Infect. 2006, 64, 313-325.

Liu, X. O.; Atwater, M.; Wang, J. H.; Huo, Q. Colloid. Surface. B 2007, 58, 3-7.

Livermore, D. M. Clin. Microbiol. Rev. 1995, 8, 557-&.

Lockman, P. R.; Mumper, R. J.; Khan, M. A.; Allen, D. D. Drug Dev. Ind. Pharm. 2002, 28, 1-13.

Login, R. B.; Merianois, J. J.; Biss, R. B.; Garelick, P. U.S. Patent 5183901, 1992.

Lyczak, J. B.; Cannon, C. L.; Pier, G. B. Clin. Microbiol. Rev. 2002, 15, 194-222.

Lynch, A. S.; Robertson, G. T. Annu. Rev. Med. 2008, 59, 415-428.

Martinez, A. W.; Phillips, S. T.; Carrilho, E.; Thomas, S. W.; Sindi, H.; Whitesides, G. M. Anal. Chem. 2008, 80, 3699-3707.

Mathur, S.; Singh, R. Int. J. Food Microbiol. 2005, 105, 281-295.

Maughan, N. J.; Lewis, F. A.; Smith, V. J. Pathol. 2001, 195, 3-6.

Maughan, N. J.; Lewis, F. A.; Smith, V. J. Pathol. 2001, 195, 3-6.

McFeters, G. A. Drinking water microbiology; Springer: New York, 1990.

McKee, E. E.; Ferguson, M.; Bentley, A. T.; Marks, T. A. Antimicrob. Agents Chemother. 2006, 50, 2042-2049.

McMurry, L.; Petrucci, R. E. J.; Levy, S. B. Proc. Natl. Acad. Sci. U.S.A. 1980, 77, 3974-3977.

Mennink-Kersten, M.; Donnelly, J. P.; Verweij, P. E. Lancet Infect. Dis. 2004, 4, 349-357.

Merritt, J. H.; Kadouri, D. E.; O'Toole, G. A. Curr. Protoc. Microbiol. 2005, 1B, 1.1.

Miranda, O. R.; Chen, H. T.; You, C. C.; Mortenson, D. E.; Yang, X. C.; Bunz, U. H. F.; Rotello, V. M. J. Am. Chem. Soc. 2010, 132, 5285-5289.

Miranda, O. R.; Li, X. N.; Garcia-Gonzalez, L.; Zhu, Z. J.; Yan, B.; Bunz, U. H. F.; Rotello, V. M. J. Am. Chem. Soc. 2011, 133, 9650-9653.

Morrow, J. B.; Arango, C.; Holbrook, R. D. J. Environ. Qual. 2010, 39, 1934-1941.

Mout, R.; Moyano, D. F.; Rana, S.; Rotello, V. M. Chem. Soc. Rev. 2012, 41, 2539-2544.

Moyano, D. F.; Goldsmith, M.; Solfiell, D. J.; Landesman-Milo, D.; Miranda, O. R.; Peer, D.; Rotello, V. M. J. Am. Chem. Soc. 2012, 134, 3965-3967.

Moyano, D. F.; Rotello, V. M. Langmuir 2011, 27, 10376-10385.

Mulligan, M. E.; Murrayleisure, K. A.; Ribner, B. S.; Standiford, H. C.; John, J. F.; Korvick, J. A.; Kauffman, C. A.; Yu, V. L. Am. J. Med. 1993, 94, 313-328.

Murata, H.; Koepsel, R. R.; Matyjaszewski, K.; Russell, A. J. Biomaterials 2007, 28, 4870-4879.

Nandwana, V.; Mout, R.; Yeh, Y. C.; Dickert, S.; Tuominen, M. T.; Rotello, V. M. J. Inorg. Organomet. Polym. 2013, 23, 227-232.

Neu, H. C. Science 1992, 257, 1064-1073.

Newton, C. R.; Graham, A. PCR, 2nd ed. ; Bios Scientific: Oxford, 1997.

Nichols, W. W.; Dorrington, S. M.; Slack, M. P. E.; Walmsley, H. L. Antimicrob. Agents Chemother. 1988, 32, 518-523.

Nikaido, H. J. Bacteriol. 1996, 178, 5853-5859.

Nostro, A.; Roccaro, A. S.; Bisignano, G.; Marino, A.; Cannatelli, M. A.; Pizzimenti, F. C.; Cioni, P. L.; Procopio, F.; Blanco, A. R. J. Med. Microbiol. 2007, 56, 519-523.

Ochman, H.; Lawrence, J. G.; Groisman, E. A. Nature 2000, 405, 299-304.

O'Connell, K. M. G.; Hodgkinson, J. T.; Sore, H. F.; Welch, M.; Salmond, G. P. C.; Spring, D. R. Angew. Chem. Int. Ed. 2013, 52, 10706-10733.

Park, J. K.; Jung, J.; Subramaniam, P.; Shah, B. P.; Kim, C.; Lee, J. K.; Cho, J. H.; Lee, C.; Lee, K. B. Small 2011, 7, 1647-1652.

Parsek, M. R.; Singh, P. K. Annu. Rev. Microbiol. 2003, 57, 677-701.

Patange, S. B.; Mukundan, M. K.; Kumar, K. A. Food Control 2005, 16, 465-472.

Pedley, S.; Bartram, J.; Rees, G.; Dufour, A.; Cotruvo, J., A. Pathogenic mycobacteria in Water; World Health Organization (WHO): London, 2004.

Peer, D.; Karp, J. M.; Hong, S.; FaroKhzad, O. C.; Margalit, R.; Langer, R. Nat. Nanotech. 2007, 2, 751-760.

Pelossof, G.; Tel-Vered, R.; Elbaz, J.; Willner, I. Anal. Chem. 2010, 82, 4396-4402.

Perkins, S. D.; Mayfield, J.; Fraser, V.; Angenent, L. T. Appl. Environ. Microbiol. 2009, 75, 5363-5372.

Phillips, R. L.; Miranda, O. R.; You, C. C.; Rotello, V. M.; Bunz, U. H. F. Angew. Chem. Int. Ed. 2008, 47, 2590-2594.

Pickering, S. U. J. Chem. Soc. 1907, 91, 2001-2021.

Prigent-Combaret, C.; Vidal, O.; Dorel, C.; Lejeune, P. J. Bacteriol. 1999, 181, 5993-6002.

Pruss, A.; Kay, D.; Fewtrell, L.; Bartram, J. Environ. Health Perspect. 2002, 110, 537-542.

Qu, H. O.; Caruntu, D.; Liu, H. X.; O'Connor, C. J. Langmuir 2011, 27, 2271-2278.

Rai, A.; Prabhune, A.; Perry, C. C. J. Mater. Chem. 2010, 20, 6789-6798.

Ramsden, W. Proc. R. Soc. London 1903, 72, 156-164.

Redl, F. X.; Black, C. T.; Papaefthymiou, G. C.; Sandstrom, R. L.; Yin, M.; Zeng, H.; Murray, C. B.; O'Brien, S. P. J. Am. Chem. Soc. 2004, 126, 14583-14599.

Redl, F. X.; Black, C. T.; Papaefthymiou, G. C.; Sandstrom, R. L.; Yin, M.; Zeng, H.; Murray, C. B.; O'Brien, S. P. J. Am. Chem. Soc. 2004, 126, 14583-14599.

Rickard, A. H.; McBain, A. J.; Ledder, R. G.; Handley, P. S.; Gilbert, P. FEMS Microbiol. Lett. 2003, 220, 133-140.

Roberts, R. R.; Hota, B.; Ahmad, I.; Scott, R. D.; Foster, S. D.; Abbasi, F.; Schabowski, S.; Kampe, L. M.; Ciavarella, G. G.; Supino, M.; Naples, J.; Cordell, R.; Levy, S. B.; Weinstein, R. A. Clin. Infect. Dis. 2009, 49, 1175-1184.

Romling, U.; Balsalobre, C. J. Intern. Med. 2012, 272, 541-561.

Rotem, S.; Mor, A. Biochim. Biophys. Acta Biomembr. 2009, 1788, 1582-1592.

Ryder, C.; Byrd, M.; Wozniak, D. J. Curr. Opin. Microbiol. 2007, 10, 644-648.

Ryman-Rasmussen, J. P.; Riviere, J. E.; Monteiro-Riviere, N. A. Toxicol. Sci. 2006, 91, 159-165.

Safarik, I.; Safarikova, M.; Forsythe, S. J. J. Appl. Bacteriol. 1995, 78, 575-585.

Saha, K.; Agasti, S. S.; Kim, C.; Li, X. N.; Rotello, V. M. Chem. Rev. 2012, 112, 2739-2779.

Saha, K.; Bajaj, A.; Duncan, B.; Rotello, V. M. Small 2011, 7, 1903-1918.

Saha, K. M., D. F.; Rotello, V. M. Mater. Horiz. 2014, 1, 102-105.

Sastry, M.; Lala, N.; Patil, V.; Chavan, S. P.; Chittiboyina, A. G. Langmuir 1998, 14, 4138-4142.

Schaffer, C.; Messner, P. Microbiology 2005, 151, 643-651.

Schwartz, V. B.; Thetiot, F.; Ritz, S.; Putz, S.; Choritz, L.; Lappas, A.; Forch, R.; Landfester, K.; Jonas, U. Adv. Funct. Mater. 2012, 22, 2376-2386.

Seil, J. T.; Webster, T. J. Int. J. Nanomedicine 2012, 7, 2767-2781.

Shen, L. L.; Mitscher, L. A.; Sharma, P. N.; Odonnell, T. J.; Chu, D. W. T.; Cooper, C. S.; Rosen, T.; Pernet, A. G. Biochemistry 1989, 28, 3886-3894.

Shen, Y.; Stojicic, S.; Haapasalo, M. Journal of Endodontics 2010, 36, 1820-1823.

Shigeta, M.; Tanaka, G.; Komatsuzawa, H.; Sugai, M.; Suginaka, H.; Usui, T. Chemotherapy 1997, 43, 340-345.

Shih, J. S.; Merianos, J. J.; Smith, T. E.; J-C., C. U. S. 5312619, 1992.

Shoji, E.; Freund, M. S. J. Am. Chem. Soc. 2001, 123, 3383-3384.

Shorten, P. R.; Pleasants, A. B.; Soboleva, T. K. Int. J. Food Microbiol. 2006, 108, 369-375.

Slowing, II; Vivero-Escoto, J. L.; Wu, C. W.; Lin, V. S. Y. Adv. Drug Delivery Rev. 2008, 60, 1278-1288.

Song, Y. J.; Qu, K. G.; Zhao, C.; Ren, J. S.; Qu, X. G. Adv. Mater. 2010, 22, 2206-+.

Spellberg, B.; Powers, J. H.; Brass, E. P.; Miller, L. G.; Edwards, J. E. Clin. Infect. Dis. 2004, 38, 1279-1286.

Steiner, M. S.; Meier, R. J.; Duerkop, A.; Wolfbeis, O. S. Anal. Chem. 2010, 82, 8402-8405.

Stewart, P. S.; Costerton, J. W. Lancet 2001, 358, 135-138.

Stoodley, P.; Conti, S. F.; DeMeo, P. J.; Nistico, L.; Melton-Kreft, R.; Johnson, S.; Darabi, A.; Ehrlich, G. D.; Costerton, J. W.; Kathju, S. FEMS Immunol. Med. Microbiol. 2011, 62, 66-74.

Storhoff, J. J.; Elghanian, R.; Mucic, R. C.; Mirkin, C. A.; Letsinger, R. L. J. Am. Chem. Soc. 1998, 120, 1959-1964.

Strachan, N. J. C.; Nicholson, F. J.; Ogden, I. D. Anal. Chim. Acta 1995, 313, 63-67.

Straub, T. M.; Chandler, D. P. J. Microbiol. Methods 2003, 53, 185-197.

Strohl, W. A.; Rouse, B.; Fisher, C. D. Microbiology; Lippincott Williams & Wilkins, 2001.

Sun, S. H.; Zeng, H. J. Am. Chem. Soc. 2002, 124, 8204-8205.

Susumu, K.; Uyeda, H. T.; Medintz, I. L.; Pons, T.; Delehanty, J. B.; Mattoussi, H. J. Am. Chem. Soc. 2007, 129, 13987-13996.

Sutherland, I. W. Microbiology-Uk 2001, 147, 3-9.

Tack, K. J.; Sabath, L. D. Chemotherapy 1985, 31, 204-210.

Taylor, E.; Webster, T. J. Int. J. Nanomedicine 2011, 6, 1463-1473.

Templeton, A. C.; Wuelfing, M. P.; Murray, R. W. Acc. Chem. Res. 2000, 33, 27-36.

Tenover, F. C. Am. J. Med. 2006, 119, S3-S10.

Thanh, N. T. K.; Rosenzweig, Z. Anal. Chem. 2002, 74, 1624-1628.

Tsien, R. Y. Annu. Rev. Biochem 1998, 67, 509-544.

Tuomanen, E.; Cozens, R.; Tosch, W.; Zak, O.; Tomasz, A. J. Gen. Microbiol. 1986, 132, 1297-1304.

Turner, A. P. F.; Magan, N. Nat. Rev. Microbiol. 2004, 2, 161-166.

Uyeda, H. T.; Medintz, I. L.; Jaiswal, J. K.; Simon, S. M.; Mattoussi, H. J. Am. Chem. Soc. 2005, 127, 3870-3878.

van de Belt, H.; Neut, D.; Schenk, W.; van Horn, J. R.; van der Mei, H. C.; Busscher, H. J. Acta Orthop. Scand. 2001, 72, 557-571.

Van Dyck, E.; Ieven, M.; Pattyn, S.; Van Damme, L.; Laga, M. J. Clin. Microbiol. 2001, 39, 1751-1756.

Vaningelgem, F.; Zamfir, M.; Mozzi, F.; Adriany, T.; Vancanneyt, M.; Swings, J.; De Vuyst, L. Appl. Environ. Microbiol. 2004, 70, 900-912.

Verma, A.; Simard, J. M.; Worrall, J. W. E.; Rotello, V. M. J. Am. Chem. Soc. 2004, 126, 13987-13991.

Verma, A.; Uzun, O.; Hu, Y. H.; Hu, Y.; Han, H. S.; Watson, N.; Chen, S. L.; Irvine, D. J.; Stellacci, F. Nat. Mater. 2008, 7, 588-595.

von Nussbaum, F.; Brands, M.; Hinzen, B.; Weigand, S.; Habich, D. Angewandte Chemie-International Edition 2006, 45, 5072-5129.

Wang, J. Small 2005, 1, 1036-1043.

Wang, P.; Huang, B. B.; Zhang, X. Y.; Qin, X. Y.; Jin, H.; Dai, Y.; Wang, Z. Y.; Wei, J. Y.; Zhan, J.; Wang, S. Y.; Wang, J. P.; Whangbo, M. H. Chemistry-a European Journal 2009, 15, 1821-1824.

Wang, Z.; Palacios, M. A.; Zyryanov, G.; Anzenhacher, P. Chem. Eur. J. 2008, 14, 8540-8546.

Waxman, D. J.; Strominger, J. L. Annu. Rev. Biochem 1983, 52, 825-869.

Wei, H.; Chen, C. G.; Han, B. Y.; Wang, E. K. Anal. Chem. 2008, 80, 7051-7055.

Wiegand, I.; Hilpert, K.; Hancock, R. E. W. Nat. Protoc. 2008, 3, 163-175.

Wiester, M. J.; Ulmann, P. A.; Mirkin, C. A. Angewandte Chemie-International Edition 2011, 50, 114-137.

Wright, A. T.; Anslyn, E. V. Chem. Soc. Rev. 2006, 35, 14-28.

Xiu, Z. M.; Zhang, Q. B.; Puppala, H. L.; Colvin, V. L.; Alvarez, P. J. J. Nano Lett. 2012, 12, 4271-4275.

Xue, L.; Liu, Q.; Jiang, H. Org. Lett. 2009, 11, 3454-3457.

Yang, S. Y.; Wang, W. C.; Lan, C. B.; Chen, C. H.; Chieh, J. J.; Horng, H. E.; Hong, C. Y.; Yang, H. C.; Tsai, C. P.; Yang, C. Y.; Cheng, I. C.; Chung, W. C. J. Virol. Methods 2010, 164, 14-18.

Yeh, Y. C.; Patra, D.; Yan, B.; Saha, K.; Miranda, O. R.; Kim, C. K.; Rotello, V. M. Chem. Commun. 2011, 47, 3069-3071.

You, C. C.; De, M.; Han, G.; Rotello, V. M. J. Am. Chem. Soc. 2005, 127, 12873-12881.

You, C. C.; Miranda, O. R.; Gider, B.; Ghosh, P. S.; Kim, I. B.; Erdogan, B.; Krovi, S. A.; Bunz, U. H. F.; Rotello, V. M. Nat. Nanotech. 2007, 2, 318-323.

Zasloff, M. Nature 2002, 415, 389-395.

Zhang, C.; Suslick, K. S. J. Am. Chem. Soc. 2005, 127, 11548-11549.

Zhang, T. C.; Bishop, P. L. Water Environ. Res 1996, 68, 1107-1115.

Zhao, Y. Y.; Jiang, X. Y. Nanoscale 2013, 5, 8340-8350.

Zhao, Y. Y.; Tian, Y.; Cui, Y.; Liu, W. W.; Ma, W. S.; Jiang, X. Y. J. Am. Chem. Soc. 2010, 132, 12349-12356.